ABSTRACT

Title of Document: GLOBAL OCEANIC MIXED LAYER PROPERTIES.

Hailong Liu, Doctor of Philosophy, 2009

Directed By: Professor James Carton
Department of Atmospheric and Oceanic Sciences
and
Senior Scientist Semyon Grodsky
Department of Atmospheric and Oceanic Sciences

In this thesis, the global oceanic mixed layer properties are explored in three aspects: variability of the oceanic mixed layer, subseasonal variability of the barrier layer/ compensated layer and comparison of bulk sea surface and mixed layer temperatures. (1) The analysis of variability of the oceanic mixed layer from 1960-2007 reveals substantial variability in the winter-spring depth of the mixed layer in the subtropics and midlatitudes. In the North Pacific an Empirical Orthogonal Eigenfunction analysis shows a pattern of mixed layer depth variability peaking in the central subtropics. This pattern occurs coincident with intensification of local surface winds and may be responsible for the SST changes associated with the Pacific Decadal Oscillation. In the North Atlantic a pattern of winter-spring mixed layer depth variability occurs that is not so obviously connected to local changes in winds or SST, suggesting that other processes such as advection are more important. Over the 48-year period the winter-spring mixed layers of both basins show deepening trends by 10-100m. (2) The strongest variability of barrier layer/ compensated layer from

monthly climatology is found over 100m in the subpolar latitudes of the North Atlantic in winter. Compensated layers in the eastern North Atlantic vary interannually associated with a North Atlantic Oscillation-like pattern of anomalous sea level pressure. In the winter a barrier layer exists in the subpolar North Pacific, while further south along the Kuroshio extension a compensated layer exists, both of which have variability of up to 60m and a significant long-term trend (shrinkage of the barrier layer in the subpolar gyre and growth of the compensated layer to the south) . These changes are also associated with meteorological shifts. (3) Mixed layer temperature (MLTT) and sea surface temperature (SST) are frequently used interchangeably or assumed to be proportional in climate studies. Historical analyses of bulk SST and MLTT from contemporaneous ocean profile observations show that globally and time averaged MLTT is lower than SST by approximately 0.1 ^{o}C. In the upwelling zone of the Equatorial East Pacific this negative MLTT-SST difference varies out of phase with seasonal SST, but on interannual timescales MLTT-SST varies in phase with SST with small differences during El Niños as a result of low solar heating and enhanced rainfall. On shorter diurnal timescales, during El Niños, MLTT-SST differences associated with temperature inversions occur in response to nocturnal cooling in presence of nearsurface freshening. Near surface freshening produces persistent shallow (a few meters depth) warm layers in the northwestern Pacific during boreal summer when solar heating is strong. In contrast, shallow cool layers occur in the Gulf Stream area of the Northwest Atlantic in boreal winter when fresh surface layers developed due to lateral interactions are cooled down by abundant turbulent heat loss.

GLOBAL OCEANIC MIXED LAYER PROPERTIES

By

Hailong Liu

Dissertation submitted to the Faculty of the Graduate School of the
University of Maryland, College Park, in partial fulfillment
of the requirements for the degree of
[Doctor of Philosophy]
[2009]

Advisory Committee:
Dr. James Carton, Chair
Dr. William Boicourt
Dr. Dake Chen
Dr. Semyon Grodsky
Dr. Sumant Nigam

Acknowledgements

First, I would like to express deep gratefulness to my advisor Dr. James Carton. In the past more than four years, he provided me the precious opportunity to be trained in the field of research and get this dissertation finished successfully. Moreover, his kindness, encouragement and support helped me to get through the hardest time in life when I felt it's not possible to move on ahead any more. Second, I would like to thank my coadvisor, Dr. Semyon Grodsky. Learning from his insightful visions and rigorous attitude for academic studies is my biggest harvest for the future career. I would also like to thank my committee members: Dr. Dake Chen, Dr. Bill Boicourt and Dr. Sumant Nigam for their valuable suggestions.

I want to thank Dr. Ming Li, who led me into Ph.D study and gave me many significant instructions in research. I also want to thank all the other staff, professors and students in the Horn Point Lab of UMCES and the Department of Atmospheric and Oceanic Sciences for the every moment in my memories.

Lastly and most importantly, I would like to express my deep gratitude and guilt to my grandparents, my parents and my wife, Cijing Zhang, for their love and support. I should and will never give up with them in my heart. .

Table of Contents

This Table of Contents is automatically generated by MS Word, linked to the Heading formats used within the Chapter text.

List of Figures

Chapter 1: Introduction

The vertical stratification of the upper ocean generally shows the presence of a near surface mixed layer of quasi-vertically uniform temperature and salinity, hence density. The properties of this quasi-vertically uniform layer reflect the impact of past turbulent mixing constrained by a wide variety of processes (**Fig. 1.1)** and through its weakened stratification it influences the future distribution of turbulent mixing.

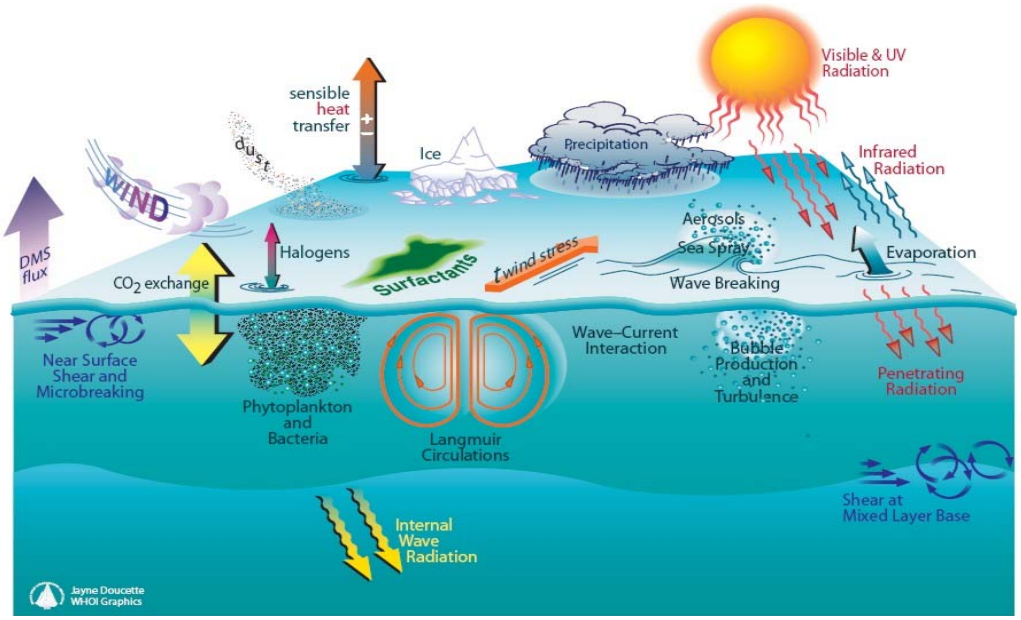

Figure 1.1 Some of the physical processes involved in oceanic mixed layer (From the Woods Hole Oceanographic Institution Graphic Services website at www.whoi.edu/graphics).

Being in direct contact with the atmosphere, it plays a central role in air-sea interaction by affecting water, gasses, heat, and momentum exchanges across the air-sea interface [*Gill,* 1982]. The temperature of the mixed layer is closely related to sea surface temperature (SST) and thus provides the lower boundary condition for

atmospheric circulation. The presences of turbulent mixing within the mixed layer and entrainment across the base of the mixed layer are key factors determining biological productivity as well as air-sea gas exchange [*Obata et al*., 1996; *Steinberg et al.*, 2001]. Motivated by improvements to the historical archive of profile observations, this dissertation reexamines several key properties of the mixed layer and their relationships to meteorological conditions.

We know that the depth of the oceanic mixed layer varies on a wide variety of timescales, from diurnal to seasonal, and on longer interannual to decadal as well (alternative ways of defining the depth of the mixed layer will be discussed in *Chapter 2*). In the past ten years a number of careful observational studies have taken advantage of the archive of historical profile observations to describe seasonal changes in mixed layer depth [*Monterey* and *Levitus*, 1997; *Kara et al*. 2000; *de Boyer Montegut et al*. 2004]. At the same time, other studies have been carried out suggesting that year-to-year changes in the seasonal maximum mixed layer depth could provide a mechanism for climate memory by allowing SST anomalies to reemerge in winters of anomalous mixed layer deepening [*Timlin et al.,* 2002*; Deser et al.*, 2003]. In *Chapter 2* I extend previous observational studies of mixed layer depth to identify patterns in year-to-year mixed layer depth variability and their connections to changes in surface forcing.

Throughout the discussion above it has been assumed that all physical properties such as temperature, salinity, and density are quasi-uniform within the mixed layer. In fact

previous studies have shown that in many parts of the ocean the depth of the layer of uniform temperature (MLT) and density (MLD) may well differ [*Sprintall* and *Tomczak*, 1992; *de Boyer Montegut et al.* 2007; *Mignot et al.*, 2007; *Yeager et al.*, 2007]. In some regions of the ocean, notably the North and western tropical Pacific, MLT may exceed MLD due to the presence of a barrier of higher salinity water in the deeper part of the uniform temperature layer [*e.g., Godfrey* and *Lindstrom*, 1989; *Lukas* and *Lindstrom* 1991]. In the tropics it has been suggested that the presence of this barrier layer may have wide-ranging impacts on air-sea interactions [e.g., *Maes et al.*, 2005; *Ffield*, 2007]. In other regions of the ocean such as the Northeast Atlantic and Southern Ocean MLD may exceed MLT due to the compensation of temperature and salinity stratification in the deeper part of the uniform density layer [*de Boyer Montegut et al.*, 2007]. Here also the consequences for climate may be substantial. In Chapter 3 I examine the observational record for evidence of year-to-year variability of these distributions and discuss the mechanisms that may have given rise to this variability.

The influence of the ocean on physical climate comes about through the role of SST in influencing the overlying atmosphere. However, the definition of SST varies considerably depending on measurement technique and application. Since the early 1980s the majority of SST observations have been made using satellite infrared and later microwave sensors. These sensors measure emissions from the upper 1mm to 1cm thick ‘skin’ of the ocean and thus provide a skin temperature estimate. These skin measurements are strongly influenced by hourly changes in surface radiation,

thermodynamic, and freshwater fluxes. Widely used SST analyses such as *Reynolds and Smith* [1994] combine these skin temperature estimates with ship intake temperatures and a limited number of buoy temperature estimates collected at depths of typically 1-5m to produce widely used analyses of SST. For the users of these analyses the residual impacts of hourly changes in surface radiation, thermodynamic, and freshwater fluxes is considered ‘noise’. In *Chapter* 4 I explore this residual noise through comparison of the profile observations with the analyses. The differences between analysis SST and ‘foundation’ temperature (approximately 10m temperature) arise through a variety of processes including impacts of the nearsurface freshening, aliasing of the diurnal cycle. Summaries and conclusions are presented in Chapter 5.

Chapter 2: Variability of the Oceanic Mixed Layer 1960-2007

2.1Introduction

The oceanic mixed layer provides a connection between atmosphere and ocean and thus plays a central role in climate variability. For example, recent studies suggest that changes in the maximum depth of the mixed layer from one winter to the next may explain the reemergence of sea surface temperature (SST) anomalies and thus persistence of wintertime SST patterns [*Alexander et al*., 2001; *Timlin et al., 2002; Deser et al., 2003*]. Here we exploit the availability of a newly expanded archive of profile observations to determine the spatial and temporal structure of mixed layer depth variability during the 48-year period 1960-2007. Our goal is to document these changes to the extent possible given the limitations of the historical observational record.

In the extratropics mixed layers undergo large seasonal depth variations as a result of seasonally varying balances in the mixed layer heat and salt budgets. Summer conditions of high sunlight and mild winds produce shallow, strongly stratified mixed layers. The maximum mixed layer depths (MLDs), in excess of 100m at 40^{o}N, occur in winter and early spring as the result of reductions in surface buoyancy flux and increases in turbulent mixing [e.g. *Monterey and Levitus*, 1997; *Kara et al*., 2002; and *de Boyer Montegut et al.*, 2004].

A number of studies have examined mixed layer dynamics at fixed mooring sites such as the *Freeland et al.* [*1997*] examination of Ocean Station Papa (50^{o}N, 145^{o}W) in the North Pacific. These examinations reveal the presence of substantial subseasonal (interannual and longer) variations of MLD. At Ocean Station Papa, *Freeland et al.* found 10-20m year-to-year depth variations as well as a long-term 6 m decade^{-1} shallowing trend. These subseasonal variations are linked to the seasonal cycle because they result from terms in the heat and salt balances of the mixed layer that are important when the mixed layer is deepening. The variations are masked by the appearance of shallow mixed layers in summer.

In addition to understanding temporal variations of MLD we would like to explore their spatial structure. For the North Pacific winter-spring mixed layer *Polovina et al.* [1995] examined the historical profile data set for the years 1977-1988 relative to 1960-1976 looking for evidence of a 'climate transition'. In contrast to the shallowing trend noted at ocean station Papa, they found a 30-80% deepening in MLD in the subtropics between these two time periods. The authors ascribe this dramatic change to the deepening of the Aleutian low pressure system and the consequent intensification of surface winds.

Indeed, since 1960 meteorological conditions in the subtropical North Pacific do appear to have undergone a transition [*Bond et al.*, 2003]. The period prior to the mid-1970s is characterized by winters with warm subtropical SSTs, cool eastern tropical SSTs, weakened midlatitude westerly winds and Aleutian low pressure

system (the negative phase of the Pacific Decadal Oscillation, PDO) [*Mantua et al.*, 1997]. More recent decades are characterized by conditions where these anomalies are reversed (the positive phase of the PDO). Incidentally, the transition seems to have induced corresponding changes in the ecosystem of the North Pacific because of the impact of changing MLD on nutrient supply to the mixed layer [*Polovina et al.*, 1995*; Chavez et al.*, 2003; *Chai et al.*, 2003]. Studies of the anomaly mixed layer heat balance in this region [see *e.g. Alexander et al.*, 2002; *Qu*, 2003] indicate the importance of forcing by surface heat flux, while Ekman transport acts to dampen temperature anomalies.

Like the North Pacific, the wintertime climate of the subtropical-to-subpolar North Atlantic is also subject to decadal variability. Since the 1960s this region has experienced a gradual increase in the latitude and strength of wintertime storms as reflected in an increasing value of the North Atlantic Oscillation (NAO) Index [*Hurrell, 1995*]. These decades have also seen a warming of SST and rising upper ocean heat storage in the subtropical gyre and cooling and freshening in the subpolar gyre [*Dickson et al., 2000; Flatau et al., 2001; Curry et al., 2003; Boyer et al., 2005; Levitus et al., 2005*].

One subtropical Atlantic location where the decadal trends of mixed layer properties have been explored is at Hydrostation S (32^{o}N, 64^{o}W) in the Sargasso Sea. There *Michaels and Knap* [*1996*] reviewed historical mixed layer properties from 1955 through 1994 relying mainly on bottle data and found quasi-decadal timescale

variations and variations with periods longer than the Hydrostation S record. In late 1950s through 1960s the time-series show winter MLDs of 200-450 m. After 1970, the mixing is shallower (100-300m), with short periods of deeper MLDs. Our own re-examination of the Hydrostation S bottle data shows that the winter MLD deepened since 1990. So, the linear trend of winter MLD over the whole period 1960-2005 is quite weak. Before 1980, interannual deepening events of winter MLD at the Hydrostation S were found to be correlated with the El Niño events in the Pacific, but this correspondence is less evident in the records after 1980. The relationship to SST was explored by *Bates* [*2001*] who found negative relationship (r=-0.56) for MLD/SST correlation.

The most dramatic changes of the mixed layer occur in the North Atlantic subpolar gyre. At the Ocean Weather Station Bravo in the Labrador Sea the upper and intermediate layers have cooled and freshened during the past 3–4 decades causing deeper mixed layers. These changes have apparently been caused by the changes in storminess associated with the rising NAO Index [*Dickson et al.*, 2002]. At the station M at 66N, 2E in the Norwegian Sea, in contrast, the winter MLD has no significant long term trend. At this eastern North Atlantic location outside the subpolar gyre the mixed layer cannot penetrate through the base of the nearsurface water mass known as Atlantic Water (~300m), and thus here MLD variability is mostly governed by horizontal advection rather than surface forcing [*Nilsen* and *Falck*, 2006].

Low frequency changes in MLD in the tropics are somewhat different than those at higher latitudes. *Wang and McPhaden* [2000] and *Cronin and Kessler* [2002] both examine the moored time series at 110^{o}W in the eastern equatorial Pacific and show that increases in MLD are associated with *decreases* in winds and *increases* in SST, rather than the reverse. In an analysis of observations since 1992 *Lorbacher et al.* [2006] examine the spatial structure of MLD variations associated with the 1997 El Niño and show an out of phase relationship between changes in MLD in the eastern and western equatorial Pacific (see their **Fig. 2.16**).

In this study we take an advantage of the 7.9 million stations contained in the newly available World Ocean Database 2005 [*Boyer et al., 2006*], Argo floats from 1997 to 2007 as well as recent work on mixed layer estimation by *de Boyer Montegut et al.* [2004] to reexamine the geographic and temporal variability of mixed layer properties during the 45-year period 1960-2007. We begin with a brief comparison to the alternative analysis of *White* [*1995*] and an examination of the impact of limitations in the salinity profile database on data coverage. The remainder of the paper examines interannual and decadal variability in the northern hemisphere and tropical mixed layer and the relationship between subseasonal changes in MLD, winds, and SST.

2.2 Data and Methods

The estimates of mixed layer properties presented here are based on the combined set of temperature and salinity vertical profiles from all available instruments contained in the World Ocean Database 2005 archive for the period 1960 through 2004 and Argo floats from 1997 to 2007. We use data from the mechanical bathythermographs

(MBT), expendable bathythermographs (XBT), conductivity-temperature-depth casts (CTD), as well ocean station data (OSD), moored buoys (MRB), and drifting buoys (DRB). The final seven years from 1960 to 2007 of the data contain an increasing number of profiles from the new ARGO system, causing the amount of salinity information to increase dramatically. This approach (based on individual vertical profiles) minimizes possible dependence of the results on biases in temperature and salinity if these biases are depth independent for each profile.

Many different criteria have been suggested in the literature for determining the depth of the base of the mixed layer [see *de Boyer Montegut et al., 2004;* and *Lorbacher et al., 2006* for the recent discussions]. Here we generally follow the methodology of *de Boyer Montegut et al.* [*2004*] who define this depth for each profile based on the temperature- or density-difference from the temperature or density at a reference depth of 10 m. This reference depth was *shown* to be sufficiently deep to avoid aliasing by the diurnal signal, but shallow enough to give a reasonable approximation of monthly SST.

Our temperature-based criterion defines MLD as the depth at which temperature changes by $|\Delta T| = 0.2^{o}$C relative to its value at 10m depth. The large 0.2^{o}C value is used following *de Boyer Montegut et al.* [*2004*] to reduce the sensitivity of the results to errors in the temperature profile measurements. Here we define the depth of the mixed layer by the *absolute difference* of temperature, $|\Delta T|$, rather than only the *negative difference* of temperature because of the possibility of temperature

inversions in salt-stratified situations. For comparison, an alternative analysis by *White* [*1995*], uses a reference level of 0m and an even larger ΔT =1^{o}C temperature criterion.

In addition to a temperature-based estimate of MLD, if profiles include both temperature and salinity (approximately 25% of all casts), we also compute a density-based MLD estimate. The increase in density, $\Delta\sigma$, which defines the depth of the base of the mixed layer is chosen, following the variable density criteria of *Monterey and Levitus* [1997], to be locally compatible with the temperature-based estimates (that is, $\Delta\sigma = \partial\sigma / \partial T \times 0.2^{o} C$). This study relies primarily on temperature-based estimates because of their superior spatial and temporal coverage (unless specified, the acronym MLD, standing for mixed layer depth, will refer to the temperature-based estimates exclusively). The differences between the two estimates are briefly discussed in Section 2.3.

In our processing we have eliminated all profiles if flagged by the World Ocean Database quality control procedure. One condition we reconsider before rejecting a profile is its vertical resolution. We retain profiles with coarse vertical resolution within the mixed layer itself. But we reject the profile if the vertical resolution is insufficient to resolve the bottom of the mixed layer (if the deepest horizon within the mixed layer is separated from the shallowest horizon below the mixed layer by more than 20% of the mixed layer depth estimate), or if the profile is shallower than the

MLD. This latter restriction is important because insufficient vertical resolution leads systematically to under-estimation of MLD.

After estimating MLD, mixed layer temperature, and mixed layer salinity at each profile location we then apply subjective quality control to remove 'bulls eyes' and bin the data into 2^{o}x2^{o}x1mo bins with no attempt to fill in empty bins. The data coverage provided by each instrument is illustrated in **Fig.2.1a,** expressed as the number of data filled points for each monthly grid (there are approximately 11000 ocean grid points on a 2x2 deg grid). The data coverage is relatively sparse. Even the XBT data never covers more than 20% of the ocean surface in a month.

As indicated in **Fig.2.1a**, the data coverage provided by each instrument is inhomogeneous in time. Moreover, significant changes in instrumentation have occurred at the beginning of the 1970s due to the introduction of high vertical resolution XBTs. We evaluate possible introduction of instrument bias into the MLD estimates by comparing the December-April MLD calculated from high vertical resolution data (XBT) with MLD calculated from low vertical resolution data (MBT) during 1970-1975 (**Fig. 2.1b**). The mean MBT-based MLD in the North Atlantic (0N to 70N) is 67m while the XBT-based MLD is 74m. The mean MBT-based MLD in the North Pacific is 67m while the XBT-based MLD is 66m. The comparison shows little evidence of instrument bias in the MLD estimates.

Much of the interesting variability of the mixed layer is linked to a particular phase of the seasonal cycle. Thus, in many of the analyses presented here we examine year-to-year variations of seasonal or bi-season average values. For comparisons to surface winds and SST we rely on the NCEP/NCAR reanalysis [*Kalnay et al., 1996*] and Hadley Center SST analysis [*Rayner et al., 2003*].

2.3 Gross Statistics

The climatological monthly maximum and minimum MLDs are shown in **Fig. 2.2** (lefthand panels show estimates based on temperature, while middle panels show estimates based on density). In the Northern Hemisphere the seasonal maximum depths occur in the subpolar North Atlantic in winter and early spring, with depths exceeding 150m in a region extending well into the western subtropical Atlantic. There the temperature-based estimates of MLD are shallower by around 50m in boreal winter than the density-based estimates because of compensation of temperature and salinity contributions to density (**Figs. 2.2a, 2.2b,** also see **Fig. 2.9** in *de Boyer Montegut et al., 2004* for comparisons). Maximum MLDs in the North Pacific are somewhat shallower than the North Atlantic, falling in the range of 100-200m. Both regions have shallow 10-30m capping mixed layers in boreal summer and fall.

In the tropical Pacific the maximum MLD may exceed 75m in the central basin, decreasing to less than 40m in the east. In the western equatorial Atlantic the temperature criterion indicates the presence of mixed layers deeper than 75m, but the

density-based criterion shows that this region of high precipitation and river discharge has a barrier layer at a shallower depth [*Pailler et al., 1999; Foltz et al., 2004*]. The maximum MLD develops by the end of February-March in the North Pacific and Atlantic (**Figs. 2.2j, 2.2k**). The annual phase of the maximum mixed layer changes approaching the equator reflecting the seasonal changes in winds and clouds over the tropics. In the Indian Ocean MLDs in excess of 75m appear in the Arabian Sea during the Southwest Monsoon beginning in June (**Figs. 2.2a, 2.2j**).

We compare our analysis to the analysis of *White (1995)* (**Fig. 2.2**, righthand panels). This alternative analysis has been used extensively to examine the impact of interannually varying mixed layers on winter SST in northern oceans [e.g. *Schneider et al., 1999; Alexander et al., 1999; Timlin et al., 2002; Deser et al., 2003*]. The differences in the analysis procedures lead to deeper estimates of MLD in the *White* analysis in the North Pacific as well as the North Atlantic during winter and spring when the upper ocean is weakly stratified. The summer mixed layers, in contrast, are generally shallower in northern latitudes and so the annual range of MLDs is larger and implied entrainment greater in the *White* analysis than in either our temperature-based or density-based analyses. These differences can be attributed to the larger $\Delta T=1C$ criterion (referenced to the surface rather than to 10m depth temperature) adopted in the *White* analysis. In the tropics, mixed layers in the *White* analysis show a similar or smaller annual range, implying similar rates of entrainment produced by the mixed layer deepening (compare **Figs. 2.2g** and **2.2i**). Maximum deepening of the

mixed layer and thus maximum entrainment occurs approximately a month later in the *White* analysis.

We next consider the root-mean-square variability in MLD about its climatological monthly average (**Fig. 2.3**). Here data is segregated by season and is only plotted if available for at least 15 of the 45 years. The available data is mainly confined to the Northern Hemisphere, coastal zones of the Southern Hemisphere, and parts of the west Pacific. The largest variability is confined to the subpolar Atlantic in winter and spring where values in excess of 100m are common. Winter-spring mixed layer variability in the Kuroshio extension region of the western North Pacific (40-75m) is weaker than that in the Gulf Stream and Gulf Stream extension regions of the North Atlantic where it ranges 50-100m. In all of these regions the variability of MLD is 25-50% of the seasonal maximum MLD (compare **Figs. 2.2** and **2.3**). Elsewhere the variability is less than 40m. In the tropics variability in the range of 15-30m occurs in all seasons in the Pacific and during the monsoon season (JJA) in the Arabian Sea. Low variability, below 15m, is a feature of the subtropical oceans during summer as well as the eastern tropical Pacific and Atlantic where the mixed layer is shallower. A zonal band of weak variability is particular noticeable along 10N in boreal fall and winter in the Pacific and Atlantic Oceans (**Figs. 2.3a, 2.3d**). This low variability band is the result of the shoaling of the thermocline on the northern side of the North Equatorial Counter Current.

The corresponding estimates of MLD variability for the *White* [*1995*] analysis (**Fig. 2.3** righthand panels) also have a higher level of MLD variability in the winter Hemisphere. But MLD variability is substantially lower in the highest variability region of the North Atlantic, a difference that probably reflects the higher spatial averaging of the *White* analysis. In the North Pacific the seasonal timing and geographic location of the maximum variability both differ. The maximum MLD variability according to the *White* analysis is shifted towards the Gulf of Alaska sector of the eastern North Pacific with low variability in the Kuroshio extension region of the western North Pacific. The maximum variability is concentrated in boreal winter and spring (in line with our estimates) but persists into the boreal summer in the central North Pacific. In the *White* analysis the tropics have significantly lower variability throughout the year than in our analysis.

Throughout much of mid latitudes the normalized standard deviation of MLD during the month of maximum deepening exceeds 30% of its depth (**Fig.2.3e**). In contrast the *White* analysis has significantly lower variability (**Fig. 2.3j**). MLD variability weakens in the tropics, but is amplified in the equatorial Pacific reflecting the ENSO variability (**Fig.2.3e**). The normalized mixed layer variability in the Atlantic is stronger than in the Pacific. This stronger variability is particularly noticeable in the southern Labrador Sea (prone to deep convection) and along the western boundary region. Higher MLD variability in the Gulf Stream area as compared to the Kuroshio extension area may be explained by lager spatial gradients of the maximum MLD (see **Fig. 3.2a**). These larger spatial gradients cause a stronger contribution of the

advective processes than elsewhere, which augments variability due to the local forcing.

The frequency dependence of the MLD variability is presented in **Fig. 2.4** by decomposing the variability into frequencies between $1yr^{-1}$ and $1/5\ yr^{-1}$ (interannual) and frequencies below $1/5\ yr^{-1}$ (decadal). In order to improve the reliability of the statistics we average the results over a winter-spring season (December–April) and a summer-fall season (July-October). During December–April most variability at both interannual and decadal frequencies is confined to higher latitudes. There the variability is at least a factor of two larger in the interannual band than the decadal band. In contrast to this, during July-October the variability at higher latitudes of the Northern Hemisphere is greatly reduced while it is increased in the Southern Hemisphere during local winter.

In the tropical Pacific the mixed layer variability has a weak seasonal dependence, while in the eastern tropical Indian Ocean and the Arabian Sea the boreal summer variability at interannual frequencies (10-15 m) is higher than that in the boreal winter variability (8-12 m). Boreal summer mixed layer variability is also higher than winter variability in the western tropical Atlantic reflecting the northward shift of the Intertropical Convergence Zone and the accompanying seasonal amplification of the southeasterly trade winds. It should be noted that the partitioning of variance in **Fig. 2.4** depends on the definition of the decadal and interannual bands. We found that for the 48-yr long time series the standard deviation of the MLD in the decadal band

drops by around 25% if the frequency separating the two bands is shifted to $f = 1/8\ yr^{-1}$.

Interestingly, part of the decadal variability reflects deepening trends in MLD in the subtropics and mid latitudes [**Fig. 5**]. In the North Pacific the most rapid changes occur early in the record from 1960-74 to 1975-1989, consistent with the independent MLD analysis of *Polovina et al.* [1995]. *Polovina et al.* have attributed this deepening of the MLD to the climate shift over the north Pacific in the mid-1970s which is reflected in changes in the PDO Index.

Detection of decadal trends is complicated by change in the ocean instrumentation discussed in Section 2. To determine the impact of instrumentation we also present decadal averages using only high vertical resolution instruments (**Fig.2.5,** XBTs and CTDs). The deepening of the mixed layer in the North Pacific between 1960-1974 and 1975-1989 seen in the 'all data' analysis is also evident in the high resolution analysis (compare **Figs. 2.5a, 2.5c** with **Figs.2.5b, 2.5d**). In contrast, there is only a weak suggestion of the mixed layer deepening in the North Pacific between 1975-1989 and 1990-2004. In the tropical Pacific and Atlantic Oceans there is little evidence of decadal trends in MLD.

In the Atlantic the 'all data' analysis suggests a steady mixed layer deepening along and south of the Gulf Stream front. The high vertical resolution analysis is patchier due to lower data coverage. North of 45N, both the 'all data' and high resolution analyses show a transition from shallow mixed layers during 1960-1974 (**Figs. 2.5a,**

2.5b) to deeper mixed layers during 1990-2004 (**Figs. 2.5e, 2.5f**). This long term deepening reflects the impact of the strengthening surface forcing and associated strengthening of westerly winds and increasing net surface heat loss.

In the North Atlantic subpolar gyre the deepening of the mixed layer has occurred while the water column has cooled and freshened [*Dickson et al*., 2002]. Because of its relationship to surface forcing as well as to entrainment cooling of the mixed layer, these variables may not be independent. We examine the potential connection between MLD and SST by computing the time regression of their anomalies with respect to the climatological seasonal cycle (**Fig. 2.6**). During all seasons this correlation analysis reveals the importance of surface forcing in northern latitudes where deeper than normal MLDs are associated with cooler than normal mixed layer temperatures. The regression coefficient is larger in winter reflecting the impact of entrainment deepening. In contrast, in the eastern half of the tropical Pacific we have the relationship frequently assumed in models of ENSO that deeper than normal MLDs are associated with warmer than normal mixed layer temperatures. A similar relationship is evident in the tropical Indian and Atlantic basins during June-August and in the western tropical Pacific during December-February, and along the western boundaries. This positively correlated relationship suggests that the anomalous heat budget of the mixed layer is dominated either by heat exchange across the bottom of the mixed layer (in the upwelling areas) or by horizontal heat advection (in the frontal areas along the western boundaries).

2.4 Variability in the Northern Oceans during Winter-Spring

Despite similar latitudes, SSTs, and presence of winter storms, mixed layers in the North Pacific and North Atlantic differ in several fundamental ways. The near-surface waters of the North Pacific are more stratified, while the higher salinity waters of the North Atlantic mixed layers are affected by episodic freshening events [*Belkin, 2004*]. In this section we explore the relationships between MLD, SST, and winds in these two regions by application of Empirical Orthogonal Eigenfunction (EOF) analysis.

The domain for the first EOF analysis spans the North Pacific and is similar to that chosen by *Bond et al.*[*2003*] for their EOF analysis of November-March SST. Our analysis is based on the five month December-April averages when the mixed layer depth is at its seasonal maximum. The primary EOF of MLD explains 9.5% of the record variance with maximum variance in the central basin between 30^{o}N-50^{o}N and positive values almost everywhere, indicating an in-phase response across the basin (**Fig. 2.7a**). The projection of the component time series on surface winds which induce wind stirring and shear instability shows that the region of maximum MLD change is almost precisely associated with the corresponding region of maximum wind speed change (**Fig. 2.7c**). The second EOF of MLD (not shown), explains 6.5% of the record variance. This second EOF has a dipole pattern with a peak in the subtropical western basin along the climatological position of the Kuroshio front and peaks of opposite phase in the northern central and eastern regions.

The principal component time series associated with this primary EOF (**Fig. 2.7b**) shows a long-term deepening trend including a rapid 10m deepening in the mid-1970s, consistent with the 15-year averages shown in **Fig. 2.5**. Superimposed on this long-term trend, the time series in **Fig. 2.7b** also reveals strong winter-to-winter fluctuations with an alternating succession of shallow and deep wintertime mixed layers in the mid-1970s through the 1980s.

Modeling studies [e.g., *Alexander et al., 2000; Xie et al., 2000*] have connected the year-to-year fluctuations in MLD to changes in local competing processes of turbulent exchange and buoyancy flux, which together regulate entrainment rate. We explore this connection by comparing the first principal component time series with the December-April PDO index reflecting low frequency changes of SST in the North Pacific. The PDO Index and the first principal component time series are positively correlated (r = 0.75 with modest smoothing) with similar year-to-year variability as well as long-term trends. Interestingly, *Cummins et al.* [2005] have demonstrated that sea level in this region also varies in phase with the PDO index, suggesting the changes of temperature and salinity penetrate throughout the upper ocean water column.

Finally, we examine the connection between winter-spring MLD and SST in the region of strong MLD-wind coherence (180^o-150^{o}W, 35^o-45^{o}N box is shown in **Fig. 2.7a**). In this region SST has a negative phase relationship with MLD where a 10m deepening of the MLD is associated with a 0.5^{o}C drop in SST (correlation is r=-0.48,

Fig. 2.8a). Thus, anomalously deep MLD is associated with anomalously cool SST. The physics of this relationship is not entirely clear. The regression patterns in **Fig.2.7c** also show a positive relationship between mixed layer deepening and surface heat loss which induces deep convection with both patterns centered at around 40N consistent with previous studies [*Alexander et al.,* 2002; *Qu,* 2003]. The strongest mixed layer response is found at around 160W just where the wind speed response peeks (compare **Figs. 2.7a, 2.7c**), while the surface heat flux pattern peeks to the east at 160E. Thus, likely both entrainment and surface heat fluxes are important in regulating year-to-year SST variations at this location in the central North Pacific.

We next turn to the North Atlantic where depth variability is a factor of two larger than the North Pacific (**Fig. 2.3**) and where variability in excess of 75m extends from the eastern subpolar region to the western subtropics. This zone is also where winter-spring MLDs extend deeper than 100m. Here we address the nature of this high variability and its connection to changes in surface meteorology.

The primary EOF in a domain extending from the equator to 70^{o}N explains 13% of the record variance and is mainly confined to the high MLD variability zone extending from the eastern subpolar region to the western subtropics (**Fig. 2.9**). The western half of this zone lies just to the east of the Gulf Stream front. The relative position of features suggests that the variability of MLD may be associated with shifts in the Gulf Stream frontal position rather than with variability of local winds. This mechanism of the North Atlantic is different with the North Pacific as the Gulf

Stream extends northeastward across the whole relatively narrower basin. Indeed, the projection of the surface winds onto the primary principal component time series shows that deepening of the MLD is correlated with increasing westerly winds at subpolar latitudes and increasing northeast trade winds in the tropics. This wind pattern resembles the wind pattern associated with strengthening of the Azores high in sea level pressure.

The corresponding principal component time series (**Fig. 2.9b**) shows that the mixed layer has deepened in this zone since the 1960s by more than 40m. A similar long term change is evident in the NAO Index, reflecting changes in the position of the storm tracks. Relationships between changes in the NAO Index and changes in the Gulf Stream frontal position have been explored by *Taylor and Stephens* [*1998*] who showed a delayed (by a few years) northward/southward shift of the front in response to amplification/attenuation of the NAO Index.

As in the case of the North Pacific, the time series shows considerable year-to-year variability. The relationship of MLD, wind, and SST variability also is not nearly as close in the North Atlantic as in the North Pacific. Time series of these variables are displayed in **Fig. 2.8b** for a rectangular box spanning the central basin (60^{o}-30^{o}W, 35^{o}-45^{o}N, see **Fig.2.9a)**. Within this box MLD and SST both exhibit a positive trend since the mid-1960s, but correlations between those variables at year-to-year timescales are quite weak.

2.5 Tropics

While mixed layer variability is weaker in the tropics than in the northern oceans (**Fig. 2.3)** some coherent features are evident. The predominant pattern of MLD variability in the tropical Pacific is coherent with the Southern Oscillation Index (SOI) and thus is associated with ENSO (**Fig. 2.10**). Here we restrict our analysis to the peak months of the mature phase of ENSO (November-March). A 10-20 decrease in the SOI, corresponding to the appearance of El Niño, is correlated with a concurrent deepening of the tropical MLD in the eastern Pacific by 5-15m and a shallowing in the western Pacific and eastern Indian Ocean by 10-20m.

In the eastern equatorial Pacific *Wang and McPhaden* [*2000*] found that the strong El Niños of 1982-3 and 1997 were associated with mixed layer deepenings of 30m or more at 0^{o}N, 110^{o}W [*Cronin and Kessler, 2002* also examine the 1997 event]. The weakening of upwelling associated with these deepening mixed layers was found to be an important modification of the mixed layer heat budget at this location. In **Fig. 2.11a** we determine a similar relationship for oceanic variables averaged over the NINO3 region (150^{o}W-90^{o}W, 5^{o}S-5^{o}N). Averaged annually (to improve the statistics), the vertical excursions of MLD reduce to a more modest 10m. However, there remains a similarly close relationship between increasing SST and a deepening mixed layer (with a ratio of 0.1^{o}C/m) and NINO3 MLD leading NINO3 SST by a few months (**Fig.2.11c)**, as well as between increasing NINO3 SST and decreasing zonal wind speed in the west (**Figs. 2.11a, 2.11b**). Winds in the west lead SST in the east by a few months (**Fig.2.11c**). In the western equatorial Pacific we find, similar to

Wang and Mcphaden, that substantial variations in MLD are evident (**Fig. 2.11b**), which lag variations in local winds by several months (**Fig.2.11c**). These MLD variations are not closely related to variations in local SST (**Fig. 2.11b**) suggesting a minor impact of entrainment on the mixed layer heat balance in the west.

The extension of the ENSO response into the mid latitude North Pacific has been examined by *Alexander et al.* [2002] (see their **Fig.2.9**). Consistent with their results, we find anomalous mixed layer deepening in the central North Pacific in the latitude range 30N to 45N during El Ninos. This anomalous deepening of the mixed layer occurs concurrent with anomalous cooling (**Fig.2.8a**, see also Fig.5 of *Alexander et al*. 2002) suggesting the importance of anomalous surface heat loss. In contrast, in the tropics the mixed layer warms as it deepens (**Figs. 2.6** and 2.**10a**) in response to heat exchanges across the base of the mixed layer.

As discussed in the Introduction, it has been suggested that anomaly mixed layer patterns can persist from one winter to the next in conjunction with the re-emergence of SST patterns. We explore the persistence of MLD patterns between successive winters by examining the regression of the SOI index on the next winter (Y+1) anomaly MLD. The midlatitude mixed layer during the next winter (**Fig.2.10b**) shows the persistence of a deepening pattern around 35N with shallowing to the north and south. Interestingly, net surface flux response does not show similar persistence. In the tropics, in contrast, the mixed layer is anomalously shallow during the following winter.

The extension of the ENSO response into the eastern tropical Indian Ocean (**Fig. 2.10a**) is also evident in our examination of the primary EOF of MLD during December-February (**Fig. 2.12a**). The spatial pattern of the mixed layer response associated with this EOF, which explains 9.5% of the record variance, has a maximum in the eastern tropics. The pattern extends further south along the Sumatra coast, with a minimum south of the equator in the central basin. The corresponding principal component time series shows that this pattern is closely related to the SOI so that MLD along the equator in the east is shallow during El Niños. Interannual variations of the mixed layer during boreal winter seem to be connected to the local wind response to ENSO. MLD variations are confined primarily to the eastern and central basin and reflect changes of the equatorial and coastal upwelling in the east and the pattern of Ekman pumping produced by the cyclonic winds in the south central basin (**Fig. 2.12a**) [see also *Murtugudde et al.*, 1999; *Potemra and Lukas*, 1999; and *Grodsky et al*., 2001].

In contrast to the conditions in December-February, the primary EOF during the peak season of the Southwest Monsoon in boreal summer reveals MLD variability confined to the western basin (**Fig. 2.12b**). During this season variations in MLD are associated with changes in the strength of the monsoonal winds, as also suggested in recent studies by *Prasad* [*2004*] and *Babu et al.* [*2004*].

2. 6 Summary and Discussion

In this work we apply the methodology of *de Boyer Montegut et al*. [2004] to construct a monthly analysis of global mixed layer depth (MLD) during the 48-year

period 1960-2007 based on profiles from the new WOD05 data set and Argo floats. The data set is limited in temporal and geographic coverage, and thus averaging is required to identify year-to-year variability. The problem of limited data is magnified since much of the MLD variability is linked to the seasonal cycle.

Despite the data limitations (The present spatial coverage of Argo floats is enough to study the basin pattern of MLD variability in the Southern Hemisphere. But several years of time coverage is not enough for the subseasonal variability even though from a statistical view it is possible. So we restrict our analysis to the Northern Hemisphere and tropics) we explore the historical record for variability that is coherent with variability appearing in winds and SST. We begin by comparing the new analysis with the widely used analysis of *White* [1995]. Our analysis differs in having shallower winter mixed layers, especially in the North Pacific. Our analysis also has shallower summer mixed layers, while the climatological peak in entrainment rate occurs a month earlier than in the *White* analysis. The distribution of MLD variability about its climatological monthly cycle also differs between the two data sets, with shifts in amplitude, structure, and seasonality.

We next consider the spatial and temporal structure of MLD variability in each of the three ocean basins and their relationship to winds and SST. In the Pacific the highest variability occurs in the subtropics and midlatitudes in the western half of the basin during boreal winter-spring. During this season 2/3 of the variability occurs at frequencies less than 1/5 yr^{-1}. An EOF decomposition of winter-spring MLD in the

North Pacific reveals that some of this interannual variability is associated with a stationary pattern with a maximum in the domain 180E-150^{o}W, 35^{o}-45^{o}N. The time variability of this primary EOF closely resembles the winter-spring PDO Index, reflecting a correspondence between increases in the MLD and increases in local wind speed. SST varies out of phase with wind speed, and thus increases in winter-spring SST are associated with shallower than normal MLD.

In boreal summer MLD variability in both the Pacific and Atlantic is reduced and tropical variability becomes more distinct. There the largest coherent signal is associated with ENSO. During an El Niño the annually averaged MLD in the eastern Pacific is deeper by 10m (and thus there is a positive correlation between SST and MLD), while MLD in the western Pacific and the eastern Indian Oceans is shallow by 10-15m.

In the Atlantic the highest variability also occurs in the subtropics and midlatitudes during boreal winter-spring, and with much of the variability at interannual frequencies. An EOF analysis shows that the maximum coherent MLD variability occurs in a zone extending along the eastern edge of the Gulf Stream in the western subtropics northeastward toward the eastern subpolar region. In contrast to the North Pacific, the MLD variability in this region is not closely related to variations in local wind speed, and does not result in coherent variations in winter SST.

A notable feature of both the central North Pacific and North Atlantic is the presence of trends that have caused the mixed layer to deepen by 10-40m over the past 48 years. In the North Pacific this deepening trend is matched by a corresponding increasing trend in the PDO Index. The presence of this trend in PDO, indeed, explains much of the decadal variability in the North Pacific MLD. Strikingly, much of the change in MLD occurred early in the record, prior to the 1980s. In the North Atlantic this deepening trend is likewise reflected in a positive trend in the NAO Index.

The salinity data coverage is still a limiting factor to address the interannual variations of the barrier and density compensated layers.

2.7 Figures

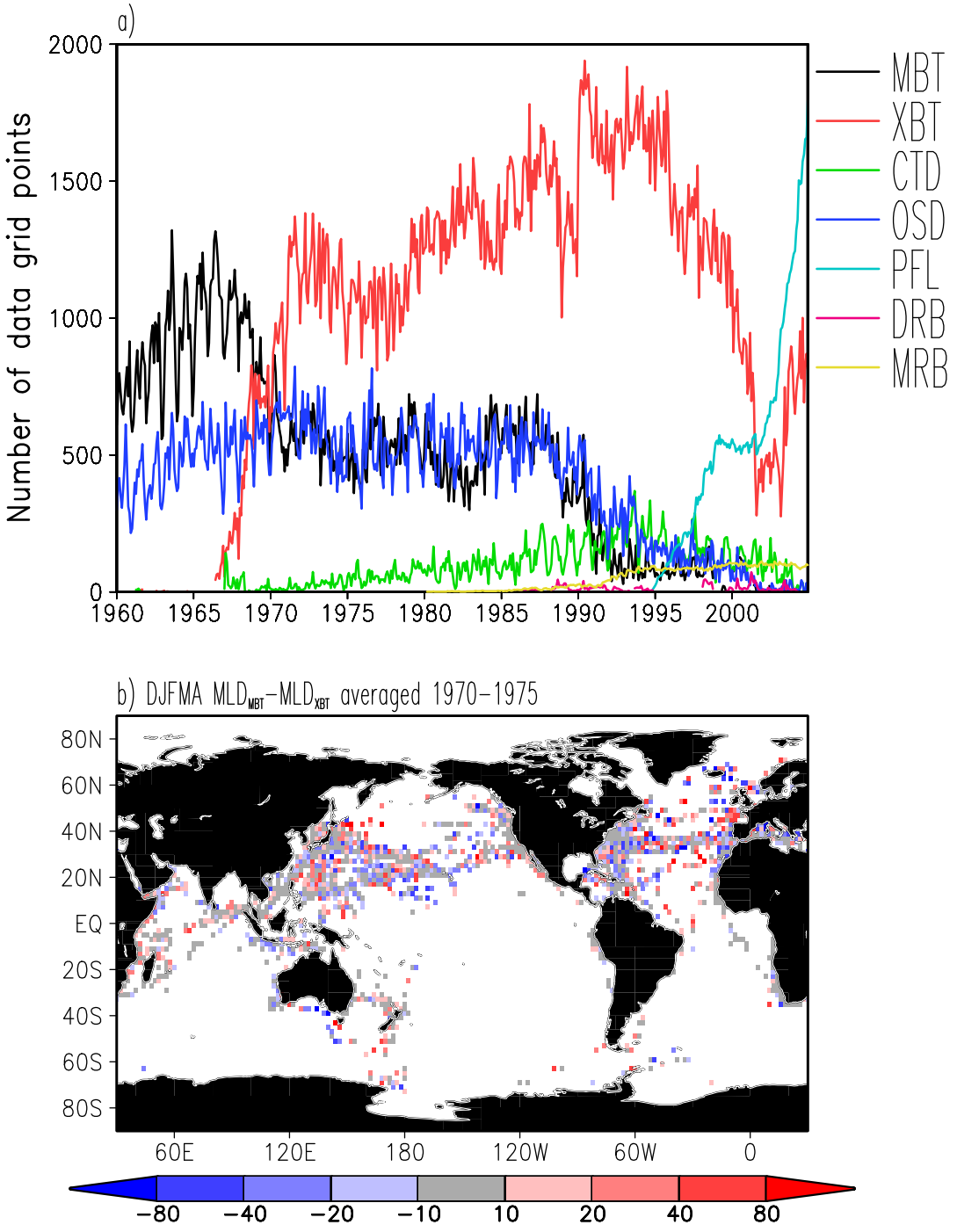

Figure 2.1. (a) Number of grid points on a 2x2 deg grid filled with data. Data are stratified by instruments. Instrument abbreviations are the same as those adopted in the NODC World Ocean Atlas. Full ocean surface coverage corresponds to approximately 11,000 points. (b) December-April MLD difference (in meters) between MBT-based and XBT-based estimates where both observations are available for the same month.

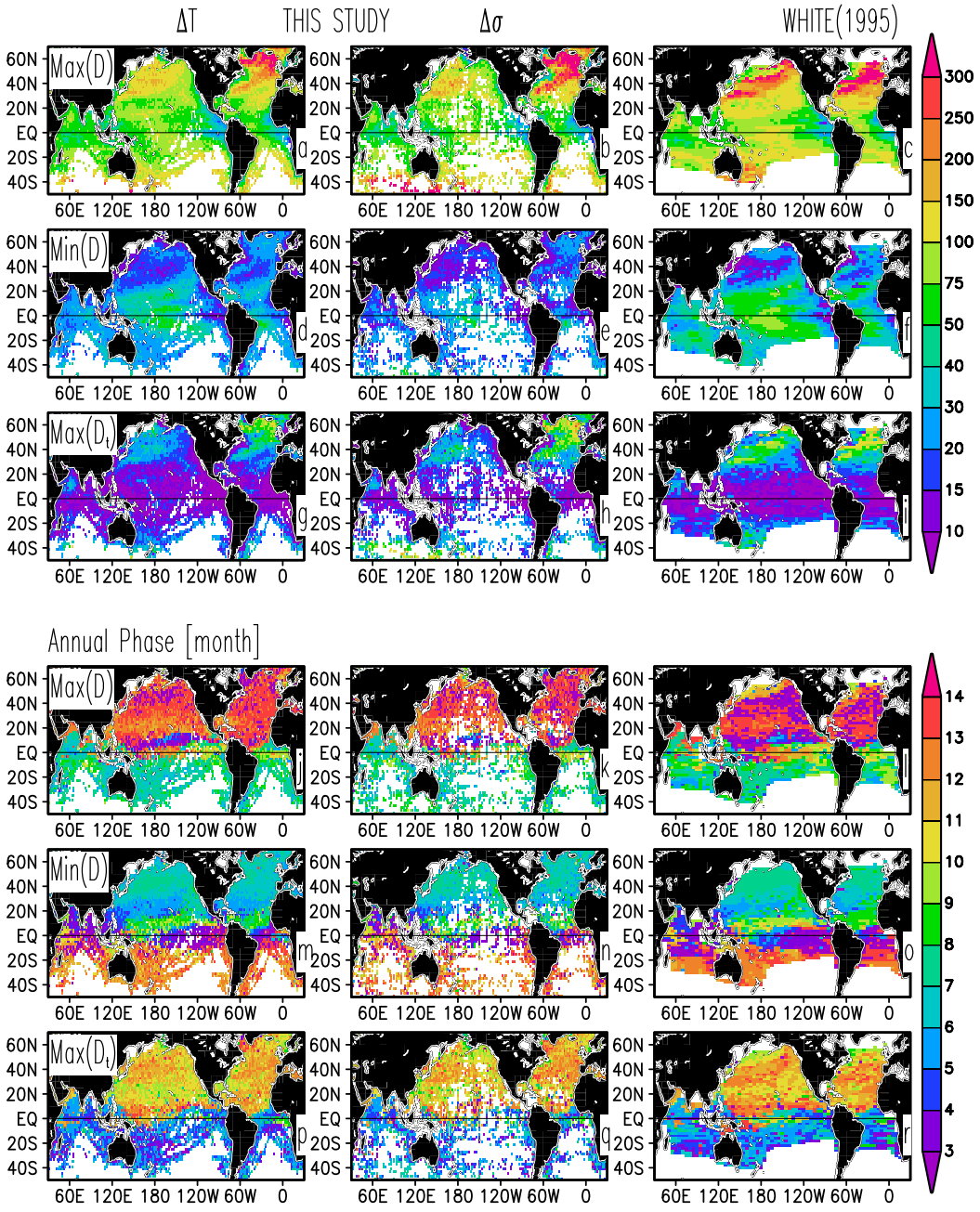

Fig. 2.2 Monthly climatology of the MLD extremes computed over the 1960-2007period. Left and middle columns show extremes based on the temperature-based definition ($|\Delta T|$=0.2 ^{o}C) and the variable density-based definition. Righthand column shows extremes based on the *White (1995)* analysis averaged over a similar period (1960-2003). Maximum MLD (a,b,c), minimum MLD (d,e,f), maximum entrainment rate (g,h,i), and the month (annual phase) of maximum MLD (j,k,l), minimum MLD (m,n,o), and maximum entrainment rate (p,q,r). Multiply entrainment rate in (g) by $C_p \rho * \Delta T$ = -0.3 to convert to entrainment heat flux in Wm^{-2}. Estimates

are plotted only if observations are available for at least 15 years. Units are meter, meter/month, and month. Month color scale begins in March in order to align with seasonal changes.

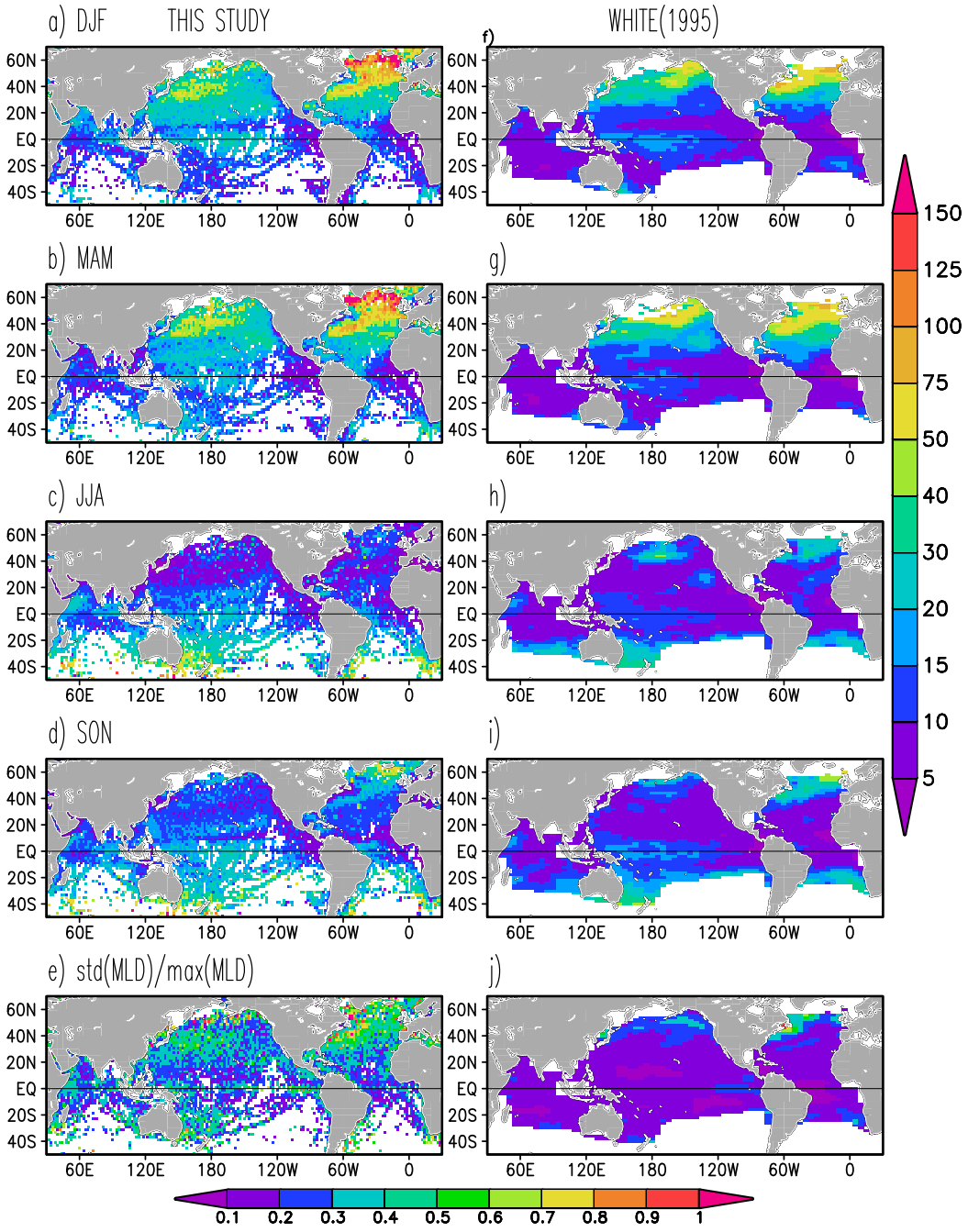

Fig. 2.3 Standard deviation of mixed layer depth from its climatological seasonal average computed over the full 48-year period. Lefthand panels show results for this study. Estimates are plotted only if observations are available for at least 15 years. Righthand panels show results for the *White (1995)* analysis over 1960-2003. Units

are meters. Color scaling is shown with righthand palette. Two bottom panels show the normalized standard deviation of MLD during the month of maximum deepening.

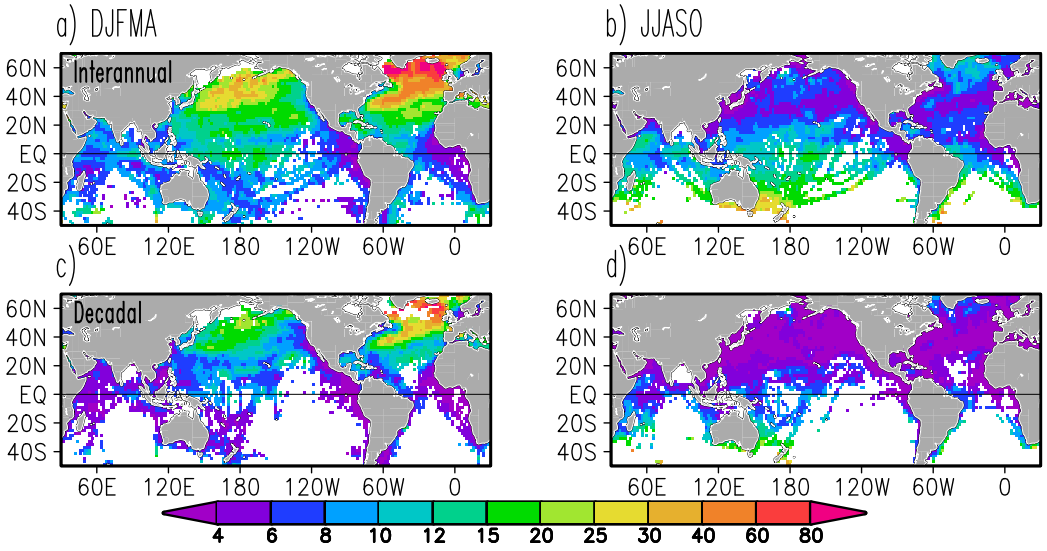

Figure 2.4 Root-mean-square MLD variability separated into interannual ($1/5yr^{-1}<f<1yr^{-1}$) and decadal frequency bands ($f<1/5yr^{-1}$) and into bi-seasons (left) December-April and (right) June-October. Interannual values are masked out if a grid box has less than 10% data coverage, while decadal values are masked out if the more poorly sampled first half of the record has less than 10% data coverage. Units are meters.

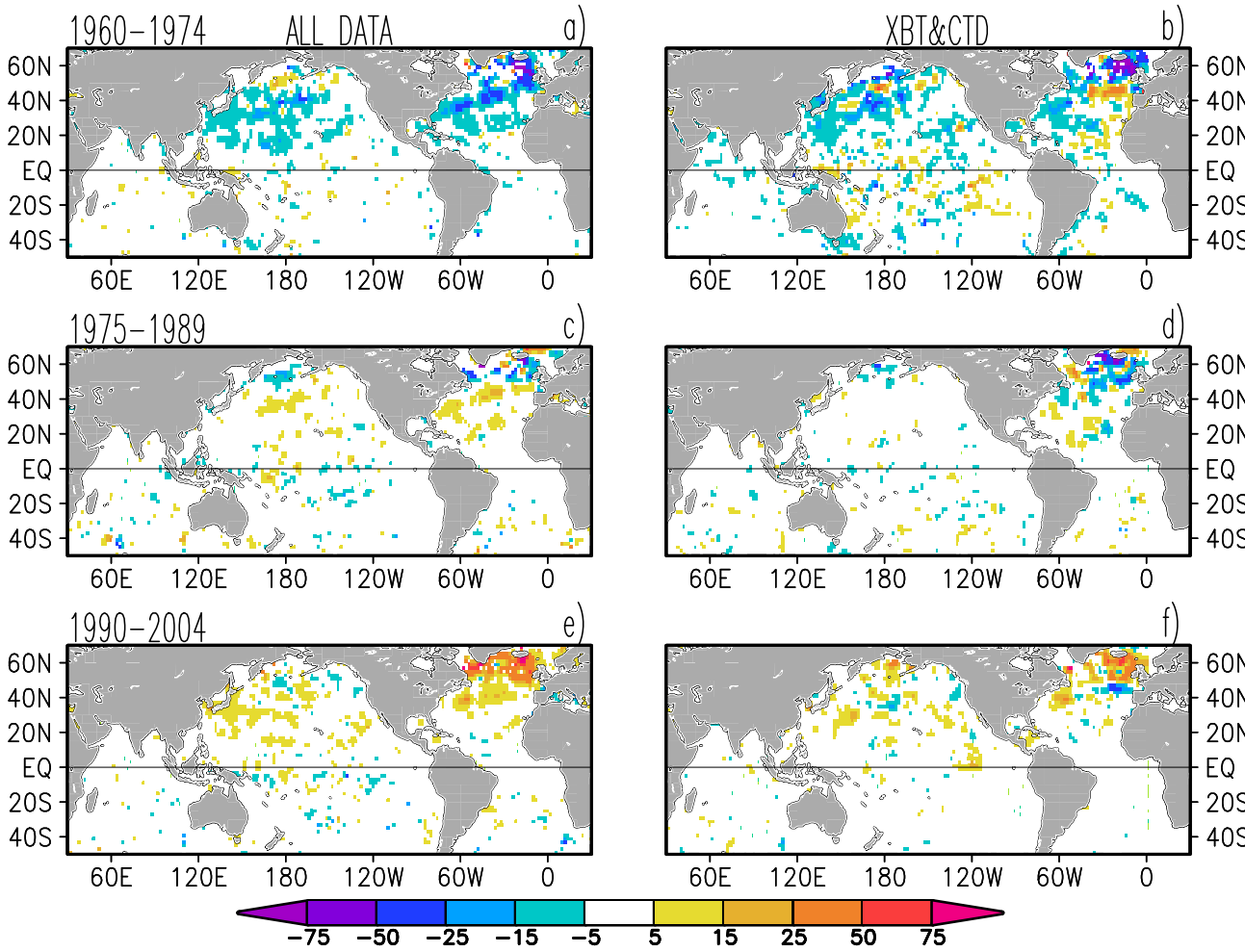

Figure 2.5 Winter-spring (December-April) MLD anomalies averaged into 15-year intervals (left) based on the whole dataset, and (right) based on the XBT and CTD data only. In the left column grid points with fewer than 15 monthly samples in any 15-year interval are masked out. A deepening trend is evident in the North Pacific and North Atlantic.

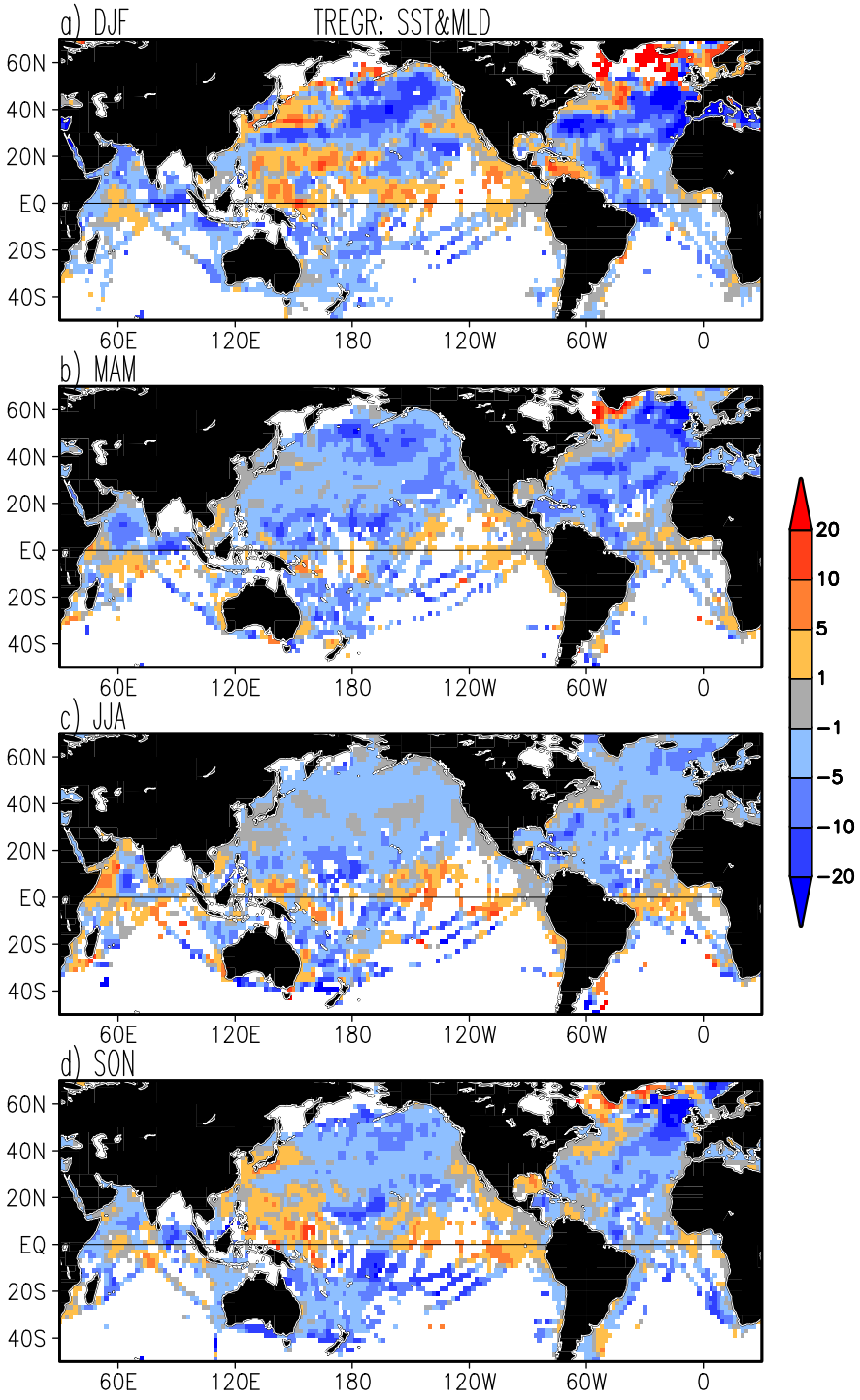

Figure 2.6 Time regression of mixed layer depth and temperature anomalies from their climatological monthly values averaged by season. Data is shown at grid points where there is at least 15 years of data. Units are m/^{o}C. Temperature is taken from profiles used to calculate MLD.

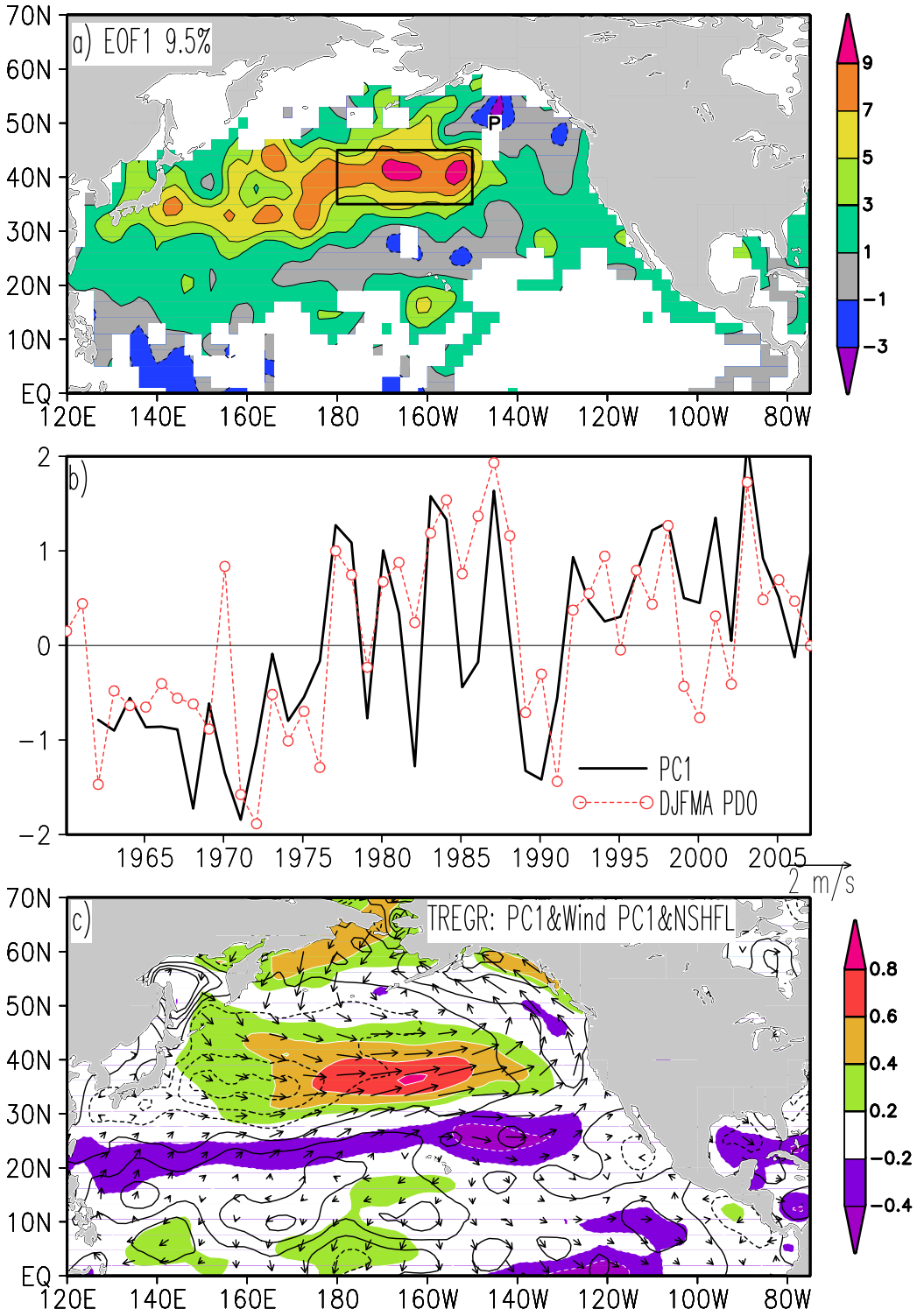

Figure 2.7 Climate variability in the North Pacific during the months December-April. (a) Spatial pattern of leading EOF of MLD. (b) Principal component time series and PDO Index time series of *Mantua et al. (1997)*. (c) Projection of anomaly

vector winds, wind speed (shading), and the net surface heat flux (contours interval 5 Wm^{-2}, negative - dashed) on the principal component time series. Location of station Papa is indicated in (a) as “P”.

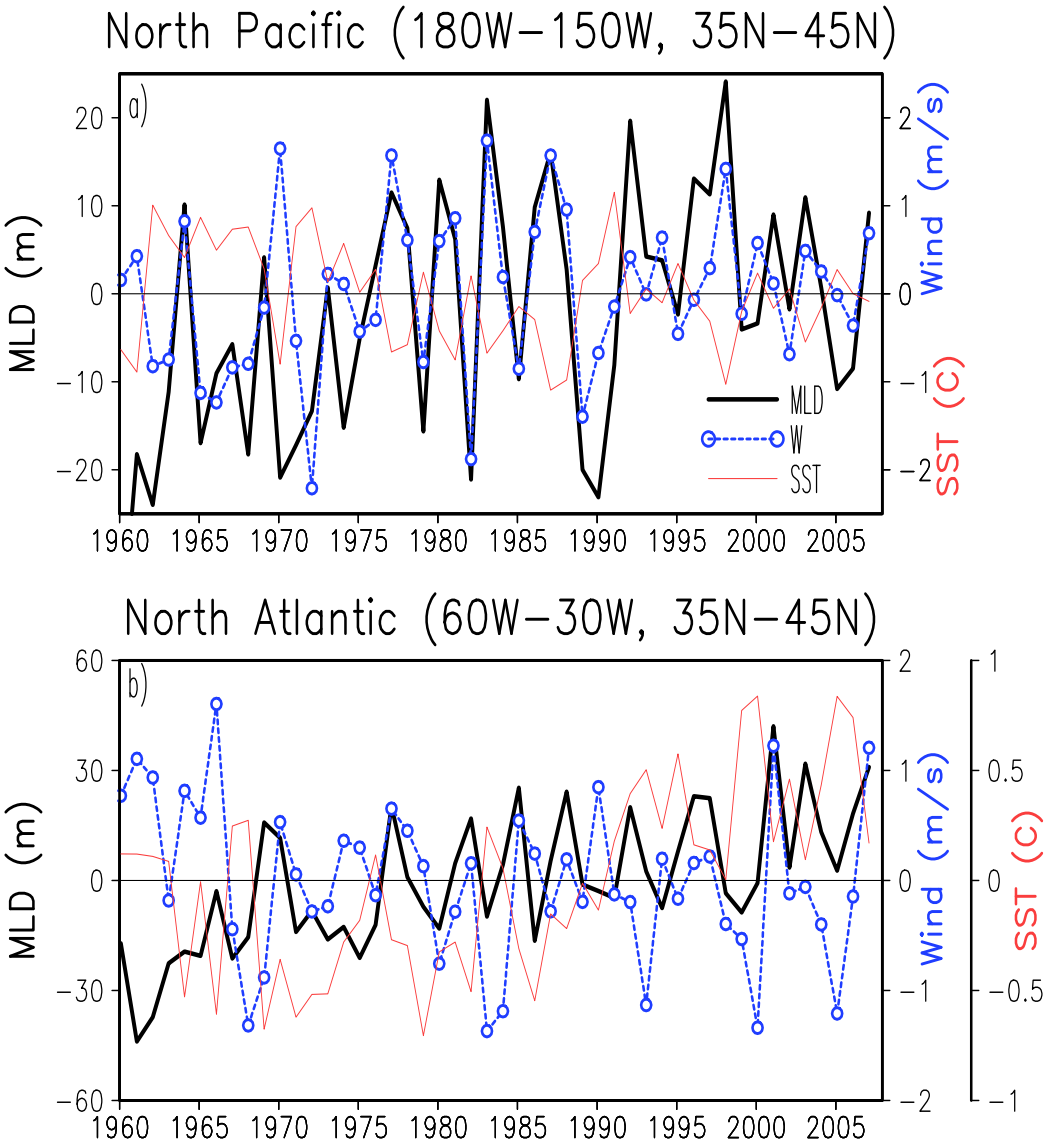

Figure 2.8 December-April anomalies averaged (a) across the central North Pacific box (defined in **Fig. 2.7**) and (b) across the central North Atlantic box (defined below in **Fig.2。 9**). The scale for mixed layer depth is shown on left (m), while scales for SST (^{o}C) and winds (ms^{-1}) are shown on right. In the Pacific the correlation between anomalous MLD and wind speed is r=0.61, while the correlation between anomalous MLD and SST is r=-0.48. In the Atlantic at decadal periods MLD and SST both show increasing trends.

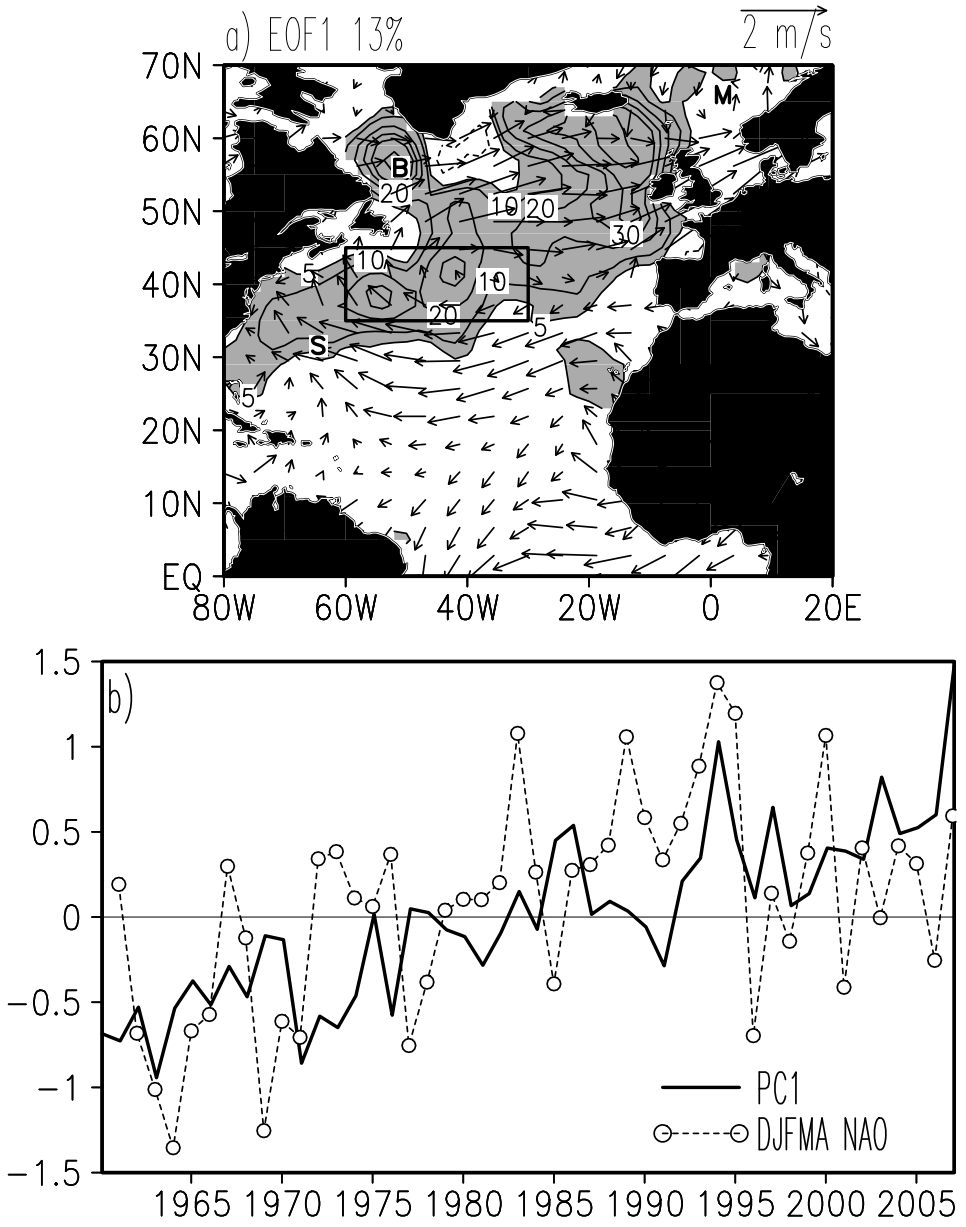

Figure 2.9 Climate variability in the North Atlantic during the months December-April (a) Spatial pattern of leading Empirical Orthogonal Eigenfunction of MLD. Projection of December-April winds on the principal component time series is overlain. (b) Principal component time series and the NAO index of *Barnston and Livezey* (1987). Locations of stations Bravo, M, and S are shown in (a) with corresponding letters.

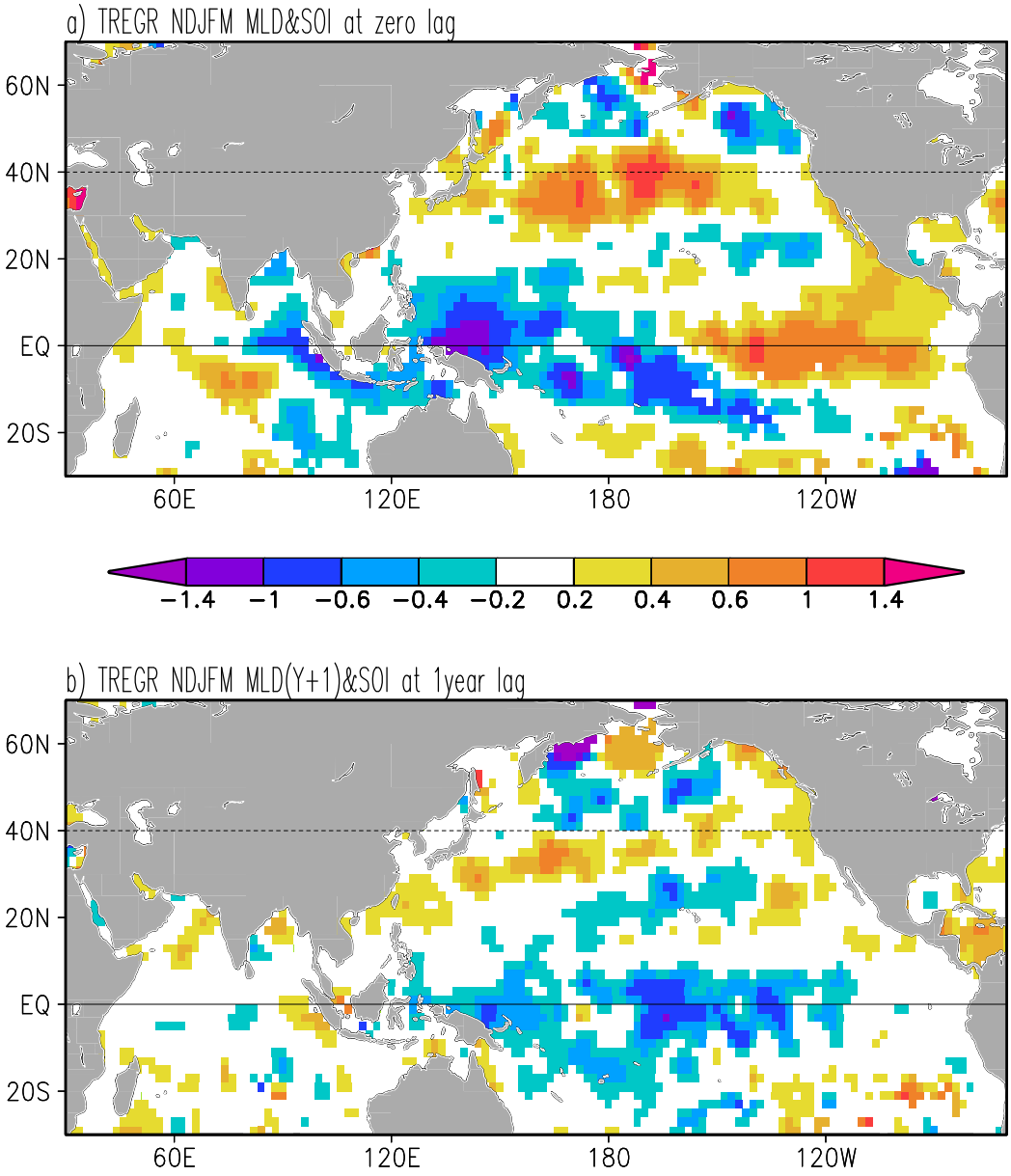

Figure 2.10 Time regression (a) of the November-March anomaly MLD and the reversed sign SOI index in the Indian and Pacific sectors. (b) Lagged regression of for the next November-March anomaly MLD(Y+1) and –SOI(Y+0). Units are m/(unit SOI).

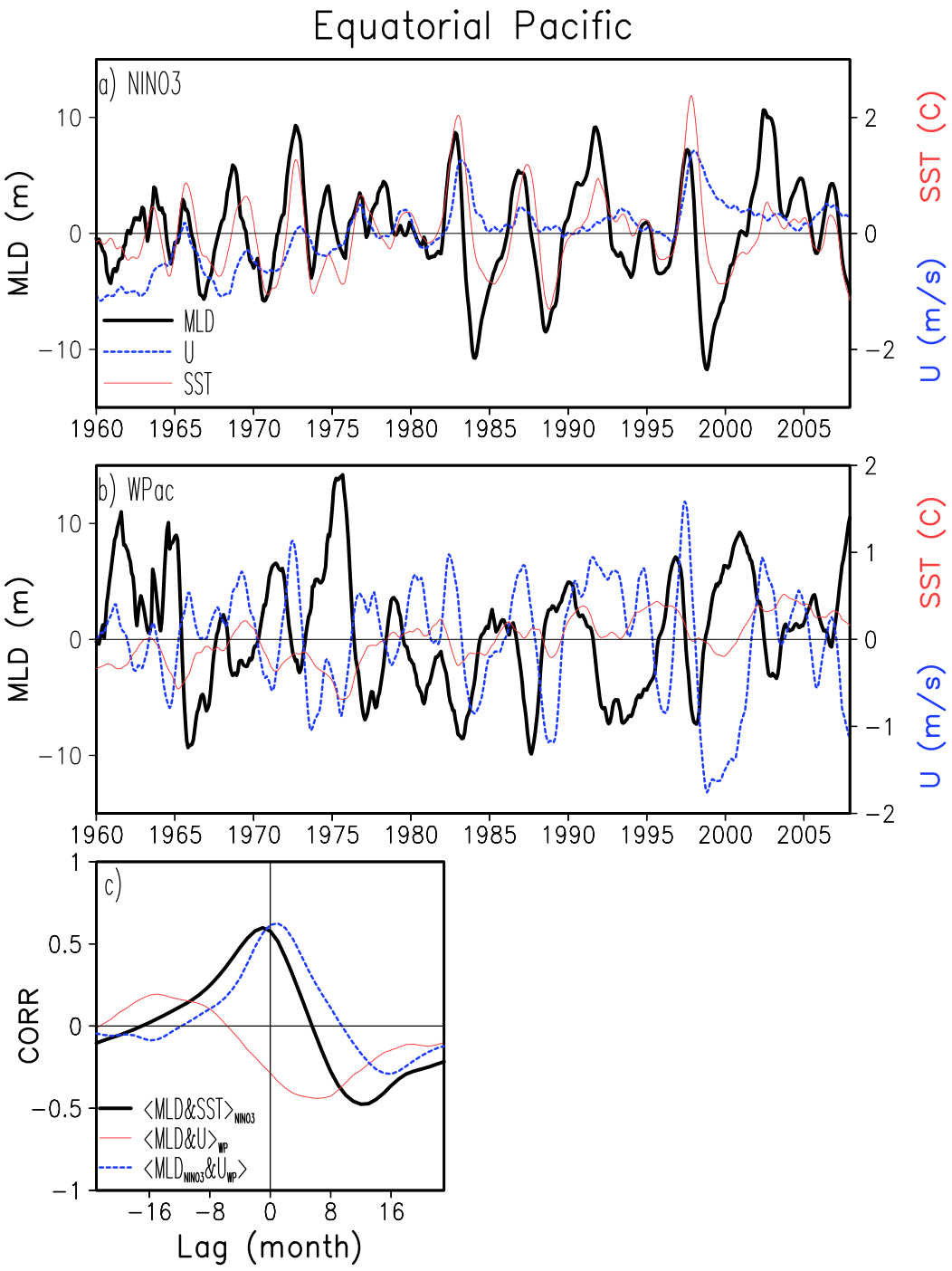

Figure 2.11 One year running mean anomaly MLD, SST, and zonal wind (*U*) (a) in the NIÑO3 box (210°-270°E, 5°S-5°N), (b) in a western Pacific box (135°-180°E, 5°S-5°N). (c) Lag correlation among *monthly averaged* NIÑO3 and western Pacific variables. Positive lags imply that the second variable leads the first.

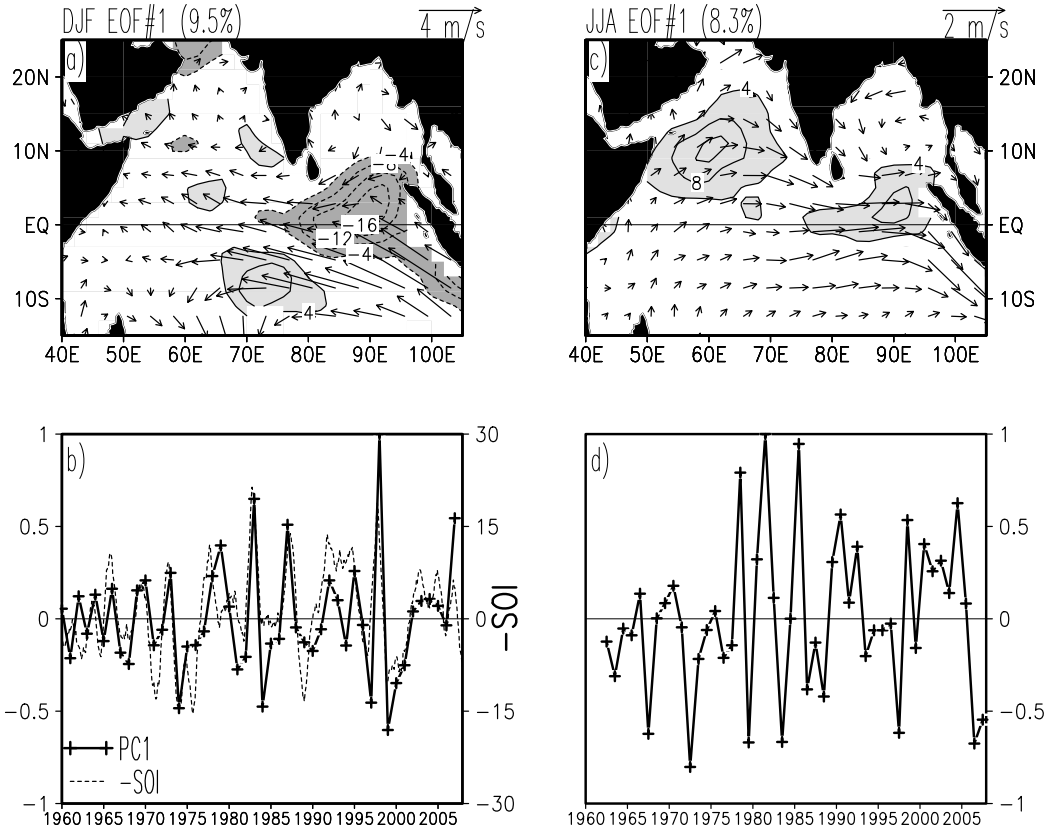

Figure 2.12 Variability in the Indian Ocean sector during (left)the season of the mature phase of ENSO SSTs (DJF) and (right) during the season of the Southwest Monsoon (JJA). **(**a,c) Spatial patterns of leading Empirical Orthogonal Eigenfunction of MLD; Time regression of winds onto the EOF time series is overlain. (b,d) Corresponding principal component time series (solid). The SOI index for DJF is overlain in (b). Correlation of PC1 and -SOI time series is 0.75.

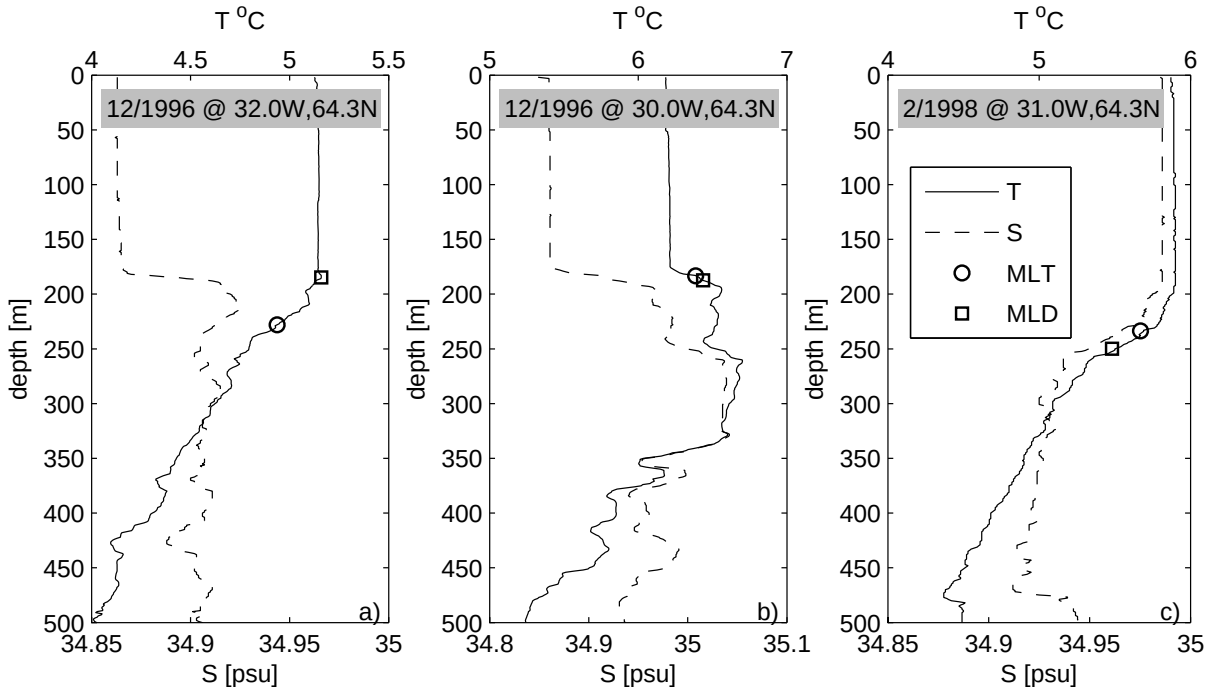

Figure A Sample *T* and *S* vertical profiles taken in the north Atlantic during winter. *MLT* and *MLD* are the mixed layer depth estimates based on the $|\Delta T|$=0.2 °C and $\Delta\sigma = \partial\sigma / \partial T \cdot 0.2^{o}$C, respectively.

Chapter 3: Observed subseasonal variability of oceanic barrier and compensated layers

3.1 Introduction

The ocean mixed layer is a nearsurface layer of fluid with quasi-uniform properties such as temperature, salinity, and density. The thickness of the mixed layer and its time rate of change both strongly influence the ocean's role in air-sea interaction. However, the thickness of the nearsurface layer of quasi-uniform temperature, MLT, may differ from the thickness of the nearsurface layer of quasi-uniform density, MLD. MLT may be deeper than MLD when positive salinity stratification forms a barrier layer (BL=MLT-MLD) as was originally found in the western equatorial Pacific [*Lukas and Lindstrom 1991*]. Elsewhere MLT may be shallower than MLD when negative salinity stratification compensates for positive temperature stratification (or the reverse situation) to form a Compensated Layer (CL=MLD-MLT) [*Stommel and Fedorov, 1967; Weller and Plueddemann, 1996*]. Modulation of the thicknesses of BLs and CLs from one year to the next [e.g., *Ando and McPhaden, 1997*], which can occur by a variety of processes including changes in surface freshwater flux, Ekman pumping, and horizontal advection, may cause a similar modulation of air-sea interaction. Here we examine the global historical profile data set covering the period 1960-2007 for corresponding year-to-year variations in the BL/CL thickness distribution.

Four surveys; *Sprintall* and *Tomczak* [1992], *Tomczak* and *Godfrey* [1994], *de Boyer Montegut et al.* [2007], and *Mignot et al.* [2007]; provide an observational description of the seasonal cycle of BL/CL distribution over much of the global ocean. BLs are a persistent feature of the tropics as well as high latitudes during winter. In high latitudes BLs occur where freshening in the near-surface is produced by excess of precipitation over evaporation, river discharge, or ice melting [*de Boyer Montegut et al*., 2007] and may be most evident in regions where upward Ekman pumping acts against the effects of vertical mixing such as occurs in the subpolar gyre [*Kara et al.,* 2000]. BLs are also observed equatorward of the salty subtropical gyres in the fresher tropics where subduction leads to a shallow subsurface salinity maximum [*Sato et al*., 2006]. The North Pacific provides an example of this, the result of southward subduction of salty North Pacific Subtropical Mode Water [as originally suggested by *Sprintall* and *Tomczak*, 1992]. BLs also occur in the Southern Ocean south of the Polar front as a result of near surface freshening and weak thermal stratification [*e.g. de Boyer Montegut et al*., 2004].

BLs also occur seasonally in the tropics in regions of high rainfall and river discharge such as the Arabian Sea and Bay of Bengal where layers as thick as 20-60m have been observed [*Thadathil* et al., 2008]. Similarly, BLs occur in the western Equatorial Pacific under the Intertropical Convergence Zone and South Pacific Convergence Zone [*Lukas and Lindstrom*, 1991] and in the western tropical Atlantic [*Pailler et al.,* 1999, *Ffield*, 2007].

Much less is known about subseasonal variations in BL/CL. In their examination of mooring time series *Ando and McPhaden* [1997] show that BLs do have interannual variability in the central and eastern Pacific, and conclude that the major driver is precipitation variability associated with El Nino. At 0^{o}N 140^{o}W, for example, the BL thickness increases from 10m to 40m in response to the enhanced rains of the 1982-3 El Nino. In contrast, *Mignot et al.* [2007] suggest that changes in zonal advection of high salinity water in response to El Nino winds are important in regulating BLs in midbasin. In the west an observational study by *Cronin and McPhaden* [2002] is able to document the response of the mixed layer to intense westerly wind bursts and accompanying precipitation and show how these lead to both the formation and erosion of BLs.

CLs in contrast may result from excess evaporation such as occurs in the subtropical gyres or by differential advection where it leads to cooler fresher surface water overlying warmer saltier subsurface water [*Yeager* and *Large*, 2007]. *de Boyer Montegut et al.* [2004] summarize several additional possible mechanisms of CL formation, such as subduction induced advection, Ekman transport, slantwise convection and density adjustment. CLs are most prominent in the eastern subpolar North Atlantic and in the Southern Ocean [*de Boyer Montegut et al.*, 2007]. In the eastern North Atlantic a CL is formed by a transport of warm and salty North Atlantic Current overlying fresher colder water. Further east the North Atlantic Current splits into a northern branch comprising the Norwegian and Irminger Currents, and the southward Canary Current all of which also develop CLs.

In our current study we build on previous observational examinations of the seasonal cycle of BL/CL development, to explore year-to-year variability. This study is made possible by the extensive 7.9 million hydrographic profile data set contained in the World Ocean Database 2005 [*Boyer et al*., 2006] supplemented by an additional 0.4 million profiles collected as part of the Argo observing program. We focus our attention primarily on the Northern Hemisphere because of its higher concentration of historical observations.

3.2 Data and Methods

This study is based on the combined set of temperature and salinity vertical profiles archived in the World Ocean Database 2005 for the period 1960-2004 and provided by Argo floats from 1997 to 2007. The first dataset was adopted from the study of variability of the oceanic mixed layer by *Carton et al.* [2008] where the details of data quality control and processing are detailed.

Mixed layer depth is defined here following *Carton et al*. [2008] which in turn combines the approaches of *Kara et al.* [2000] and *de Boyer Montegut et al.* [2004]. The mixed layer depth is the depth at which the change in temperature or density from its value at the reference depth of 10m exceeds a specified value (for temperature: $\Delta T = \left|0.2^{o} C\right|$). The reference depth was shown to be sufficiently deep to avoid aliasing by the diurnal signal, but shallow enough to give a reasonable approximation of monthly SST. The value of $\Delta T = \left|0.2^{o} C\right|$ is chosen following *de*

Boyer Montegut et al. [2004] as a compromise between the need to account for accuracy of mixed layer depth retrieval and the need to avoid sensitivity of the results to measurement error. The absolute temperature difference instead of the negative temperature difference is used following *Kara et al.* [2000] in order to accommodate for temperature inversions that are wide spread at high latitudes. The specified change in density used to define the density-based mixed layer depth follows the variable density criterion [*e.g. Monterey and Levitus*, 1997] to be locally compatible with the temperature-based estimates, (i.e. $\Delta\sigma = (\partial\sigma / \partial T) \times 0.2^0 C$). In this study the thickness (or width) of either a barrier layer or compensated layer is defined as a difference of isothermal mixed layer depth and isopicnal mixed layer depth, MLT-MLD. As a result of these definitions a positive MLT-MLD difference indicates the presence of a BL while a negative difference indicates the presence of a CL. We compute BL/CL thicknesses for each profile which are then passed through a subjective quality control to eliminate outliers and binned into $2^o \times 2^o \times 1$ month bins without attempt to fill in empty bins.

In order to quantify the relative impact of temperature and salinity stratification within BLs and CLs we introduce a bulk Turner Angle defined following *Yeager and Large* [2007] as: $Tu_b = \tan^{-1}[(\alpha\Delta T - \beta\Delta S)/(\alpha\Delta T + \beta\Delta S)]$, where $\alpha = \rho^{-1}\partial\rho / \partial T$ and $\beta = \rho^{-1}\partial\rho / \partial S$ are the expansion coefficients for temperature, T , and salinity, S . In this study the changes in temperature and salinity ΔT and ΔS are defined between the top, $z_t = \min(MLT, MLD)$, and the bottom, $z_b = \max(MLT, MLD)$, of either a BL or CL based on analysis of individual vertical profiles. The bulk Turner

angle is then evaluated from spatially binned values of ΔT and ΔS. **Fig. 3.1** shows the correspondence between values of ΔT, ΔS, bulk Turner Angle, and the presence of BLs and CLs. Angles less than -72^o correspond to situations where positive salinity stratification compensates for negative temperature stratification, a common occurrence at subpolar latitudes. Angles in the range -72^0 to 45^0 correspond to positive stratification of temperature and salinity, creating a BL. Angles greater than 45^o correspond to situations where positive temperature stratification compensates for negative salinity stratification, as occurs at the northern edges of the Circumpolar Current.

We explore the role that surface forcing plays in regulating mixed layer properties through comparison of the BL/CL distribution to fluxes from the NCEP-NCAR reanalysis of *Kalnay et al*. [1996]. Satellite QuikSCAT scatterometer winds [see *Liu,* 2002], which begin in mid-1999, are used to characterize the finer scale spatial patterns of wind-induced Ekman pumping. We also examine the Climate Prediction Center Merged Analysis of Precipitation (CMAP) of *Xie* and *Arkin* [1997] which covers the period 1979 -present.

The results of observational analysis of subseasonal variability of BL and CL are compared to 140-year long control simulation by the NOAA's Geophysical Fluid Dynamics Laboratory global coupled climate model [CM2.1, *Delworth et al.,* 2006] with the mixed layer prediction based on the *K*-profile parameterization (KPP) mixed layer scheme of *Large et al.* [1994]. The model simulates reasonably well the

atmospheric and oceanic variability from the diurnal time scale through multicentury climate change.

3.3 Results

We begin with a brief review of features of the mean and seasonal distribution.

3.3.1 **Time Mean and Seasonal Patterns**

Global seasonal patterns of BL/CL display many features previously revealed by previous analyses *(de Boyer Montegut et al*., 2007). Throughout the year there are persistent BLs in the tropics in areas of high precipitation (**Figs. 3.2a, 3.2b**). In particular, BLs are thick under the Intertropical Convergence Zone (ITCZ) and the South Pacific Convergence Zone. BLs are generally thickest in the western side of the tropical Pacific and Atlantic Oceans reflecting higher levels of rain as well as the presence of Amazonian rivers discharge. BLs are thickest on the eastern side of the tropical Indian Ocean due to the presence of the Java and Sumatra high precipitation area [*Qu* and *Meyers,* 2005]. In mid latitudes the BL/CLs are mainly a phenomenon of winter and early spring. In boreal winter the BLs thicker than 60 m are observed in the North Pacific subpolar gyre (**Fig. 3.2a**). Similarly strong BLs occur in the Atlantic Ocean north of the Gulf Stream north wall, again in phase with the seasonal increase of precipitation.

Sea surface salinity (SSS) increases drastically across the Gulf Stream front leading to a switch from the BL regime north of the front to a CL regime south of the front (**Fig.**

3.2a). Thick CLs (thicker than 30m) are also observed along the Gulf Stream due to cross-frontal transport of low salinity water. And even thicker CLs (thicker than 60m) are observed further northeast along the path of the North Atlantic Current as its warm, salty water overlies cooler, fresher water. Interestingly, despite the presence of warm and salt western boundary currents in both the Atlantic and Pacific Oceans, the winter CLs are much less pronounced in the North Pacific than the North Atlantic. Explanation for the difference likely lies in the higher surface salinity of the Atlantic (**Fig. 3.2a**) and consequently larger values of ΔS (**Fig. 3.3a**).

CLs are also evident in the southern subtropical gyres of the Pacific and Atlantic Oceans as well as the South Indian and South-west Pacific Oceans (**Fig. 3.2b**) regions to the south of the surface salinity maximum lying along 30^{o}S across the Indian Ocean into the western Pacific. The presence of CLs in this region reflects the northward advection of cold and fresh water which subducts under the water of the surface salinity maximum [*Sprintall* and *Tomczak*, 1993; note correspondence between CL in **Fig. 3.2b** and ΔS in **Fig. 3.3b**].

This proposed mechanism for CL formation is similar to that used to explain BL formation in subtropical gyres [*e.g. Sato et al.*, 2006]. In particular, the southern Indian Ocean BLs north of 30S form as the result of salty water which subducts in the region of subtropical salinity maximum along 30S and is advected northward under relatively fresh surface water (see **Fig. 3.2b**). Similar meridional dipole-like patterns with CLs to the south and BLs to the north of local subtropical SSS maxima are seen

during austral winter in the South Pacific and the South Atlantic in the regions of the downward wind driven vertical velocity (**Fig. 3.2b**). In addition to the subduction mechanism, the local rainfall in the southern Intertropical Convergence Zone [*Grodsky* and *Carton*, 2003] may contribute to freshening of the mixed layer along ~10S in the South Atlantic during austral winter. In the Northern Hemisphere the areas of CLs in the North Pacific and Atlantic Oceans extend well north of the downward Ekman pumping regions (**Fig. 3.2a**) suggesting that horizontal transport of warm salt waters by the western boundary currents plays a role.

Spatial patterns of BL/CL (**Fig. 3.2)** are in close correspondence with the spatial patterns of the vertical changes of salinity, ΔS , (**Figs. 3.3a, 3.3b**). As expected, the barrier layers are distinguished by a stable salinity stratification, $\Delta S < 0$, where salinity increases downward below the mixed layer. In contrast, compensated layers have unstable salinity stratification, $\Delta S > 0$. As discussed above, regions of fresh mixed layer trace major areas of precipitation (like the Intertropical Convergence Zone) and river runoff (the Bay of Bengal). Different type of BL is observed on the equatorward flanks of subtropical salinity maxima. In these areas the ocean accumulates salt due to an excess of evaporation over precipitation. Here the equatorward propagation of subducted water produces meridional dipole-like BL/CL and ΔS structures that are most pronounced during local winter in the Southern Hemisphere (**Figs. 3.2b, 3.3b**). Here barrier layers are observed to the north of SSS maxima where mixed layer tops saltier water below while compensated layers are observed to the south where mixed layer is saltier than thermocline.

Vertical change of temperature, ΔT, in the depth range between MLT and MLD is limited by the definition of the temperature-based mixed layer. In fact, if the uniform temperature layer is deeper than the uniform density layer (barrier layer), temperature difference across the barrier layer is limited by magnitude of the difference criterion of 0.2C. If a uniform density layer is deeper than a uniform temperature layer (density compensation), temperature difference across the CL may be arbitrary. In fact, these relatively large ΔT in excess of 0.2C are observed in CL regions during local winter (**Figs. 3.3c, 3.3d**).

Spatial patterns of the bulk Turner angle (**Figs. 3.3e, 3.3f**) indicate that majority of CL cases is associated with saltier and warmer mixed layers overlaying fresher and colder water beneath $Tu_b > 45^o$. Compensated layers widen during the cold season that is seen in higher values of Tu_b during local winter in comparison with local summer. Another type of a warm and saltier CL can be formed below a fresh and cold mixed layer, $Tu_b < -72^o$. This type of density compensation is observed only in small regions of the Labrador Sea and the Antarctica during the local cold season.

3.3.2 **Subseasonal Variability**

The subseasonal variations of BL/CL thickness are similar in amplitude to the seasonal variations (compare **Fig. 3.4** and **Fig. 3.2**). This subseasonal variability generally weakens towards the tropics reflecting stronger temperature stratification of the upper ocean at low latitudes but is large in the western Atlantic and Pacific due to subseasonal variations in precipitation and river discharge, similar to the seasonal

cycle. The highest variability of BL/CL thickness of up to 100m occurs in the North Atlantic.

To understand the sources of this low frequency variability we next consider variability separated by season and roughly 15-year averaging periods (**Fig. 3.5**). During the first periods 1960-1975 thick BLs are evident during the cold season in the North Pacific, tropical western Pacific and western Atlantic, northern Indian Ocean, and Southern Ocean (the latter being evident even in austral summer). CLs during this early period appear primarily in the eastern North Pacific. Little can be said about the existence of BLs in the Southern Ocean in austral winter due to the lack of data during this period. By the last period, 1991-2007 several changes are evident. In the Northern Hemisphere during boreal winter CLs have appeared in the subtropical North Pacific and have strengthened in the eastern North Atlantic. Strong CLs are also evident on the northern side of the Circumpolar Current in austral winter (in fact these may have existed earlier but simply not been observed). By this last period the extensive winter BLs in the North Pacific had declined as well. In order to clarify the trends in these we next examine monthly time series describing four regions: (1) BLs in the subpolar North Pacific (2) CLs in the subtropical North Pacific; (3) CLs in the eastern North Atlantic; and (4) BLs in the western equatorial Pacific (the regions outlined in **Fig. 3.5**).

The monthly time series of the northern subpolar North Pacific BL region and the subtropical CL region both show long-term trend towards thinner BLs and thicker

CLs interrupted by occasional years reversing the trend **(Figs. 3.6a, 3.6b)**. Indeed, the subtropical CL region actually supported a ~10-20m thick BL prior to 1980s. One direct cause of this change from BL to CL seems to be the gradual deepening of the late winter-spring mixed layer in the central North Pacific noted by *Polovina et al.* [1995] and *Carton et al.* [2008]. This observed 20 m deepening into the cooler, fresher sub-mixed layer water has the effect of strengthening density compensation [the 'spice injection' mechanism is discussed by *Yeager* and *Large*, 2007]. *Carton et al.* [2008] attribute the cause of mixed layer deepening to changes in the atmospheric forcing associated with the deepening of the Aleutian sea level pressure low after 1976. These changes led to strengthening of the midlatitude westerlies and the ocean surface heat loss in the North Pacific, hence the deepening of the mixed layer. The deepening of the mixed layer has opposite impacts on width of compensated layers and barrier layers. It widens CLs by injecting saltier water from the mixed layer into fresher thermocline. In contrast, stronger atmospheric forcing normally destroys near-surface BLs by stronger mixing. In fact, these accorded long-term changes of BLs shrinking and CLs widening are observed in the North Pacific (**Figs. 3.6a, 3.6b**).

Similarity in the long-term temporal changes of BL/CL thickness in the NP/BL and NP/CL boxes suggests a corresponding similarity in the long-term changes of the atmospheric forcing in both boxes. In fact, these temporal changes project on the wind pattern associated with changes in the Aleutian pressure low (**Fig. 3.7**). Widening of CLs (that corresponds to the inverse of regression patterns shown in **Fig. 3.7a**) is linked to strengthening of westerly winds and latent heat loss (hence, deeper

mixed layers) in the NP/CL box. Winds also strengthen in the NP/BL box to the north. This wind strengthening destroys BLs but may be not the only reason of shrinking BLs. Deepening of the Aleutian low amplifies anomalous dry northerly winds to the east of the low that decreases moisture transport from the south and thus reduces precipitation that is vital for BL formation (**Fig. 3.7b**).

Observed variability of the north Pacific BL/CL is dominated by long-term changes (**Figs. 3.6a, 3.6b**) that project onto mean sea level pressure pattern corresponding to strengthening of the Aleutian low (**Fig. 3.7**). But these regression patterns may lack statistical confidence because the long-term temporal changes are not well resolved by available observations. To overcome this limitation we resort on 140 year control run of the GFDL CM2.1 global coupled model.

Like in observations (**Fig. 3.2a**), in late winter - early spring the model simulates BL in the north Pacific north of approximately 35N and CL south of the BL region (**Fig. 3.8a**). In fact, two CL region are identified. The first region locates in the Kuroshio-Oyashio confluence at approximately 40^{o} N in the northwestern Pacific. The second region extends across the north Pacific along approximately 30^{o} N. This latter basin-wide pattern (the model NP/CL region) is collocated with the subtropical sea surface salinity maximum (SSS=35psu) and is bounded in the north by the northern edge of the downward Ekman pumping (W_{Ek}, **Fig. 3.8b**).

Simulated CL width varies seasonally reaching maximum by the end of cold season, so its March values follow closely the CL width envelope (**Fig. 3.8c**). March CL width varies on periods ranging from interannual to multi-decadal. In March of 1953 simulated CL is the strongest (up to 25m wide) while in a few years, in March of 1956, CL is shrunk and replaced by weak 10m wide BL. We next examine changes in the surface meteorology and vertical salinity between the two contrasting years.

Climatological W_{Ek} is downward south of 35N that produces corresponding subduction area (**Fig. 3.8b**). Southward propagation of cold and fresh water subducted to the north of the subtropical SSS maximum produces unstable vertical salinity stratification below the region of SSS maximum while subduction of salt water of SSS maximum produces stable salinity stratification to the south. These meridional changes in the vertical salinity are clearly seen in **Fig. 3.9** during the both years. During the cold season when a saltier mixed layer deepens to the levels of lower salinity, CLs develop to the north of SSS maximum.

There is a striking difference in the wind stress between model years 1953 and 1956 manifesting in different northward extension of the downward W_{Ek} (**Fig. 3.9**). In the 1953 the northward extension of downward W_{Ek} is similar to the climatological mean. During this year (**Fig. 3.9a**) the isohaline contours are tilted southward reflecting southward propagation of subducted water. This tilt produces unstable salinity stratification in the vertical and results in appearance of CLs to the north of 25^{o} N where MLD>MLT. In contrast to the 1953, W_{Ek} in the 1956 is mostly upward north

of the SSS maximum (**Fig. 3.9b**). This upward velocity traps precipitation near the surface (isohaline contours are tilted northward in the upper 40m) and results in shallow BLs, the regime that is normally observed further north (**Fig. 3.8a**).

Anomalous CL width and BL width (averaged over the corresponding regions shown in **Fig. 3.8a**) have different relationship with anomalous MLD (**Fig. 3.8d**). CLs (negative width) widen when the mixed layer deepens. This is in line with the spice injection mechanism discussed by *Yeager* and *Large* [2007]. In contrast, BLs (positive width) shrink when the mixed layer deepens reflecting stronger mixing that destroys near-surface BLs. Because both, CL and BL width are negatively correlated with local MLD, they are positively correlated with each other (0.5 at zero lag, not shown). This means that widening of CLs in the NP/CL box corresponds to shrinking of BLs in the NP/BL box in line with observations in **Figs. 3.6a**, 3.**6b**.

Like in observations (**Fig. 3.7**), temporal changes of simulated CL width (**Fig. 3.8c**) project on a wind pattern associated with changes of the Aleutian low. Vertical expansion of CL (more negative CL width) correlates with strengthening of Aleutian low and midlatitude westerly winds. The strengthening of westerly winds deepens mixed layer and amplifies subduction in the CL box, thus increasing the vertical extent of compensated layers.

Correspondence between temporal changes of BL/CL width and atmospheric pressure patterns seen in both, observations and simulations in the north Pacific suggests that

similar correspondence with local atmospheric patterns may take place in the north Atlantic. But the time series of variations in CL region of the North Atlantic is striking in showing primarily year-to-year variations (**Fig. 3.6c**) even though the winter-spring meteorology of this region does exhibit decadal variations frequently referred to as the North Atlantic Oscillation [*Hurrell*, 1995]. We suspect that some of this variability is the result of the smaller spatial scales of variability relative to the North Pacific which has been insufficiently sampled by the historical observing systems. During the past ten years when the data coverage has been increasingly extensive (due to implementation of the Argo floats) CL thickness in the North Atlantic CL region has undergone 15m variations from year-to-year with thick layers in 1999, 2002-3, and 2006-7 and thinner layers during the other years (**Fig. 3.10a**). This pattern of CL variation is related to the strength of the subtropical high in sea level pressure (**Fig. 3.10a**). Indeed, a regression of sea level pressure, latent heat flux, and winds on CL thickness in the North Atlantic CL box shows basin-scale relationships (**Fig. 3.10b**). Vertical expansion of CLs (more negative CL width) corresponds to NAO-like pattern of the atmospheric pressure with stronger Azores high and deeper Iceland low. This pressure pattern strengthens winds and latent heat losses in the east while weakens them in the central and western subtropics (**Fig. 3.10b**). Anomalously strong winds and net surface heat losses suggest deepening of the mixed layer that, in turn, expands width of CLs by the spice injection mechanism. This is in line with 2002-3 and 2006-7 data when anomalously thick CLs in the NA/CL box occur in phase with anomalously deep mixed layers. But in 1999 this relationship is opposite (**Fig. 3.10a**). This may suggest that alternative mechanisms

including salt advection play a role. Indeed, in the north-east it is clear that advection plays a central role in variability of the mixed layers [*Nilsen* and *Falck*, 2006 show this process at work in the Norwegian Sea].

Finally, we consider year-to-year variability of the BL region of the tropical Pacific. BL thickness in the western Pacific west of 160^{o}E, which is generally 10-20m, varies in thickness coherently with the value of the Southern Oscillation Index (**Fig. 3.11c**). The eastward shift of precipitation during El Nino decreases precipitation west of 160^{o}E by 20% or 1 mm/dy (in response to a 20 unit decrease of the SOI) and as a result BLs shrink by 20% or 2-5m (**Figs. 3.11a, 3.11b**). Thus, in this region variations in BL thickness respond primarily to surface freshwater flux. East of 160^{o}E BLs are thinner and occur at much shallower depths so that they are affected more strongly by solar radiation, advection and entrainment.

3.4 Conclusions

This study examines subseasonal changes in the distribution of a key aspect of the oceanic mixed layer – the presence of barrier or compensated layers (BLs and CLs) – based on analysis of profiles of temperature and salinity covering the years 1960-2007. Because of data limitations we focus mainly on the Northern Hemisphere and tropics. The processes that regulate subseasonal variability of BL/CL thickness are similar to those which regulate their seasonal appearance: fluctuations in surface freshwater flux, Ekman pumping, and horizontal advection. Thus, the spatial

distribution of subseasonal variability reflects aspects of the subseasonal variability of these forcing terms.

The most striking interannual variability of BL width occurs in the rainy tropical oceans with deep thermoclines such as the Arabian Sea and Bay of Bengal in the Indian Ocean and the western tropical Pacific under the Intertropical Convergence Zone and the South Pacific Convergence Zone. Precipitation in these regions varies strongly interannually. During high precipitation years the mixed layers in these regions show capping fresh layers and thick BLs. In contrast, during low precipitation years mixed layer salinities increase and BL thickness decreases. Thus, in the western Equatorial Pacific between 120^{o}E and 160^{o}E, the BL thickens by 2m to 5m during La Nina while during the El Nino the BL thickness thins by a similar amount. In the central and eastern equatorial Pacific variations of BL thickness are not nearly as well correlated with the phase of ENSO. We think this happens because in the central basin salt advection plays an important role in regulating BL thickness as well, while further east the mixed layer shallows and mixed layer entrainment variability becomes increasingly important.

In the subtropics and midlatitudes during late winter-spring we find alternating regions of CLs and BLs in the climatological analysis. The northern tropics of both the Pacific and Atlantic (the southern edge of the subtropical gyres) show broad regions of BLs where salty subtropical surface water formed further north has subducted, advected equatorward, and affected the water properties of the winter

mixed layer. Within the evaporative subtropical North Pacific and eastern North Atlantic we find CLs resulting from mixed layers with positive temperature stratification but negative salinity stratification. In the eastern subpolar North Atlantic this CL merges with a subpolar CL resulting from negative temperature stratification but positive salinity stratification. In the North Pacific, strengthening of the Aleutian pressure low during successive winters, thus strengthening the midlatitude westerly winds has led to deeper mixed layers, cooler SSTs, and a long-term increase in the thickness of this CL. Further north in the North Pacific a supolar BL region is evident, which does not have a counterpart in the North Atlantic. The same changes in meteorology which include an have led to an increase in dry northerly winds which in turn cause a thinning of this BL from ~40m before 1980s to ~ 20m afterwards.

In the North Atlantic the broad area of CL also undergoes fluctuations in thickness associated with surface meteorology. In this basin the fluctuations in winter thickness also seem to vary in response to meteorological changes associated with changes of the Azores sea level high pressure. Estimation of the timescale of variability is more difficult in this basin as the analysis is more noisy. Here our analysis focuses on the changes that are apparent in the shorter 1997-2007 period when the data coverage is better. During this period the thickness of the winter-spring CL in the northeastern Atlantic undergoes 4-5 year timescale fluctuations in thickness from 45m to 60m thick in phase with the strengthening/weakening of the Azores high.

Determining the basin-scale structure of BL/CL structure tests the limits of the historical observing system. Further progress in understanding BL/CL variability and its role in air-sea interactions will likely require development of models that can provide reasonable simulations of observed variability.

3.5 Figures

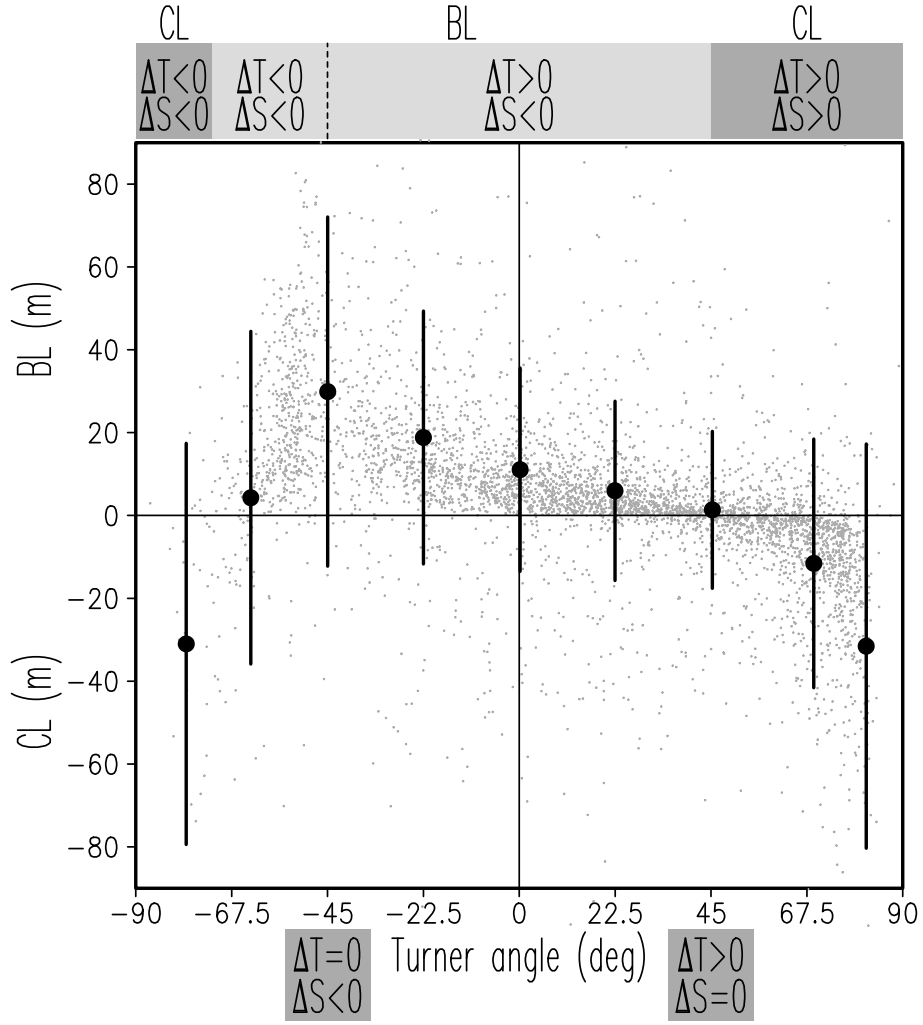

Figure 3.1. Climatological January-March barrier layer/compensated layer thickness versus the bulk Turner angle evaluated using temperature (ΔT) and salinity (ΔS) difference between the top and bottom of a barrier or compensated layer. Grey dots are data, vertical bars show the mean and the standard deviation for consecutive 22.5^0 interval of the Turner angle. The Turner angle range -72^0 to 45^0 corresponds to BL. CL occurs outside this interval.

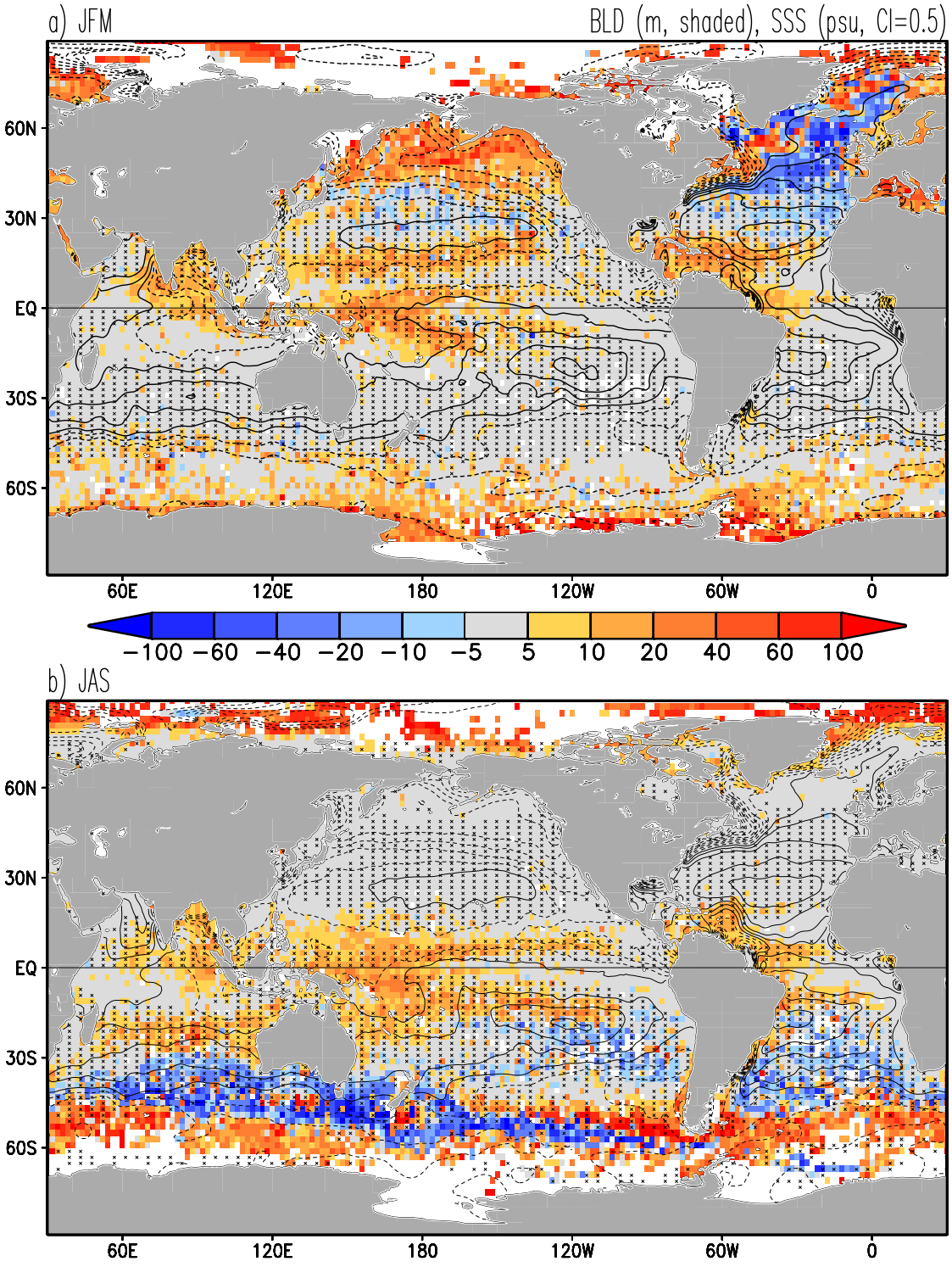

Figure 3.2. Climatological (a) January-March and (b) July-September barrier layer width (positive) and compensated layer width (negative). Climatological sea surface salinity (>35psu solid contours, below 35psu dashed contours) and downward wind-

driven vertical velocity (hatching) are overlain. Salinity data are from *Boyer et al.* (2006).

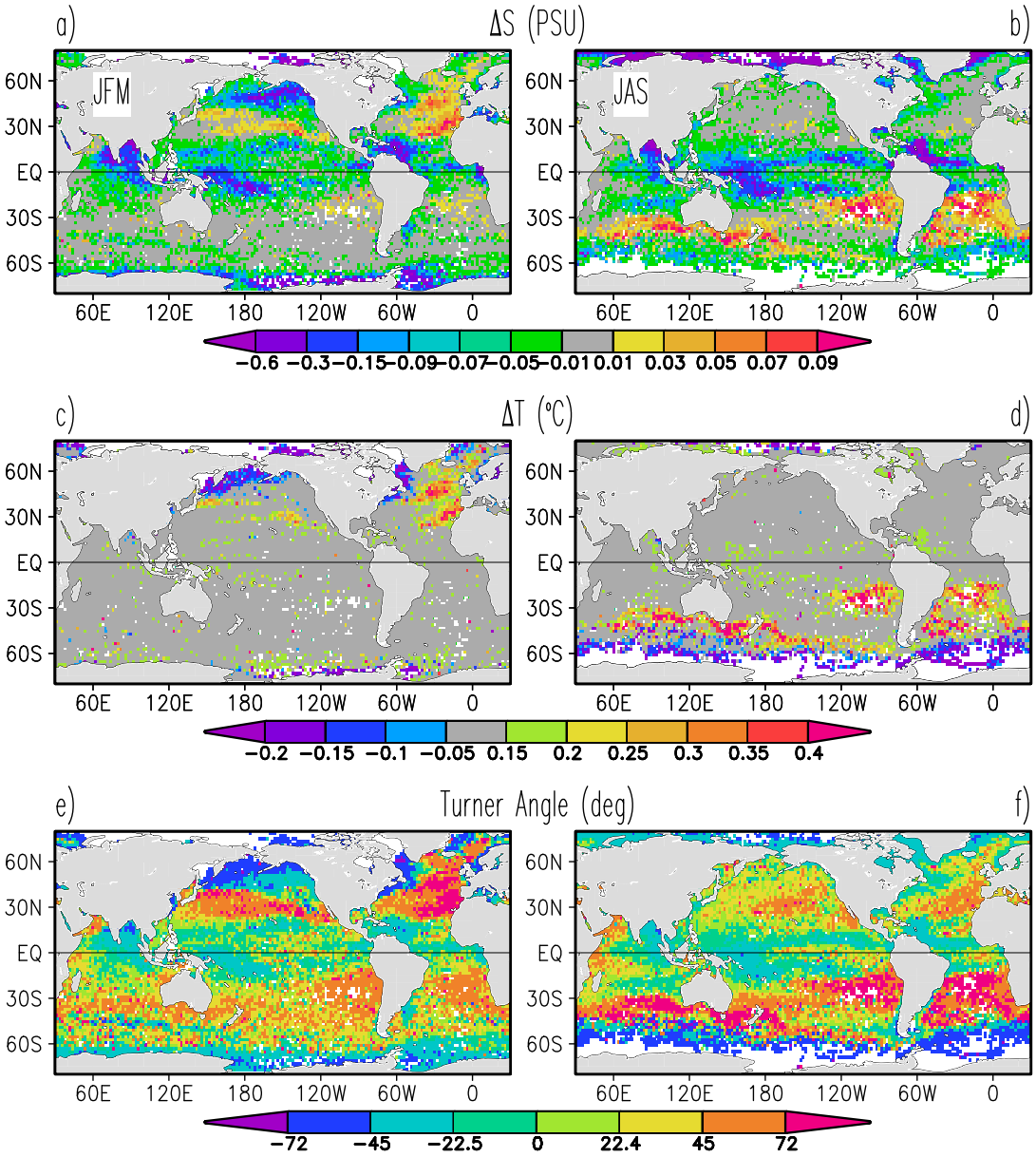

Figure 3.3. (a,b) Salinity (ΔS) and (c,d) temperature (ΔT) difference between the top z_t = min[MLT, MLD] and the bottom z_b =max[MLT, MLD] of barrier/compensated layer, (e,f) bulk Turner angle calculated from ΔS and ΔT between the same two depths. (left) January - March (JFM) values, (right) July - September (JAS) values. Turner angles in the range from -72° to 45° corresponds to barrier layers, while compensated layers occur outside this range

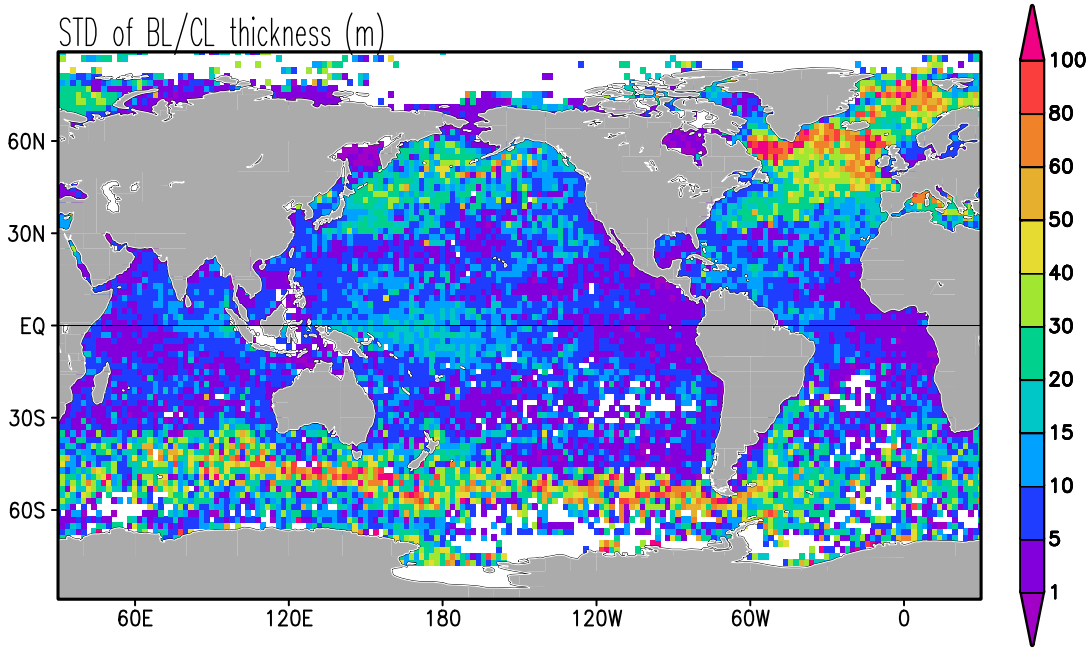

Figure 3.4. Standard deviation (STD) of monthly anomalous BL/CL thickness.

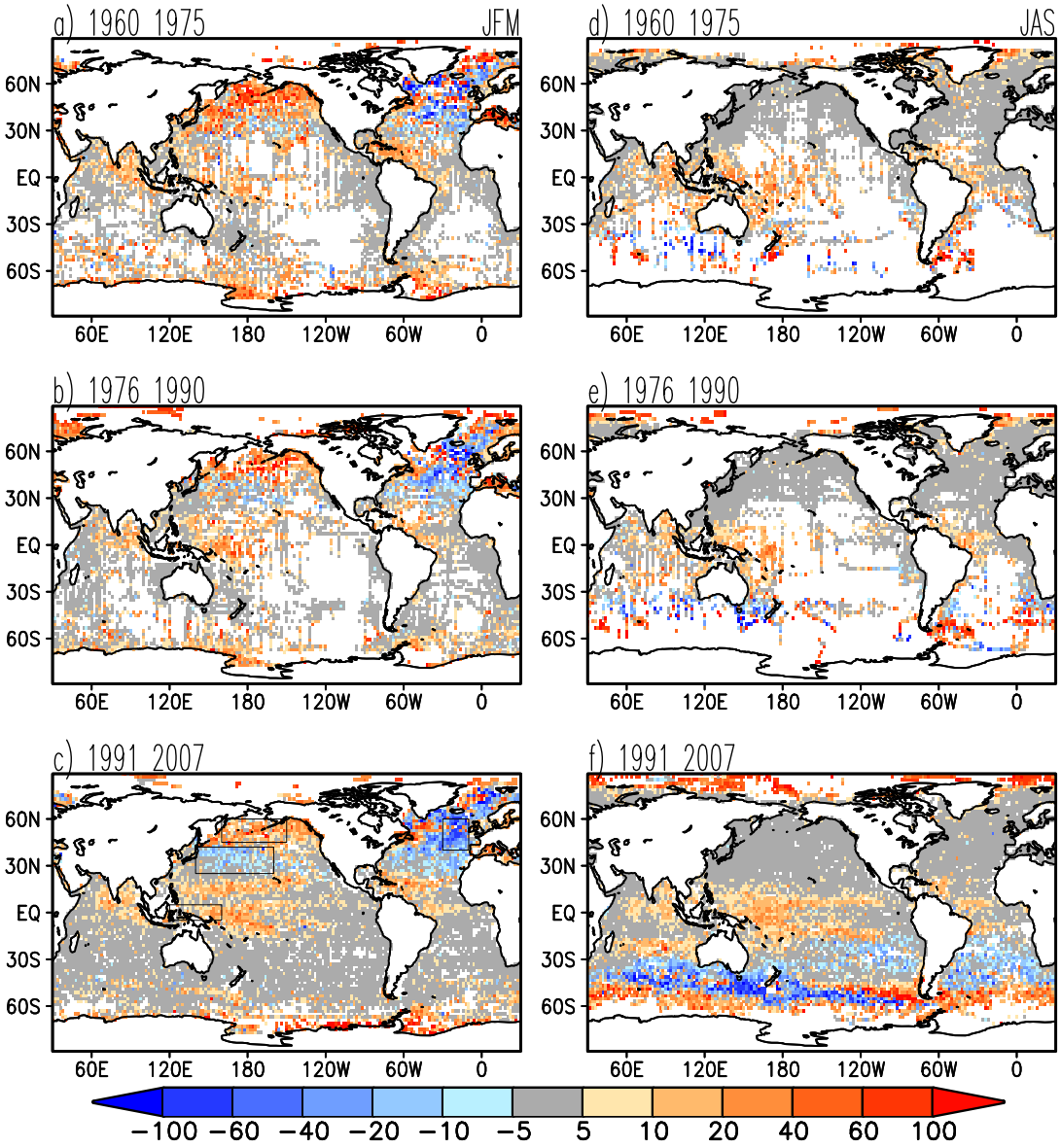

Figure 3.5. Quasi-decadal mean barrier layer (positive) and compensated layer (negative) thickness in (left) northern winter and (right) austral winter. Rectangles in (c) show locations of the North Pacific barrier layer box (NP/BL 140°E-140°W, 50°-60°N), North Pacific compensated layer box (NP/CL 140°E-160°W, 25°-35°N), equatorial Pacific barrier layer box (EP/BL 120°E-160°E, 5°S-5°N), and North Atlantic compensated layer box (NA/CL 30°W-10°W, 40°-60°N)

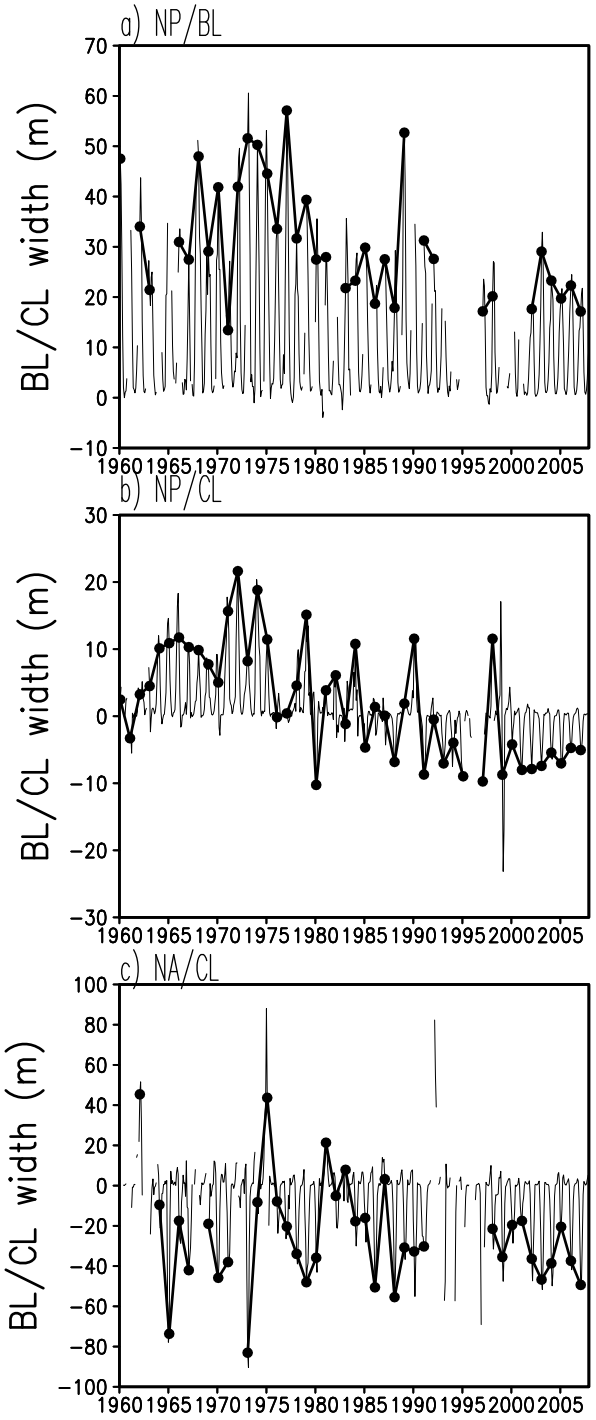

Figure 3.6. Box averaged BL/CL width in (a) North Pacific barrier layer region, (b) North Pacific compensated layer region, and (c) North Atlantic compensated layer region. Thin lines are monthly average values, bold lines are January-March average values. JFM values are shown if at least 10 data points are available. Box locations are shown in Fig. 3.5c.

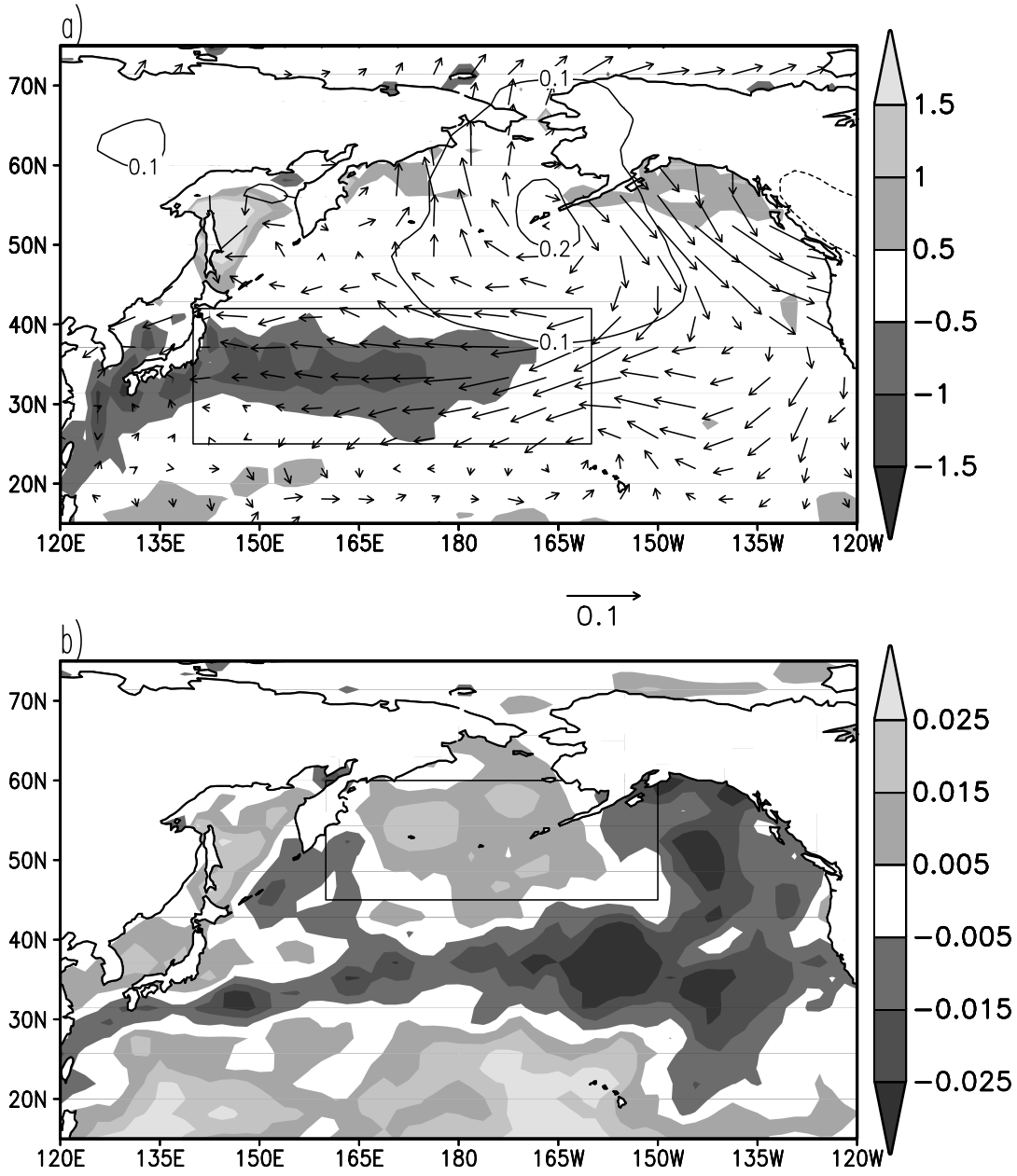

Figure 3.7. Time regression of JFM barrier layer thickness in (a) North Pacific compensated layer box on latent heat flux (Wm^{-2}/m, shading), winds (ms^{-1}/m, arrows), and sea level pressure (mbar/m); (b) North Pacific barrier layer box on precipitation (mm h^{-1}/m). See also Fig.3.5c for box locations. Atmospheric parameters are from the NCEP/NCAR Reanalysis.

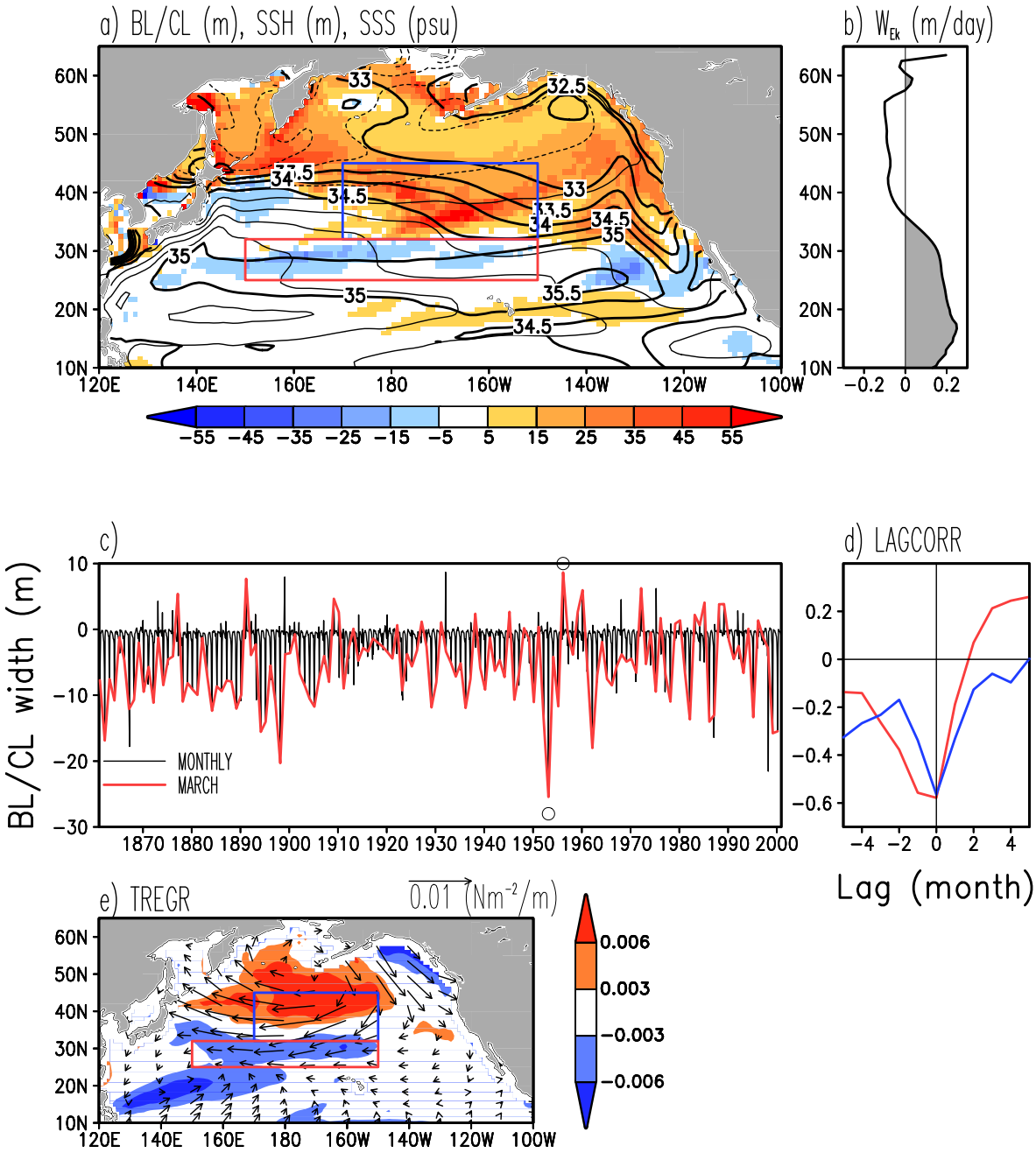

Figure 3.8. CM2.1 model simulations in the north Pacific. (a) March climatological BL/CL width with climatological sea surface height (SSH, CI=0.2m) and sea surface salinity (SSS, bold contours) overlain. CL and BL boxes are drawn in red and blue, respectively. (b) Zonally averaged March climatological Ekman pumping (positive – downward is shaded gray). (c) Time series of the box-averaged CL width. Two contrasting model years with thick (1953) and thin (1956) CL are marked by 'o'. (d) Lagged correlation of anomalous (blue) box-averaged CL width and MLD, (red) box-averaged BL width and MLD. (e) Time regression of March box-averaged CL width on wind stress and Ekman pumping.

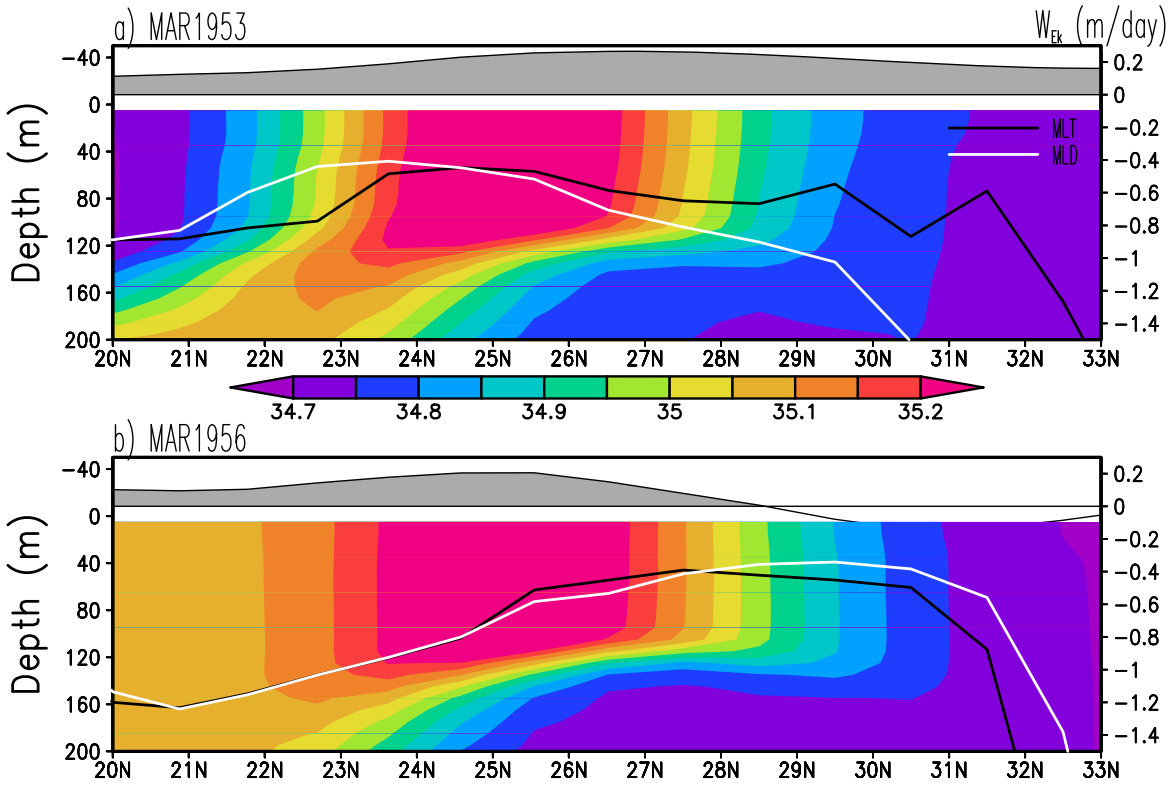

Figure 3.9. Latitude-depth section of salinity along 180E for March of the two contrasting model years with thick (1953) and thin (1956) CL. Ekman pumping (positive – downward is shaded gray) is shown against the right-hand vertical axes.

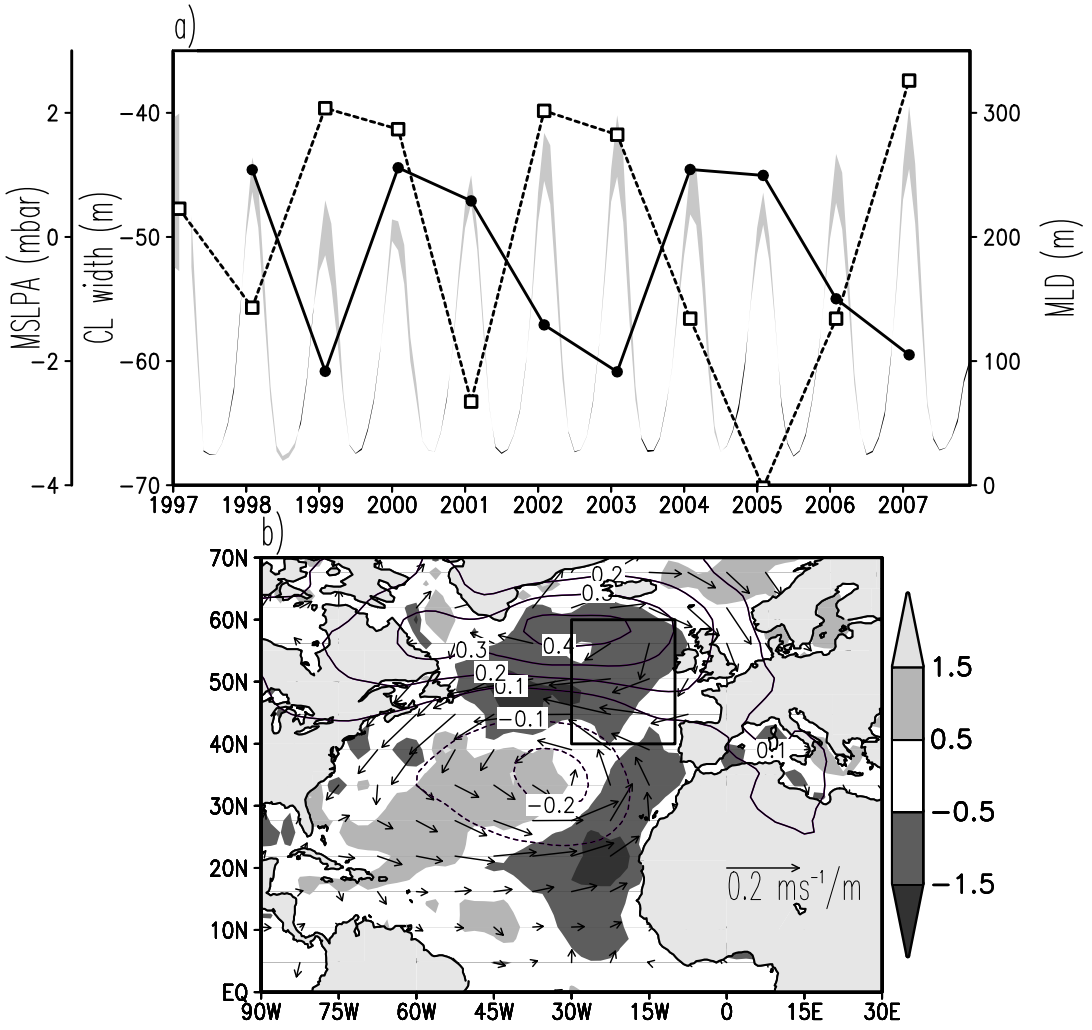

Figure 3.10. (a) JFM compensated layer width (solid) and monthly mixed layer depth (compensated layer depth range between MLT and MLD is shaded) averaged in the North Atlantic compensated layer box, JFM anomalous mean sea level pressure (dashed) averaged 40W-30W, 30N-40N. (b) Time regression of the 1997-2007 JFM compensated layer width on latent heat flux (Wm^{-2}/m, shaded), anomalous mean sea level pressure (mbar/m, contours), and winds (ms^{-1}/m, arrows).

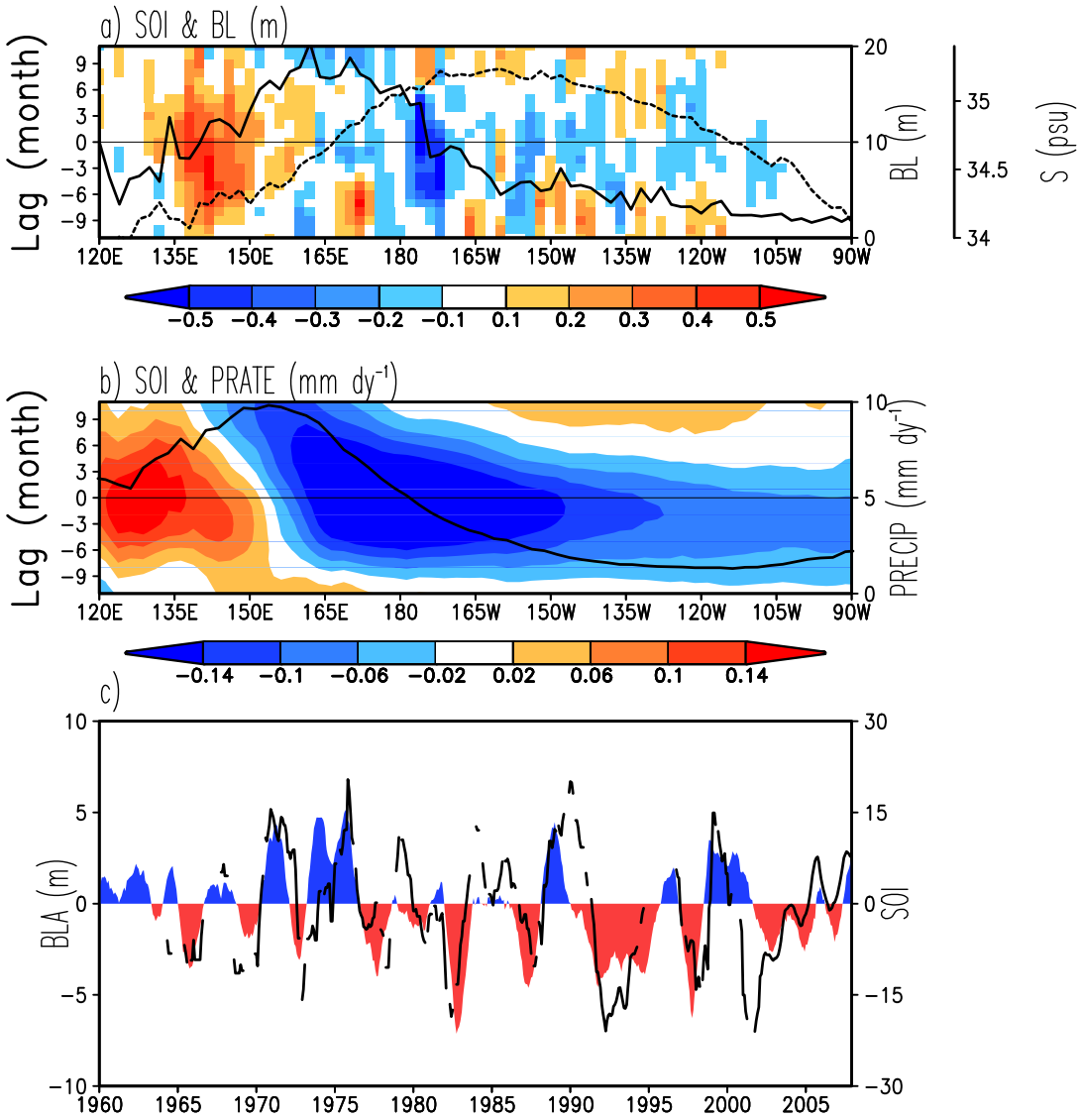

Figure 3.11. Lag regression of SOI index on 5S-5N averaged (a) anomalous barrier layer width, (b) precipitation. Time mean BL width (solid), salinity(dashed), and precipitation are shown against right hand vertical axes. Precipitation is *Xie and Arkin* (1997). (c) Time series of annual running mean SOI (shaded) and anomalous BL width averaged in the western equatorial Pacific box (120E-160E, 5S-5N). See Fig. 3.5c for the box location.

Chapter 4: Comparison of bulk Sea Surface and Mixed Layer Temperatures

4.1 Introduction

SST is a difficult parameter to define because the ocean has complex and variable vertical stratification complicated by the presence of laminar and turbulent boundary layers as well as varying meteorological fluxes[1]. The most prolific measurements of SST are satellite radiance measurements, which sample the sub-millimeter skin temperature several times a day. Operational centers then modify these measurements based on comparison to *in situ* observations to produce gridded estimates of temperature of the upper ~1-5 m, referred to as the bulk SST [*e.g., Reynolds and Smith*, 1994; *Reynolds et al*, 2002; *Rayner et al*., 2003]. But many applications, including studies of climate [*Manabe* and *Stouffer*, 1996; *Deser et al.*, 2003; *Seager et al.*, 2002], biogeochemical cycles [*Doney et al.*, 2004], and fisheries [*Block et al*., 1997] require estimates of the average mixed layer temperature. In general we may expect MLTT to be lower than SST by a few tenths of a degree. This difference reflects the time average effect of the nearsurface suppression of turbulence by daytime warming or by positive freshwater flux.

The upper 10 m of the ocean has complex and variable vertical temperature stratification. This variation in stratification occurs more frequently under conditions in which the ocean surface fluxes cause gains or losses of heat or freshwater or in

[1] See the GODAE Global High Resolution SST Pilot Project at http://www.ghrsst-pp.org/SST-Definitions.html

situations of strong horizontal exchange. Surface fluxes are responsible for a distinct diurnal cycle in the temperature in the uppermost few meters over wide areas of the ocean when winds are weak and solar heating is strong [*Stuart-Menteth et al.,* 2003; *Gentemann et al.,* 2003; *Clayson* and *Weitlich,* 2007; *Kawai* and *Wada*, 2007]. This diurnal cycle is particularly prominent in upwelling areas such as the eastern equatorial Pacific where vertical advection of cool water leads to shallow stratification and thus shallow mixed layers [*Deser* and *Smith*, 1998; *Cronin* and *Kessler*, 2002]. In the warm pool region of the western equatorial Pacific diurnal warming arises because the excess rainfall forms a nearsurface barrier layer of low salinity water even though the seasonal thermocline is rather deep [*Soloviev* and *Lukas,* 1997].

Impact of diurnal warming on SST is addressed by applying various corrections [see *e.g. Donlon et al*., 2007] assuming that the diurnal thermocline is destroyed by nocturnal convection. But, the diurnal cycle of temperature may be significantly altered over some oceanic regions affected by the surface freshening or upwelling where MLTT differs seasonally from bulk SST. In this study we compare historical analyses of bulk SST by *Rayner et al.* [2003] and *Smith* and *Reynold*s [2003] with contemporaneous temperature and salinity profile observations to identify the conditions giving rise to systematic differences between mixed layer temperature and bulk SST and to identify the regions where this difference is essential. These historical analyses of bulk SST are widely used in climate studies and for ocean model validations. Although using bulk SST instead of satellite SST eliminates part

of the diurnal warming signal that contributes to the deviation of MLTT from skin SST, it also eliminates contribution of satellite SST bias. In this sense we focus on the difference between MLTT that is simulated by majority of ocean models and the reference bulk SST that is used to validate ocean models.

The mixed layer is defined as the near-surface layer of uniform properties such as temperature and salinity. The presence of weak stratification and the nearness to atmospheric momentum sources give rise to values of the Richardson number consistent with flow instabilities and thus a high potential for turbulent motion. Under conditions where density is primarily determined by temperature *de Boyer Montégut et al.* [2004] (with a generalization introduced by *Kara et al*., 2000a) define the base of the seasonal mixed layer to be the depth at which temperature changes by 0.2C from its value at 10m reference depth. From this we can define a seasonal MLTT as the vertical average temperature of the mixed layer, which when multiplied by the depth of the mixed layer and the specific heat of seawater gives the heat capacity of the layer of ocean in direct contact with the atmosphere on seasonal timescales.

The near surface processes that affect the monthly difference, *dT*=MLTT-SST, are dominated by the integrated effect of diurnal warming. But, a variety of processes including rain, river discharge, or lateral interactions may produce fresh barrier layers that trap the heat near the surface by shoaling the penetration depth of wind stirring and nocturnal convection [*Lukas* and *Lindstrom*, 1991; *Soloviev* and *Lukas*, 1997]. Moreover, stable salinity profiles may permit nocturnal temperature inversions due to

radiative cooling [*Anderson et al.,* 1996; *Cronin* and *Kessler*, 2002] with magnitudes comparable to those of diurnal warming. Barrier layers are observed over wide ocean areas; in particular, they are produced by abundant rainfall and river discharge in the tropics, an excess precipitation over the North Pacific, and lateral exchanges across the western boundary currents [*de Boyer Montégut et al*., 2007]. In all these areas we also expect significant stratification of near surface layers that affect the difference between MLTT and SST.

4.2 Data and Methods

The mixed layer properties for this study are estimated from individual temperature profiles provided by World Ocean Database 2005, WOD05 [*Boyer et al.,* 2006], for 1960 through 2004. We use data from the mechanical bathythermographs (MBT), expendable bathythermographs (XBT), conductivity-temperature-depth casts (CTD), ocean station data (OSD), moored buoys (MRB), and drifting buoys (DRB). The final four years of the database contain an increasing number of profiles from the new Argo system (PFL). The Argo profiles through 2007 are obtained from the Argo Project web site. For better characterization of the tropical Pacific region, the data provided by the TAO/TRITON moorings [*McPhaden et al.,* 1998] are also used.

The mixed layer depth (MLD) may be defined in a number of different ways. In this study we use the concept of the isothermal mixed layer depth that is evaluated from individual vertical profiles based on the temperature difference from the temperature at a reference depth of 10 m [*de Boyer Montégut et al.,* 2004]. This reference depth

was shown to be sufficiently deep to avoid aliasing by the diurnal signal, but shallow enough to give a reasonable approximation of monthly mixed layer depth. It is worth noting that in some areas of shallow mixed layer, such as the Black Sea, or in areas of strong upwelling, the thermocline may shoal above the 10m reference level. In these particular areas our estimates of MLD may be biased deep and estimates of MLTT may be biased cold. In this study the isothermal MLD is defined as the depth at which temperature changes by $|\Delta T| = 0.2^{o}$C relative to its value at 10m depth. Following *Kara et al.* [2000a], the isothermal MLD is defined by the *absolute difference* of temperature, $|\Delta T|$, rather than only the *negative difference* of temperature. Temperature inversions ($\Delta T > 0$) are most common at high latitudes. They are accompanied by stable salinity stratification to achieve positive water column stability, and, thus, may be used as an indicator of the base of the mixed layer. The same definition of isothermal mixed layer depth has been used by *Carton et al.* [2008] who show that the absolute temperature difference criterion works reasonably well even at high latitudes in the North Atlantic where the thermal stratification is relatively weak.

An alternative definition of the mixed layer depth (based on the dynamical stability criterion) defines it as the depth of a density uniform layer. Vertically-averaged temperature of the uniform temperature layer is the same as vertically averaged temperature of the uniform density layer if the latter layer is not deeper than the former (barrier layer). If a uniform density layer is deeper than a uniform temperature layer (density compensation), their average temperatures may be different. Here we

follow *de Boyer Montégut et al.* [2004] and define the mixed layer as a layer vertically uniform in both temperature and salinity. Hence, the mean mixed layer temperature is the same as the mean temperature of an isothermal layer. The mean temperature of an isothermal layer is referred in this study as the mixed layer temperature.

The mixed layer temperature is evaluated as the temperature vertically averaged above the base of the mixed layer using trapezoidal numerical integration, assuming uniform temperature above the reference depth, $T(z<10m)=T(z=10m)$. Vertical sampling of temperature varies from approximately 10m for low resolution MBTs to approximately 1m for high resolution sensors, such as CTDs. The method of vertical integration chosen is not important because the MLTT is evaluated over the layer quasi-homogeneous in temperature. By assuming temperature constant above 10m a large portion of daytime heat gain is excluded that makes MLTT estimates appear more like nighttime vertically averaged temperature. We introduce this assumption in order to make use of XBT and Argo data that constitute a good portion of the ocean profiles inventory. In their current configuration these two instruments are not designed to sample the upper few meters below the surface. In particular, the Argo floats don't sample the upper 5m of the ocean while the upper 4m XBT temperature is biased by 'start-up' adjustment [*Kizu* and *Hanawa*, 2002]. After estimating MLTT at each profile location we then apply subjective quality control to remove 'bulls eyes' and bin the data into 2^{o}x2^{o}x1mo bins with no attempt to fill in empty bins.

Mixed layer temperature is compared with bulk SST provided by Met Office Hadley Centre sea ice and sea surface temperature (HadISST1) of *Rayner et al.* [2003] and by extended analysis (version 2) of *Smith* and *Reynold*s [2003]. Both products provide globally complete monthly averaged grids spanning the late 19th century onward. HadISST1 combines a suite of historical and modern in situ near surface water temperature observations from ships and buoys with the recent satellite SST retrievals, while the *Smith* and *Reynold*s [2003] data is mostly based on in-situ measurements. Neither of these products use the vertical temperature profiles from WOD05. In order to reduce the impact of diurnal effects the UK Met Office HadISST1 utilizes only the night satellite SSTs (available beginning in 1981) and adjusts them to match *in-situ* measurements collected by voluntary observing ships, drifters, and buoys [*Rayner et al.* 2003]. The NOAA National Climatic Data Center SST extended analysis uses both day and night satellite SSTs only to evaluate the spatial structure of analysis SST while relying on the same *in situ* observations to adjust their SST analysis to reflect water temperature at an effective depth of ~1-5 m [*Smith* and *Reynold*s 2003]. A more precise definition of this analysis depth is impractical for either product because of the variety of depths at which the *in situ* observations are available. SST adjusted to temperature at a few meters depth is referred to here and after as bulk SST or simply SST. Adjustment to measurements taken from a few meters depth (where the diurnal signal is relatively weak) effectively attenuates but doesn't eliminate impacts of transient near surface processes on bulk SST completely. Most recently the Global Ocean Data Assimilation Experiment High Resolution SST Project has introduced the concept of 'foundation SST', defined as the temperature at a depth of 10m, below the

depth of the diurnal cycle. But this 10m depth temperature, which generally lies within the mixed layer, has not been measured frequently enough to calibrate the analyses.

The local response of the mixed layer to the forcing from the atmosphere is simulated using the one-dimensional hybrid mixed layer model of *Chen et al*. [1994]. This model is based on the Kraus-Turner-type bulk mixed layer physics for the first shallowest layer. This first layer depth is determined by a turbulent energy balance equation and its temperature and salinity are determined by budget equations forced by surface fluxes and entrainment. The entrainment across the base of the first layer provides a communication between the mixed layer and the ocean beneath that is represented in sigma-layers. This model is capable of simulating the three major mechanisms of vertical turbulent mixing in the upper ocean wind stirring, shear instability and convective overturning. The model is forced by 6-hour surface fluxes provided by the NCEP/NCAR atmospheric reanalysis of *Kalnay et al*. [1996].

4.3 Results

We begin by examining the average *dT* based on the 1960-2004 WOD05 dataset (Fig. 4.1a). Because of the distribution of observations, only the Northern Hemisphere is well sampled. On average, MLTT is colder than bulk SST by about 0.1^{o}C, with large anomalies <-0.4°C north of the Kuroshio-Oyashio extension and along the Equator in the eastern Pacific, and large anomalies >0.4°C anomalies (temperature inversions) in the Gulf Stream region.The results are similar for the two

bulk SST analyses, but only results based on HadISST1 are shown in **Fig.4.1**. The equatorial Atlantic shows negative anomalies as well, but not as large as those in the equatorial Pacific. Spatial patterns of dT don't change much if a density-based mixed layer depth is used (compare **Figs. 4.1a** and **4.1b**), but data coverage is reduced due to a lack of salinity data.

To illustrate the relationship between MLTT and bulk SST in the Southern Hemisphere we examine averaged dT using Argo profile data set which, although is more homogenous spatially, is mainly restricted to 2004onward (**Fig. 4.1c**). The Argo results in the Northern Hemisphere show only a few differences from the distribution of dT based on the WOD05 data set. In the Labrador Sea positive values of dT are now more evident, indicating nearsurface temperature inversions. In contrast, the subtropical North Atlantic and North Pacific both show negative values in the regions of weak winds where diurnal warming of the nearsurface is a frequent occurrence. In the Southern Hemisphere large negative anomalies of dT based on Argo data are evident in the South Pacific west of Chile as well as southwest of Australia and South of Cape of Good Hope. We next focus on the Northern Hemisphere patterns because they are evaluated from longer time records than those from the southern counterparts. To explore the causes of the largest anomalies of dT we next examine in detail the time changes in the three regions in the Northern Hemisphere identified in **Fig. 4.1**.

These three regions are distinguished by persistently shallow nearsurface stratification due to either upwelling or impact of the barrier layers (nearsurface

freshening) that trap warming (cooling) in the near surface. On the other hand, the air-sea interactions are particularly strong over these regions. It is illustrated by climatological maps of the net surface heat gain by the ocean. During the northern winter (**Fig. 4.2a**) the turbulent heat loss in excess of 200 Wm^{-2} occurs over the warm western boundary currents in the Pacific and in the Atlantic due to strong air-sea temperature contrast which leads to enhanced evaporation and sensible heat loss over areas of warm SSTs. In northern summer (**Fig. 4.2b**) the ocean gains heat in excess of 100 Wm^{-2} in the northwestern Pacific and over the shelf waters north of the Gulf Stream. While the seasonal increase in the ocean heat gain in summer is explained by the seasonal cycle of insolation, the geographical location of the areas of strong ocean heat gain is linked to the spatial patterns of SST. Both areas of strong ocean heat gain in the north Pacific and Atlantic Oceans are located to the north of sharp SST fronts. Although solar radiation decreases gradually with latitude, the evaporation decreases abruptly across the SST front. As a result of these spatial changes the ocean gains more heat north of the subtropical SST front in the Pacific and north of the Gulf Stream north wall in the Atlantic (**Fig. 4.2b**). The ocean also gains heat at a rate exceeding 100 Wm^{-2} in the eastern equatorial Pacific cold tongue (**Fig. 4.2b**) due to abundant solar radiation and relatively weak local latent heat loss over cool SSTs in the cold tongue. In the cold tongue the heat gain is compensated by entrainment cooling. In the near surface it produces remarkable magnitudes of diurnal warming. We shall next analyze the origins of persistently shallow stratifications in these three regions.

4.3.1 **Eastern Equatorial Pacific**

The equatorial Pacific thermocline shoals eastward in response to annual mean easterly winds that, along with entrainment cooling, form a tongue of cool water in the east. Here, in the cold tongue, the ocean gains heat from the atmosphere in excess of 100 Wm^{-2} (**Fig.4.2b**) that is compensated by entrainment cooling. In response to this surface heat flux the near-surface ocean develops substantial diurnal warming of SST, in excess of 0.2°C [*Deser* and *Smith,* 1998]. Here, average dT is approximately -0.4^{o}C (Fig. 3a) with more negative values (MLTT<SST) in March when SST reaches its monthly maximum and diurnal warming is large (**Fig. 4.3b**) [*Cronin* and *Kessler*, 2002]. In contrast, on interannual timescales dT is weak (MLTT ≈ SST) when El Niño warms SST, the mixed layer deepens, solar radiation decreases and freshwater input increases, and dT has negative extreme during the La Niñas when the mixed layer shoals and atmospheric convection shifts westward [*Cronin* and *Kessler*, 2002; *Clayson* and *Weitlich,* 2005]. In Fig.3a this relationship is clearest after the early 1980s as the data coverage increases.

In order to understand the causes of the seasonal and interannual relationships we examine conditions at the Tropical Atmosphere Ocean/TRITON mooring at 0°N, 140°W for 1995-2001, encompassing the 1997-98 event (**Fig. 4.4a**). We focus on 0°N, 140°W location, where the records are continuous during the event. At this location 1m temperature, a proxy for SST, increases by 5°C during 1997 and then decreases

by nearly 7°C in mid-1998[2]. Coinciding with the drop in 1m temperature is a substantial development of negative dT meaning that the mixed layer has developed some near-surface temperature stratification. The negative values of dT are even more striking in 1999 and 2000 when SST increase during January-March as part of the climatological seasonal cycle at this location phases with interannual variation of dT.

To identify the mechanisms giving rise to differences in seasonal and ENSO changes in dT we examine a one-dimensional mixed layer model simulation beginning with homogeneous initial conditions (**Fig. 4.4b**). The model is forced by fluxes from the NCEP/NCAR reanalysis. These fluxes are known to have errors in shortwave radiation and other components. But comparison of the reanalysis fluxes with measurements taken at the 0N, 140W TAO/TRITON mooring indicates that reanalysis fluxes provide reasonable variability associated with ENSO (**Fig.4.4**). The model responds seasonally to weakened winds in boreal spring (**Fig. 4.4d**) with increased near-surface stratification (dT <0) as observed. The conditions arising during the onset of El Niño similar to those occurring during the first half of 1997 are somewhat different. During those months the winds also weakened, but solar heating decreased (**Fig. 4.4c**) and freshwater input increased (**Fig. 4.4d**) as a result of the eastward shift of convection. The decrease in the ocean heat gain due to decreased solar heating is accompanied by increased latent heat loss due to warmer SST (**Fig. 4.4c**). The result is weakening values of dT followed in the summer and fall by

[2] TAO/TRITON moorings measure SST at z=1m. Time mean difference of T_{1m} from HadISST1 at 0°N, 140°W is -0.3C while time correlation is 0.96.

occasional temperature inversions. In mid-1998 through early 1999, as El Niño transitioned into cooler La Niña conditions, the nearsurface again becomes strongly stratified due to enhanced solar heating and weaker latent heat loss and resulting diurnal warming of the nearsurface. Good comparison between one-dimensional mixed layer model simulation and observed dT suggests that the processes governing dT are one-dimensional and include local response of the mixed layer to changes in wind forcing and heat flux.

Intermittent temperature inversions (SST cooler than MLTT by 0.2-0.5°C) are evident in observations (**Fig. 4.4a**) and simulations (**Fig. 4.4b**). They are associated with nocturnal cooling of shallow freshwater lenses produced by enhanced rainfall (**Fig. 4.4d**). Stable salinity stratification (barrier layer) produced by local rainfall captures the nocturnal convection in the near surface layer until the cooling or wind stirring is strong enough. If the freshwater surface flux is set to zero, the one-dimensional model doesn't simulate temperature inversions [see also *Anderson et al.*, 1996].

As we have seen the stable salinity stratification produced by local rainfall may impact significantly the near surface temperature stratification. An alternative mechanism of barrier layers formation is associated with the lateral interactions. In particular, in the equatorial Pacific near the dateline, salty and warm water can be subducted under the western Pacific's warm fresh water to form barrier layers [*Lukas* and *Lindstrom*, 1991]. This advection mechanism, which is not in an one-dimensional

model's physics, may be effective near the frontal interfaces and contribute to temperature inversions during the seasons when the ocean loses heat.

4.3.2 **Gulf Stream**

In the western North Atlantic, MLTT differs from bulk SST along the Gulf Stream path (**Fig. 4.1**). This regional anomaly may result from differences in spatial interpolation of MLTT and bulk SST that may be an issue in regions of sharp SST fronts. To eliminate the potential impact of spatial interpolation, the MLTT-SST is also computed from individual CTD and Argo profiles (**Fig.4.5**). This reveals noticeable seasonal variation of MLTT-SST that is not expected if the difference in spatial interpolation dominates the signal. In summer, MLTT is colder than bulk SST in the cold sector of the Gulf Stream front due to abundant net surface heating and relatively weak evaporation over cool SSTs (**Fig. 4.5a**). Analysis of vertical profiles (**Fig.4.6a**) indicates that this heating produces a warm layer trapped in a 10-20m deep shallow fresh layer. This shallow barrier layer limits the depth of nocturnal convection and mechanical stirring above the base of halocline and thus separates the shallow near surface warm layer (that is still observed at 2 a.m. local time) from the seasonal mixed layer. This shallow warm layer affects water temperature in the depth range of 1-5m used to adjust the bulk SST analysis. This, in turn, explains the cold difference between MLTT and bulk SST observed north of the Gulf Stream north wall in summer. Negative dT in this region is statistically significant and shows up in the tail of the regional dT histogram (**Fig.4.1a**).

In contrast, an examination of the spatial structure of MLTT-SST during the winter months (**Fig. 4.5b**) shows large inversions frequently exceeding 1°C along the path of the Gulf Stream, while SST is close to MLTT in this area in summer. Winter MLTT-SST inversions are aligned along the northern wall of the Gulf Stream (**Fig.4.5b**), suggesting mechanisms involving cross-frontal interactions between contrasting water masses. Collision of warm and salty Gulf Stream water with colder and fresher shelf water produces shallow salinity stratified cold near-surface layers (**Fig.4.6b**). These layers are further cooled by oceanic net surface heat loss and eventually destroyed by passing storms. In spite of that, the ocean areas affected by the temperature inversions might be more frequently observed by satellite infrared sensors. In fact, passing winter storms that eventually destroy the inversions are usually associated in the Gulf Stream area with the cold air outbreaks and significant convection cloudiness that obscure infrared imageries of the sea surface. Winter MLTTs warmer than SSTs are observed over a spatially narrow area along the Gulf Stream north wall. As a result, their contribution is not seen in the shape of histogram evaluated over a wider area shown in **Fig.4.5b**.

Examination of the meridional variations of dT also shows the strongest temperature inversions over the warm Gulf Stream (**Fig.4.2c**). Variations of dT are similar if an alternative, gradient-based definition of the mixed layer depth is used (**Fig.4.2c**). Seasonal variations of MLTT-SST in the Gulf Stream region occur in accord with the seasonal variations of the net surface flux that displays very large heat loss over the warm Gulf Stream in winter [e.g. *Dong* and *Kelly*, 2004] and strong warming over the

cold shelf sector in summer. In distinction from the equatorial Pacific, where interannual *dT* significantly correlates with local SST, these values are weakly correlated in the Gulf Stream area (**Fig. 4.3c**).

The above discussions emphasize impacts of salinity on the near-surface temperature stratification. Next, the temperature response to the presence of the near-surface salinity gradients (occurring in the Gulf Stream area) is explored with a one-dimensional mixed layer model (**Fig.4.7**). To contrast the impact of salinity, the twin runs are compared. Each pair of model runs is forced by the same fluxes but differs in initial conditions. The first (control) run starts from the vertically homogeneous temperature and salinity while the initial salinity profile for the second run has salinity decreasing toward the surface in the upper 20 m at a rate of 0.1 psu m^{-1} (in accord with observations in **Fig.4.6**).

Fig. **4.7b** illustrates simulations during the warm season. It displays the difference in temperature between the two runs that shows an impact of the near surface freshening. In the presence of a stabilizing salinity gradient the diurnal warming is stronger during the first day of simulations (**Fig.4.7b**), but is surprisingly similar during the second day when it is limited by the shear instability of diurnal currents. Relative warming in the upper 20 m is even stronger as wind strengthens. This is explained by slower deepening of the mixed layer and weaker entrainment cooling in the salinity-stratified case. Although the one-dimensional mixed layer model simulates warmer near-surface temperature in the salinity-stratified case, the simulated temperature

stratification in the upper 10 m column doesn't exceed a few tenths of a degree in contrast with observations (**Fig. 4.6a**). This is explained in part by relatively short (only a few days long) run as well as by limitations of the model. If a strong ($\tau \sim 1$ day) relaxation of salinity to its initial conditions is introduced (to account indirectly for three-dimensional mechanisms producing a shallow halocline) the temperature gradient in the upper 10m amplifies up to 1^{o}C but never reaches values shown in **Fig. 4.6a**.

In winter the mixed layer model simulates a 1^{o}C colder mixed layer in salinity stratified case than in the control run (**Fig. 4.7d**). The difference is due to the stably stratified halocline that limits the penetration depth of wind stirring. In turn, the shallower mixed layer cools down faster due to net surface heat loss. Although the anomalous cooling of 1^{o}C compares well with observations (**Fig.4.6b**), the simulated mixed layer is relatively deep. Therefore, the stratification is weak in the upper 10 m in contrast to observations. This suggests again that lateral interactions (missing from the one-dimensional model) are important for establishing winter temperature inversions in the region, while the net surface heat loss further amplifies existing anomalies.

4.3.3 **Northwestern Pacific**

Salinity in the Northwestern Pacific decreases towards the surface. This stable halocline is produced by an annual-mean excess of precipitation over evaporation north of 30°N and is maintained by upward vertical pumping driven by a cyclonic wind curl [*Kara et al.*, 2000b]. Although the regional precipitation peaks in winter,

the near-surface freshening persists year -round. In summer, when the ocean heating is particularly strong (**Fig. 4.2b**), the shallow stably stratified halocline localizes the ocean heat uptake in the near-surface layer (**Fig.4.1**) by limiting the penetration depth of wind stirring and nocturnal convection. In distinction from the Gulf Stream region, where shallow warm layers develop mostly in the cold sector of the front, the shallow warm layers are observed randomly in the Northwestern Pacific (**Fig.4.5c**). They are not destroyed by nocturnal convection (see sample profile taken at 10 p.m. local time, Fig. 8). Meridional variations of dT follow the meridional variations of net surface heating and are similar if different a gradient-based definition of the mixed layer depth is used (**Fig. 4.2d**). Occasional SST inversions seeing in **Fig.4.5c** are associated with nocturnal cooling of freshwater lenses (profiles are not shown).

Shallow warm layers observed in the Northwestern Pacific and in the Gulf Stream region in summer are not observed in winter when the ocean loses heat to the atmosphere (**Figs.4.5b** and **4.5d**). During that season mixed layer temperatures warmer than SSTs are observed along the Gulf Stream north wall (**Fig.4.5b**) where the combination of strong heat loss and strong spatial gradient of salinity results in cooling of the near-surface salinity stratified layers. Despite similarly strong heat loss over the warm western boundary currents in the Atlantic and Pacific Oceans (**Fig. 4.2a**), the winter SST inversions are less frequently observed in the Kuroshio region in distinction from the Gulf Stream region (**Fig.4.1**). This difference may be linked to the differences in spatial patterns of salinity. In fact, the spatial gradients of salinity, vital in producing the temperature anomalies, are significantly weaker in the

Northwestern Pacific compared to the Northwestern Atlantic (see **Fig.4.9** based on data from *Antonov et al*., 2006). There also appears to be some evidence in Fig.1 that the $dT > 0$ seen in the Gulf Stream region also occurs in the Kuroshio region southeast of Japan where the salinity gradient is stronger (**Fig.4.9**). This area of temperature inversions ($dT > 0$) is weaker and narrow in scope than in the Atlantic. In addition to the basin difference in salinity other factors such as boundary current behavior could also contribute to the dT structures in these regions.

4.4 Summary

This study compares the magnitudes of two ocean temperature variables frequently used in climate studies, mixed layer temperature and bulk SST as represented by the widely used analyses of *Rayner et al.* [2003] and *Smith* and *Reynold*s [2003]. Mixed layer temperature is defined as the vertically averaged temperature above the mixed layer base, and the depth of the base here is defined following *Kara et al.* [2000a] and *de Boyer Montégut et al.* [2004] as a function of the temperature difference relative to 10m temperature. Our analysis shows that areas with shallow temperature stratification, such as upwelling zones, frequently have significant differences between mixed layer temperature and SST. Shallow temperature stratification also occurs in regions of near surface freshening (barrier layers) which limits the depth of convection and wind stirring. In both cases, shallow stratification occurs in zones of strong air-sea heat exchange. In the Northern Hemisphere the local peaks of heat gain by the ocean are observed in local summer over the areas of equatorial cold tongues

and over the areas of cold SSTs to the north of the Kuroshio Extension front and the Gulf Stream north wall. But, in winter, the ocean loses much heat over the warm SSTs of the western boundary currents.

We examine the temporal relationship between bulk SST and MLTT in the Equatorial Eastern Pacific where abundant net surface warming is compensated for by cooling across the base of the mixed layer. Here MLTT is persistently cooler than SST by approximately -0.4^{o}C. On seasonal time scales, it has a negative extreme during the boreal spring warm season when winds are weak. In contrast, on interannual timescales, the magnitude of dT = MLTT-SST increases during La Ninas and weakens during El Niños as a result of increases/decreases in solar radiation and decreases/increases in precipitation. Increased precipitation during El Niños produces freshwater stratified barrier layers leading to nocturnal cooling.

In the subtropics negative values of dT are found in the Gulf Stream area of the western North Atlantic. In summer the shallow warming in excess of 1 ^{o}C develops above the cool shelf waters to the west and north of the Gulf Stream where the ocean gains heat at a rate exceeding 100 Wm^{-2}. The presence of nearsurface freshening prevents the nighttime destruction of this shallow warm layer. In contrast, during winter the near surface layer within the Gulf Stream itself has an inverted temperature structure (time averaged dT=0.6°C) as the result of strong surface cooling in the presence of a near-surface barrier layer.

Another region where the salinity stratified barrier layers are present is the Kuroshio Extension region of the Northwest Pacific. Here the barrier layer is produced due to excess of precipitation accompanied by upward Ekman pumping preventing the vertical exchange of this freshwater. As in the case of the Gulf Stream region, the ocean gains heat in the summer at a rate exceeding 100 Wm^{-2} producing a warm surface layer during the day which has time averaged dT of -0.5 ^{o}C. In winter, MLTT and SST match in this region.

One of the persistent issues in coupled atmosphere-ocean general circulation models is a tendency to develop cold biases in the eastern equatorial Pacific [Davey et al. 2002]. However the surface temperature of such models is actually more analogous to mixed layer temperature since the uppermost ocean grid point is well below the ocean surface, and diurnal processes are generally neglected. Thus, any systematic differences in SST and MLTT are likely to be reflected in the evaluation of model SST bias. Indeed, Danabasoglu et al. [2006] have shown that adding the diurnal cycle to the daily mean incoming solar radiation does warm the model eastern equatorial Pacific SST and shoals the ocean boundary with SST observations similarly to observations. Even greater improvements to model SST estimates seem possible if the nearsurface stratification of temperature and salinity can be more accurately represented.

4.5 Figures

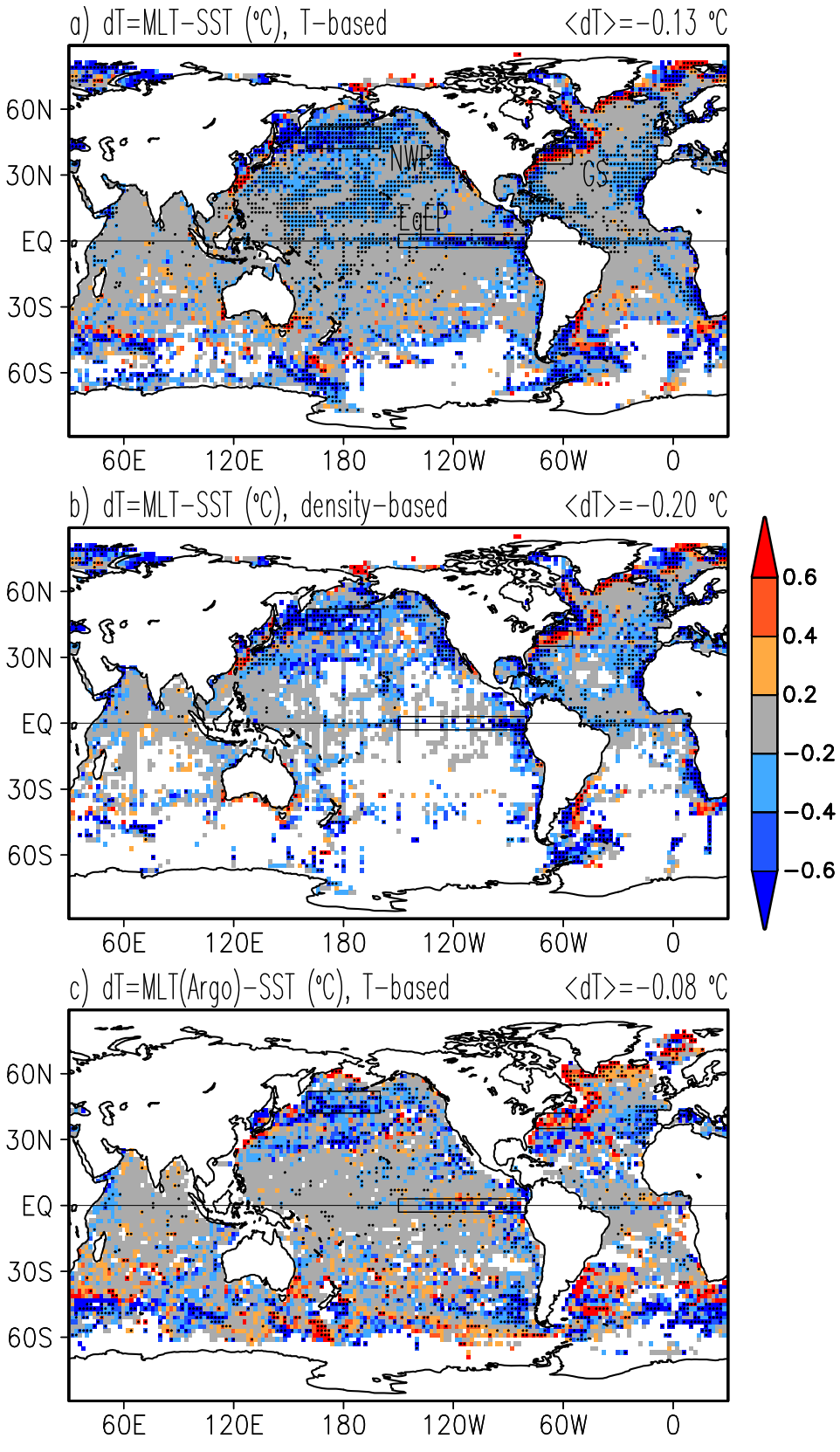
a) dT=MLT-SST (°C), T-based
<dT>=-0.13 °C
60N
30N
EQ
30S
60S
NWP
GS
EqEP
60E
120E
180
120W
60W
0
b) dT=MLT-SST (°C), density-based
<dT>=-0.20 °C
0.6
0.4
0.2
−0.2
−0.4
−0.6
c) dT=MLT(Argo)-SST (°C), T-based
<dT>=-0.08 °C

Figure 4.1. Time mean difference, dT =MLTT-SST, of mixed layer averaged temperature, MLTT, and bulk SST from HadISST1. Panels (a) and (b) show MLTT from WOD05 based on temperature-based and density-based mixed layer depth, respectively. Grid points with less than one year of data aren't shown. (c) Argo float MLTT difference from bulk SST at grid points with at least 6 months of data. Grid points where magnitude of dT exceeds standard deviation of dT are dotted. $< dT >$ is the global and time mean difference.

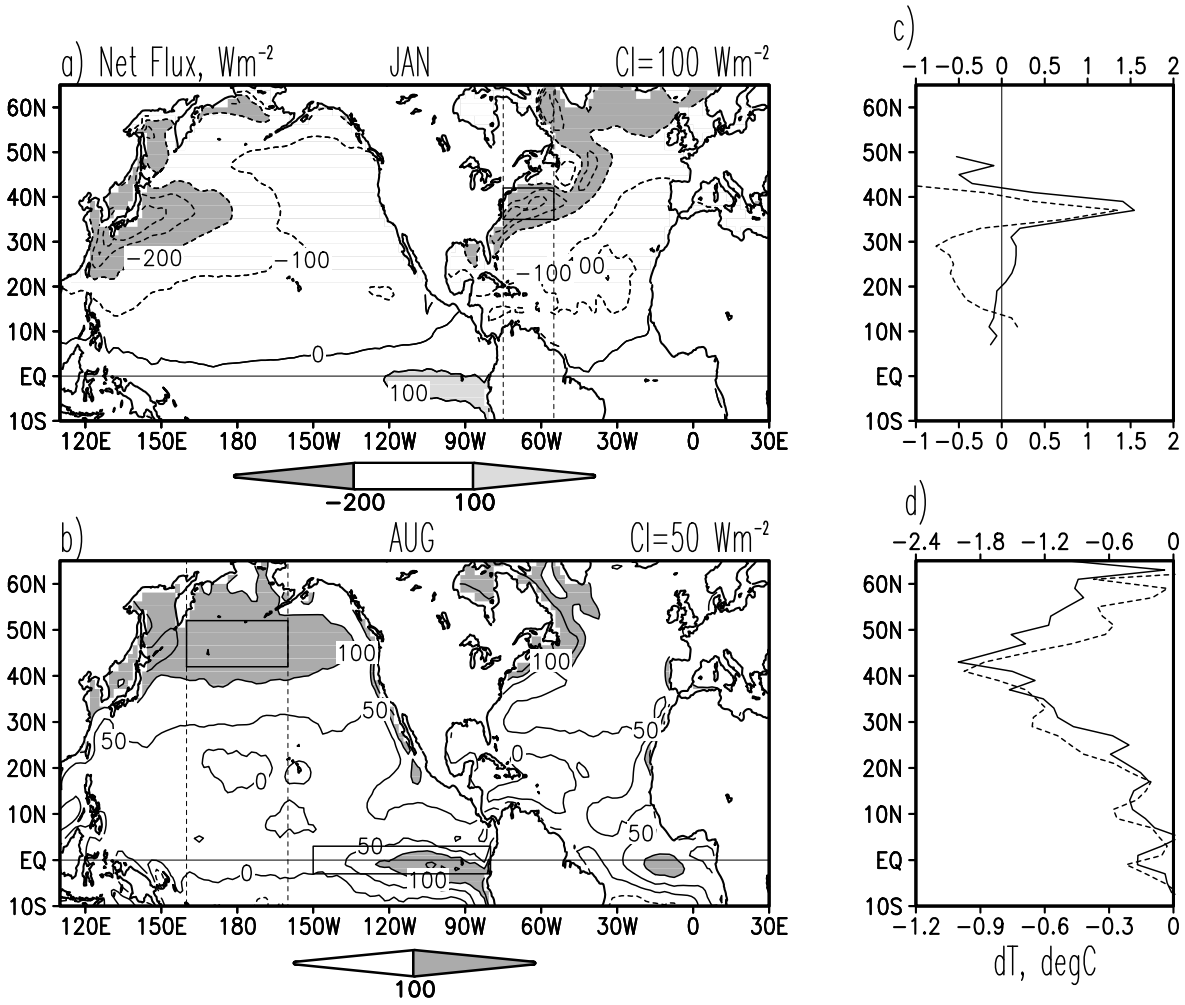

Figure 4.2. (Left) Climatological net surface heat flux for (a) January, (b) August (positive is heat gain by the ocean). Boxes show the same areas as in Fig.4.1. (Right, c/d) *dT* =MLTT-SST zonally averaged over longitude belts shown in the left panels. Solid lines show result of this study (against bottom x-axis) while dashed lines show results based on depth estimates of *Lorbacher et al.* [2006] (against top x-axis) that is based on the gradient-based definition of the mixed layer depth.

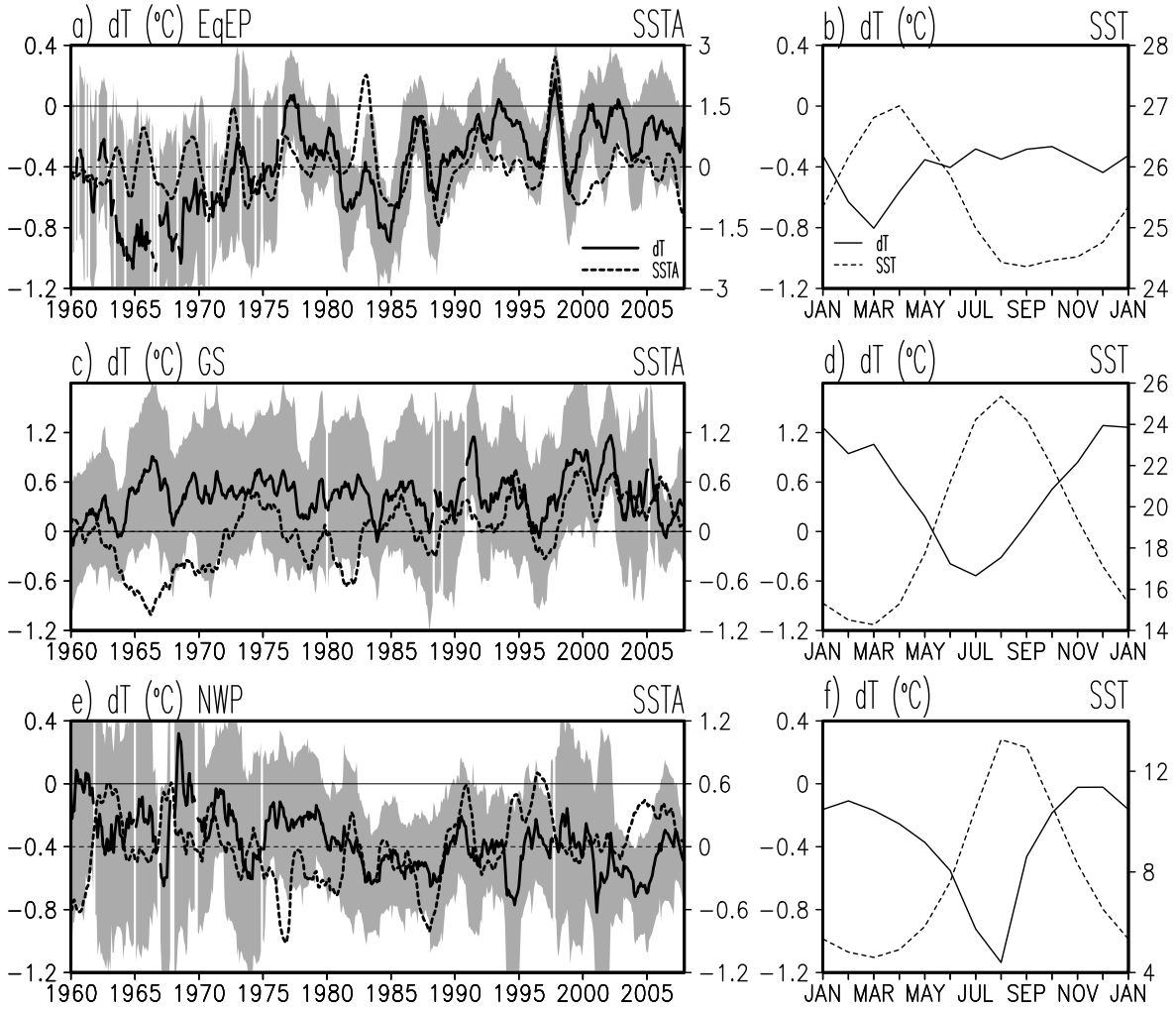

Figure 4.3. (a), (c) ,(e) Time series of annual running mean box-averaged *dT* , standard deviation of *dT* (shading), and anomalous SST for the equatorial east Pacific, Gulf Stream, and northwestern Pacific. (b), (d), (f) Seasonal cycle of box-averaged *dT* and SST based on HadISST1 data. Time series combine *dT* evaluated from WOD05 data through 2004 and Argo data afterwards.

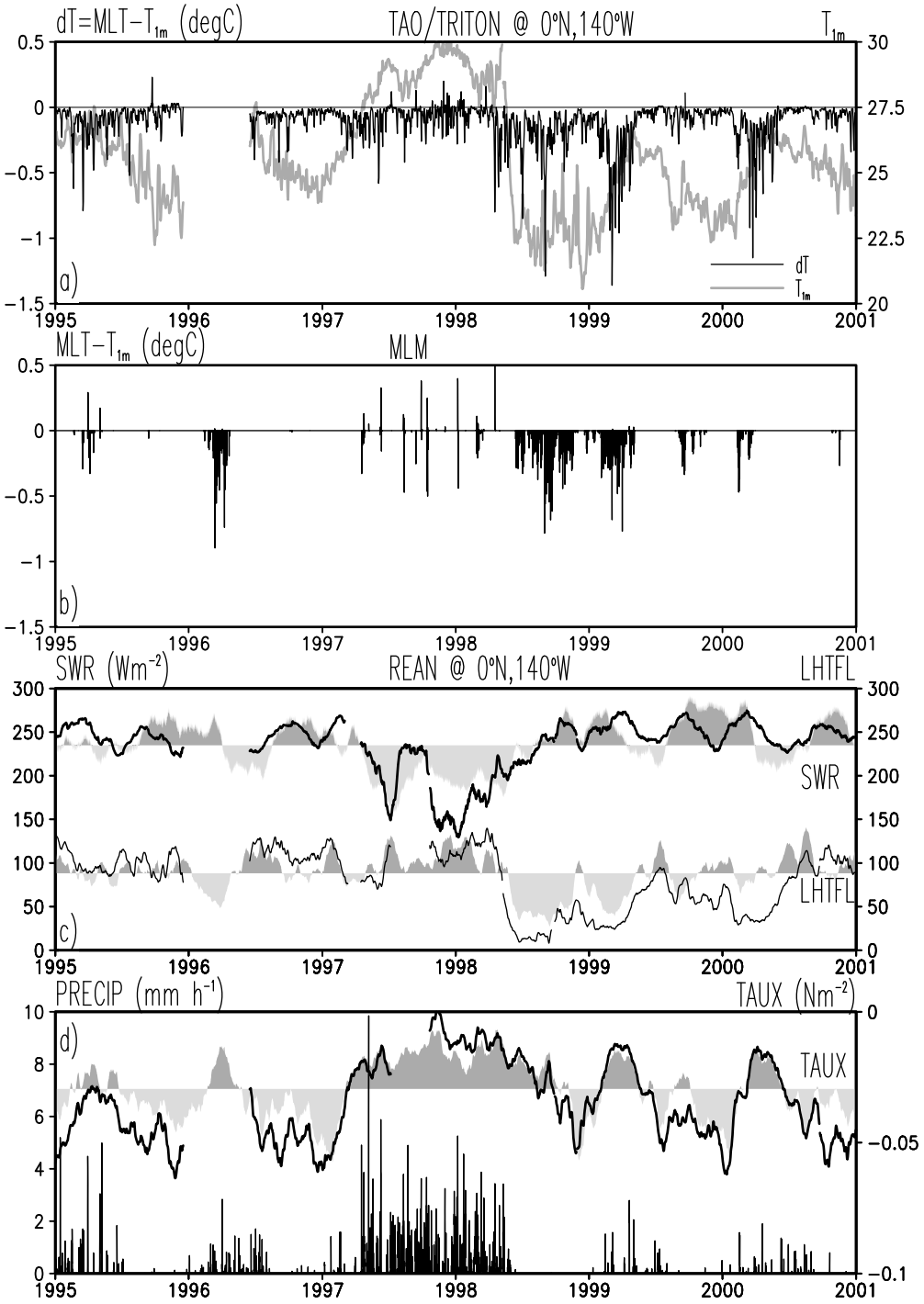

Figure 4.4. (a) Time series of 1m temperature, T_{1m}. Mixed layer temperature gradient, MLTT-T_{1m}, from (a) TAO/TRITON mooring at 0°N, 140°W and (b) mixed layer model (MLM). (c) Monthly running mean shortwave radiation (SWR) and latent heat flux (LHTFL), (d) 6-hour precipitation (PRECIP) and monthly zonal wind stress (TAUX) from the atmospheric reanalysis (shaded) and the mooring (solid).

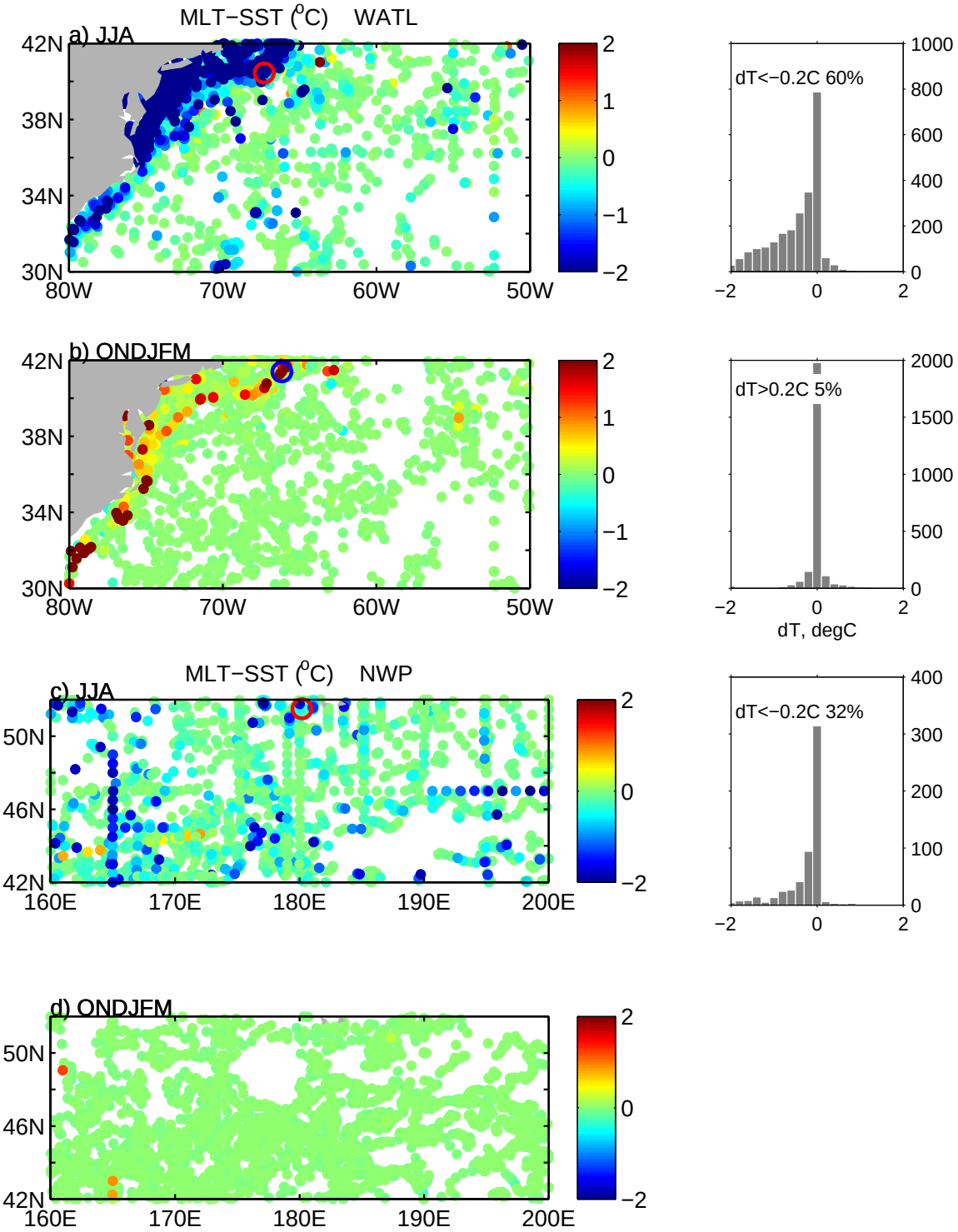

Figure 4.5. *dT* during June-August (JJA) and October-March (ONDJFM) evaluated from individual CTD and Argo profiles in (a,b) Gulf Stream area, (c,d) northwestern Pacific. Circles mark locations of vertical profiles shown in Figs. 4.6 and 4.8. Right panels show histograms of *dT* based on CTD data. Percentage of grid points with *dT* exceeding given threshold is also indicated in histograms.

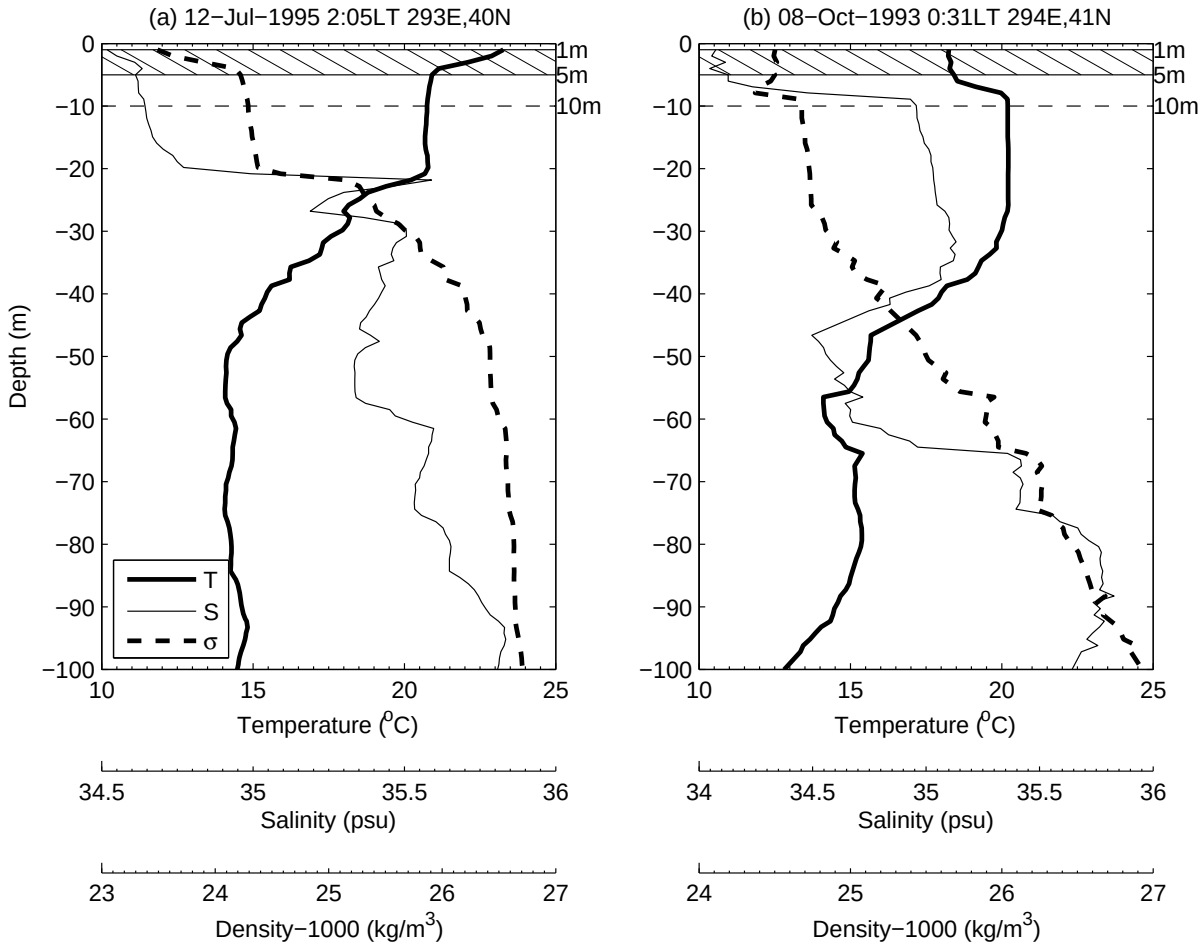

Figure 4.6. Sample temperature, salinity, and density profiles of with (a) negative and (b) positive MLTT-SST. Profiles are taken in the northwestern Atlantic in (a) summer and (b) fall at locations shown in Figs. 4.5a and 4.5b, respectively. 'LT' indicates the local sun time. Depth range between 1m and 5m is cross-hatched.

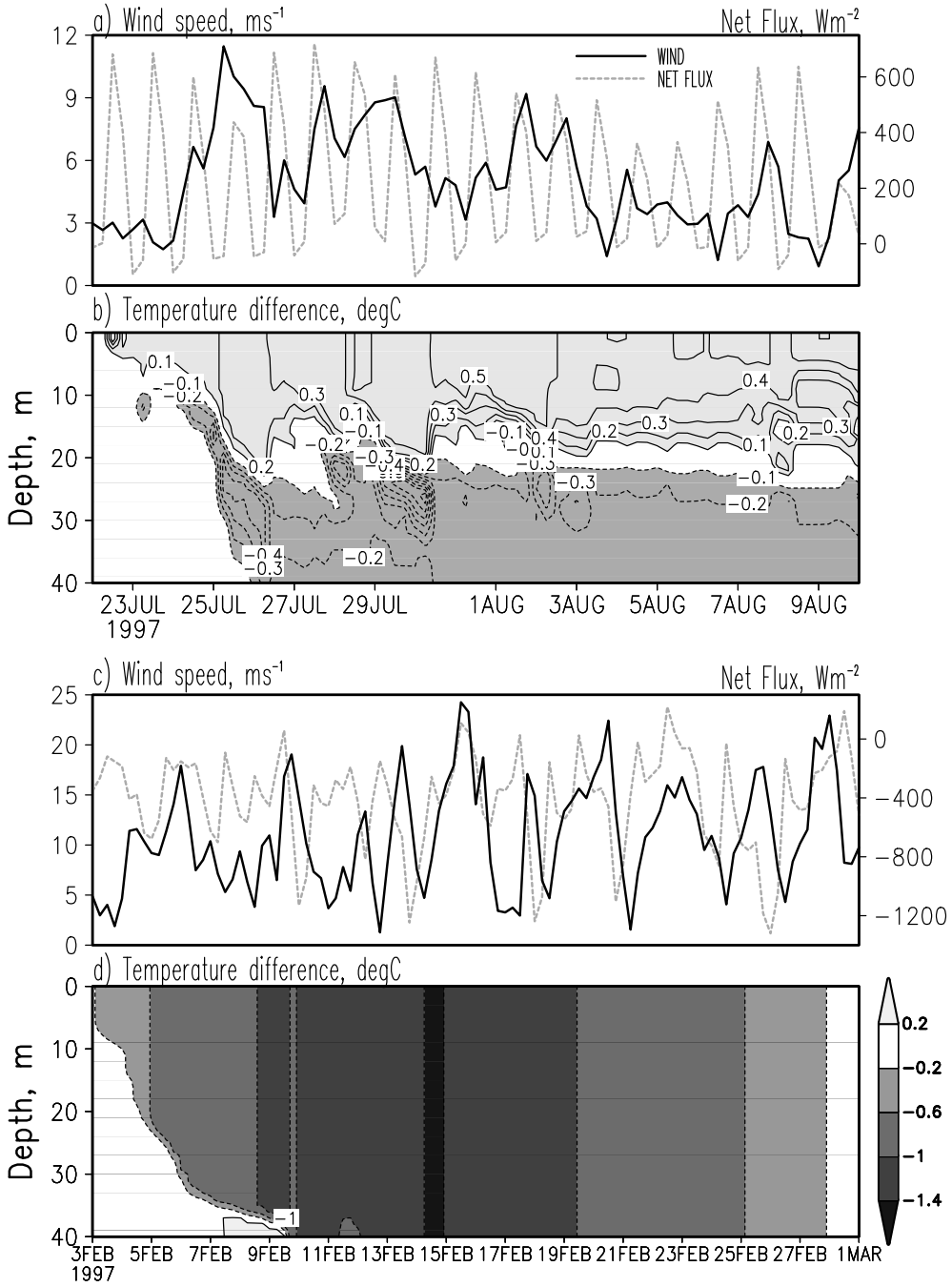

Figure 4.7. Mixed layer model response to sample winds and net surface flux in the Gulf Stream area in (a,b) summer and (c,d) winter as a function of salinity stratification. Panels (b) and (d) show temperature difference between experiment 2 and experiment 1. These two experiments have the same surface forcing, the same vertically uniform temperature initial conditions, but different salinity initial conditions. In the first experiment initial salinity is vertically uniform while in the second initial salinity has a uniform vertical gradient, $\partial S / \partial z$ =0.1 psu m^{-1}.

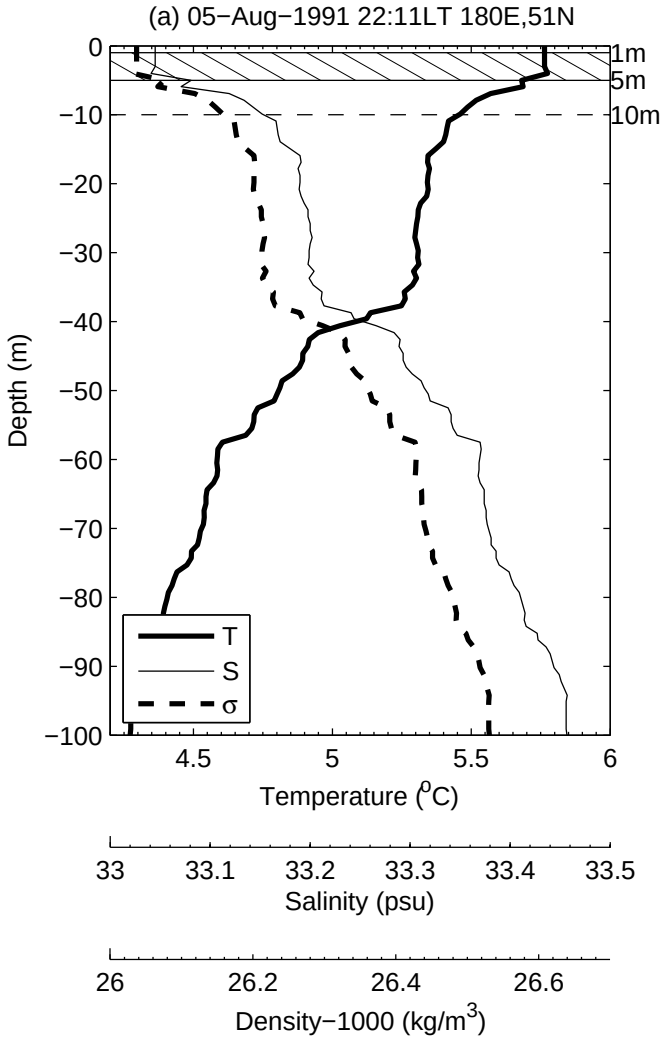

Figure 4.8 Sample temperature, salinity, and density profiles taken in the northwestern Pacific in summer at location shown in Fig. 4.5c. 'LT' indicates the local sun time.

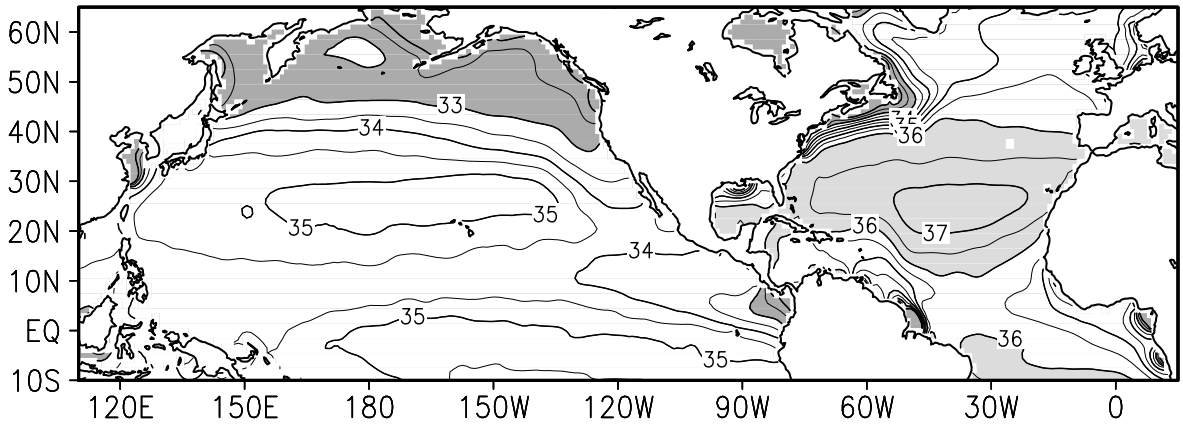

Figure 4.9. Time mean surface salinity (psu) from the WOD05. Salinities above 36 psu and below 33 psu are shaded.

Chapter 5: Remarks

In this thesis, global mixed layer properties are discussed in three topics: the variability of mixed layer depth, the variability of barrier layer/ compensated layer and comparison of sea surface temperature and mixed layer temperature. Several points including future work should be addressed about this research.

5.1 Mixed layer depth calculation

This work is based on the recent improvements of the ocean observing system represented in an increased volume of data provided by the recent World Ocean Database 2005 and Argo floats. Although the number of available temperature and salinity observations has risen tremendously during the last decade, the temporal and spatial gaps in salinity data limit observation-based studies of interannual and longer scale variability of the mixed layer. Given the fast increasing number of ARGO profiles (that provide both temperature and salinity) I expect significant improvements of our understanding of interannual variability of the mixed layer in the near future.

5.2 Numerical model simulation and data assimilation

5.2.1 **Model Simulation**

There have been significant improvements of the numerical mixed layer modeling in the recent decades from early research by *Munk and Anderson* [1948] through recent

parameterization by *Large et al*.[1994]. Although numerous approaches including differential models [e.g. *Mellor and Yamada,* 1982] and vertically integrated models (e.g. Kraus and Turner [1967], Price et al. [1986], and Chen et al., [1994]) have been explored, these one-dimensional models drift (mixed layer cools down) in multi-year runs. This drifting problem appears in both 1-D mixed layer models [Mellor 2001; Tandon and Zhao, 2004] and 2-D mixed layer models [*Michel et al.*, 2007]. Future research are challenged by the need to assess impacts of the mixed layer models drift on the global ocean simulations, and to suggest approaches to overcome the drifting problem.

5.2.2 **Data assimilation**

Mixed layer depth introduces a natural vertical scale in the upper ocean. This vertical scale should be accounted for in the ocean data assimilation to improve the upper ocean simulations.

5.3 Biophysical coupling

Some biophysical coupling models [Oschlies and Garcon, 1999; McCreary et al., 2001] examined mixed layer sensitivity on biological modeling. The coupling on the inter-annual and climatological time scale research is still limited. As far as I know, most biophysical models are also only one way between physical models and biological models. With more and more satellite data, observational nutrients, phytoplankton, zooplankton and debris data, it is challenging to improve and

diagnose biophysical modeling, revealing oceanic mixed layer role in biological system and providing our knowledge of climate change and ecosystem behavior.

Appendices

Bibliography

Anderson, S.P., R.A. Weller, and R.B. Lukas, 1996, Surface Buoyancy Forcing and the Mixed Layer of the Western Pacific Warm Pool: Observations and 1D Model Results. *J. Climate*, *9*, 3056–3085.

Alexander, M.A., C. Deser, and M.S. Timlin, 1999: The reemergence of SST anomalies in the North Pacific Ocean, *J. Clim.*, **12**, 2419-2433.

Alexander, M.A., J.D. Scott, and C. Deser, 2000: Processes that influence sea surface temperature and ocean mixed layer depth variability in a coupled model, *J. Geophys. Res*, **105**, 16823-16842.

Ando, *K. and M.J.* McPhaden *(*1997*)* Variability of surface layer hydrography in the tropical Pacific Ocean, *J. Geoph. Res.*, **102**, 23063-23078.

Antonov, J. I., R. A. Locarnini, T. P. Boyer, A. V. Mishonov, and H. E. Garcia (2006), World Ocean Atlas 2005, Volume 2: Salinity. S. Levitus, Ed. NOAA Atlas NESDIS 62, U.S. Government Printing Office, Washington, D.C., 182 pp.

Babu, K.N., R. Sharma, N. Agarwal, V.K. Agarwal, and R. A. Weller, 2004: Study of the mixed layer depth variations within the north Indian Ocean using a 1-D model, *J. Geophys. Res*, **109**, C08016, doi:10.1029/2003JC002024.

Barnston A.G., and R.E. Livezey, 1987: Classification, Seasonality and Persistence of Low-Frequency Atmospheric Circulation Patterns, *Mont. Wea. Rev*., **115**, 1083-1126.

Bates, N.R., Interannual variability of oceanic CO2 and biogeochemical properties in the Western North Atlantic subtropical gyre, 2001: *Deep-Sea Res.* II, **48**, 1507-1528.

Belkin, I.M., 2004: Propagation of the ‘‘Great Salinity Anomaly’’ of the 1990s around the northern North Atlantic, *Geophys. Res. Lett.*, **31**, L08306, doi:10.1029/2003GL019334.

Block, B. A., J. E. Keen, B. Castillo, H. Dewar, E. V. Freund, D. J. Marcinek, R. W. Brill and C. Farwell, 1997, Environmental preferences of yellowfin tuna (*Thunnus albacares*) at the northern extent of its range, *Marine Biology, 130*, 119-132, doi: 10.1007/s002270050231.

Bond, N.A. J.E. Overland, M. Spillane, and P. Stabeno, 2003: Recent shifts in the state of the North Pacific, *Geophys. Res. Lett*., **30**, doi:10.1029/2003GL018597.

Boyer, T.P., J.I. Antonov, H.E. Garcia, D.R. Johnson, R.A. Locarnini, A.V. Mishonov, M.T. Pitcher, O.K. Baranova, and I.V. Smolyar, 2006, *World Ocean Database 2005*. S. Levitus, Ed., NOAA Atlas NESDIS 60, U.S. Government Printing Office, Washington, D.C., 190 pp., DVDs.

de Boyer Montégut, C., G. Madec, A. S. Fischer, A. Lazar, and D. Iudicone, 2004, MLD over the global ocean: An examination of profile data and a profile-based climatology, *J. Geophys. Res., 109*, C12003, doi:10.1029/2004JC002378.

de Boyer Montégut, C., J. Mignot, A. Lazar, and S. Cravatte, 2007, Control of salinity on the mixed layer depth in the world ocean: 1. General description, *J. Geophys. Res., 112*, C06011, doi:10.1029/2006JC003953.

Carton, J.A., S. A. Grodsky, and H. Liu (2008), Variability of the Oceanic Mixed Layer 1960-2004, *J. Climate*, *21*, 1029–1047.

Chavez, F.P., J. Ryan, S.E. Lluch-Cota, and M. Niquen C, 2003: From anchovies to sardines and back: Multidecadal change in the Pacific Ocean, *Science*, **299**, 217-221.

Chen, D., L.M. Rothstein, and A.J. Busalacchi, 1994: A hybrid vertical mixing scheme and its application to tropical ocean model, *J. Phys. Oceanogr., 24*, 2156-2179.

Clayson, C.A., and D. Weitlich (2007), Variability of Tropical Diurnal Sea Surface Temperature. *J. Climate*, *20*, 334–352.

Cronin, M.F., and W.S. Kessler, 2002: Seasonal and interannual modulation of mixed layer variability at 0N, 110W, *Deep-Sea Research I*, **49**, 1–17.

Cummins, P. F., G. S. E. Lagerloef, and G. Mitchum, 2005: A regional index of northeast Pacific variability based on satellite altimeter data, *Geophys. Res. Lett.*, **32**, L17607, doi:10.1029/2005GL023642.

Curry, R., R. Dickson, and I. Yashayaev, 2003: Ocean evidence of a change in the fresh water balance of the Atlantic over the past four decades, *Nature*, **426**, 826-829.

Danabasoglu, G., W.G. Large, J.J. Tribbia, P.R. Gent, B.P. Briegleb, and J.C. McWilliams, 2006, Diurnal Coupling in the Tropical Oceans of CCSM3. *J. Climate*, *19*, 2347–2365.

Davey, M. K., and coauthors, 2002, STOIC: A study of coupled model climatology and variability in tropical ocean regions. *Clim. Dyn.*, *18*, 403-420.

Delworth, T.L., and Coauthors, 2006: GFDL's CM2 Global Coupled Climate Models. Part I: Formulation and Simulation Characteristics. *J. Climate*, **19**, 643–674.

Deser, C. and C. A. Smith, 1998, Diurnal and semidiurnal variations of the surface wind field over the tropical Pacific Ocean, *J. Climate, 11*, 1730–1748.

Deser, C., M.A. Alexander, and M.S. Timlin, 2003, Understanding the Persistence of Sea Surface Temperature Anomalies in Midlatitudes. *J. Climate*, *16*, 57–72.

Dickson, R.R., T.J. Osborn, J.W. Hurrell, J. Meincke, J. Blindheim, B. Adlandsvik, T. Vinje, G. Alekseev, and W. Maslowski, 2000: The Arctic Ocean response to the North Atlantic Oscillation, *J. Clim.,* **13**, 2671-2696.

Doney, S. C., and coauthors, 2004, Evaluating global ocean carbon models: The importance of realistic physics, *Global Biogeochem. Cycles*, 18, GB3017, doi:10.1029/2003GB002150.

Dong, S., and K.A. Kelly, 2004, Heat Budget in the Gulf Stream Region: The Importance of Heat Storage and Advection. *J. Phys. Oceanogr., 34*, 1214–1231.

Donlon, C., and coauthors, 2007, The Global Ocean Data Assimilation Project (GODAE) High Resolution Sea Surface Temperature Pilot Project (GHRSST-PP), *Bull. Am. Met. Society*, *88*, 1197-1213.

Ffield, A., 2007: Amazon and Orinoco River Plumes and NBC Rings: Bystanders or Participants in Hurricane Events? *J. Climate*, **20**, 316–333.

Flatau, M.K., L. Talley, and P.P. Niiler, 2003: The North Atlantic Oscillation, surface current velocities, and SST changes in the subpolar North Atlantic, *J. Clim.,* **16**, 2355-2369.

Foltz, G., S.A. Grodsky, J.A. Carton, and M. J. McPhaden, 2004: Seasonal salt budget of the northwestern tropical Atlantic Ocean along 38W, *J. Geophys. Res.*, **109**, C03052, doi:10.1029/2003JC002111.

Freeland, H., K. Denman, C. S. Wong, F. Whitney and R. Jacques, 1997: Evidence of change in the winter mixed layer in the Northeast Pacific Ocean, *Deep Sea Research Part I*, **44**, 2117-2129.

Gentemann, C. L., C. J. Donlon, A. Stuart-Menteth, and F. Wentz (2003), Diurnal signals in satellite sea surface temperature measurements, *Geophys. Res. Lett.*, *30*(3), 1140, doi:10.1029/2002GL016291.

Grodsky, S.A., J.A. Carton, and R. Murtugudde, 2001: Anomalous surface currents in the tropical Indian Ocean, *Geoph. Res. Lett.*, **28**, 4207-4210.

Grodsky, S. A., and J. A. Carton, 2003: Intertropical convergence zone in the South Atlantic and the equatorial cold tongue, *J. Climate*, **16**(4), 723-733,

Hurrell, J.W., 1995, Decadal trends in the North-Atlantic oscillation - regional temperatures and precipitation, *Science, 269*, 676-679.

Kalnay, E., and Coauthors, 1996: The NCEP/NCAR 40-year reanalysis project, *Bull. Amer. Meteorol. Soc.*, **77**, 437-471.

Kara, A. B., P. A. Rochford, and H. E. Hulburt , 2000a, Mixed layer depth variability and barrier layer formation over the North Pacific Ocean, *J. Geophys. Res., 105*, 16,803–16,821.

Kara, A. B., P. A. Rochford, and H. E. Hulburt, 2000b, Mixed layer depth variability and barrier layer formation over the North Pacific Ocean, *J. Geophys. Res., 105*, 16,783-16,801.

Kara, A. B., P. A. Rochford, and H. E. Hurlburt, 2002: Naval Research Laboratory MLD (NMLD) Climatologies, Rep. NRL/FR/ 7330–02-9995, 26 pp.

Kawai, Y., and A. Wada, 2007, Diurnal Sea Surface Temperature Variation and Its Impact on the Atmosphere and Ocean: A Review, *J. Oceanogr.*, 63, 721-744.

Kizu, S., and K. Hanawa,2002, Start-up transient of XBT measurement, *Deep-Sea Res. I, 49* (5), 935-940.

Kraus, E. B. and J. S. Turner, *1967*: A one-dimensional model of the seasonal thermocline ii, the general. theory and its consequences. Tellus, 19, 98–105.

Large, W., J. McWilliams, and S. Doney, 1994, Oceanic Vertical Mixing: A Review and a Model with a Nonlocal Boundary Layer Parameterization, *Rev. Geophys*., **32**(4), 363-403.

Levitus, S., J. Antonov, and T. Boyer, 2005: Warming of the world ocean, 1955–2003, *Geophys. Res. Lett.,* **32**, L02604, doi:10.1029/2004GL021592.

Liu, W.T., 2002: Progress in scatterometer application, *J. Oceanogr.,* **58**(1), 121-136.

Lorbacher, K., D. Dommenget, P. P. Niiler, and A. Köhl, 2006, Ocean MLD: A subsurface proxy of ocean atmosphere variability, *J. Geophys. Res.*, *111*, C07010, doi:10.1029/2003JC002157.

Lukas, R., and E. Lindstrom, 1991, The mixed layer of the western equatorial Pacific Ocean, *J. Geophys. Res*., **96**(Supplement), 3343 –3357.

Maes C., J. Picaut, and S. Belamari. 2005: Importance of salinity barrier layer for the buildup of El Niño, *J. Climate*, 18, 104-118.

Manabe, S., and R.J. Stouffer, 1996, Low-frequency variability of surface air temperature in a 1000-year integration of a coupled atmosphere-ocean-land surface model, *J. Climate*, *9* (2), 376-393.

Mantua, N.J., S.R. Hare, Y. Zhang, J.M. Wallace, and R.C. Francis, 1997: A Pacific interdecadal climate oscillation with impacts on salmon production, *Bull. American Meteor. Soc.,* **78**, 1069-1079.

McCreary, J.P., K.E. Kohler, R.R. Hood, S. Smith, J. Kindle, A. Fischer, and R.A. Weller, 2001: Influences of diurnal and intraseasonal forcing on mixed-layer and biological variability in the central Arabian Sea. *J. Geophys. Res*., **106**, 7139–7155.

McPhaden , M.J. , and Coauthors, 1998, The Tropical Ocean-Global Atmosphere observing system: A decade of progress, *J. Geophys. Res., 103*(C7), 14,169-14,240.

Mellor, G. L. and Yamada, T., 1982: Development of a turbulence closure model for geophysical fluid problems. *Rev. Geophys. Space Phys.*, **20**, 851-875.

Mellor, G.L., 2001: One-Dimensional, Ocean Surface Layer Modeling: A Problem and a Solution. *J. Phys. Oceanogr.*, **31**, 790–809.

Michaels, A.F. and A.H. Knap, 1996: Overview of the U.S. JGOFS Bermuda Atlantic Time-series Study and the Hydrostation S Program, *Deep-Sea Res.*, **43**, 157-198.

Michel, S., Chapron, B., Tournadre, J., and Reul, N., 2007: Sea surface salinity variability from a simplified mixed layer model of the global ocean, Ocean Sci. Discuss., 4, 41-106.

Mignot, J., C. de Boyer Montégut, A. Lazar, and S. Cravatte, 2007: Control of salinity on the mixed layer depth in the world ocean: 2. Tropical areas, *J. Geophys. Res*., **112**, C10010, doi:10.1029/2006JC003954

Monterey, G., and S. Levitus, 1997: Seasonal Variability of MLD for the World Ocean, *NOAA Atlas NESDIS 14*, 100 pp., Natl. Oceanic and Atmos. Admin., Silver Spring, MD.

Murtugudde, R., J. P. McCreary Jr., and A. J. Basalacchi, 1999: Oceanic processes associated with anomalous events in the Indian Ocean with relevance to 1997-1998, *J. Geophys. Res*., **105,** 3295-3306.

Nilsen, J. E. Ø., and E. Falck, 2006: Variations of mixed layer properties in the Norwegian Sea for the period 1948–1999, *Prog. Oceanogr., 70,* 58–90.

Obata, A., J. Ishizaka and M. Endoh, 1996: Global verifica-tion of critical depth theory for phytoplankton bloom with climatological in situ temperature and satellite ocean color data. *J. Geophys. Res*., **101**, 20,657–20,667.

Oschlies, A., and V. Garcon, 1999, An eddy-permitting coupled physical-biological model of the North Atlantic. Part I: Sensitivity to advection numerics and mixed layer physics, Global Biogeochemical Cycles, 13, 135-160.

Pailler, K., B. Bourle`s, and Y. Gouriou, 1999: The barrier layer in the western tropical Atlantic Ocean, *Geophys. Res. Lett*., **26**, 2069–2072.

Prasad, T. G., 2004: A comparison of mixed-layer dynamics between the Arabian Sea and Bay of Bengal: One-dimensional model results, *J. Geophys. Res.*, **109**, C03035, doi:10.1029/2003JC002000.

Price, J. F., R. A. Weller, and R. Pinkel, 1986: Diurnal cycling: Observations and models of the upper ocean response to diurnal heating, cooling, and wind mixing. *J. Geophys. Res.*, **91**, 8411-8427.

Polovina, J.J., G.T. Mitchum, and G.T. Evans, 1995: Decadal and basin-scale variation in MLD and the impact on biological production in the central and North Pacific, 1960-88, *Deep-Sea Res.,* **42***,* 1701-1716.

Potemra, J. T., and R. Lukas, 1999: Seasonal to interannual modes of sea level variability in the western Pacific and eastern Indian Oceans, *Geoph. Res. Let.*, **26**, 365-368.

Qu, T., and G. Meyers, 2005, Seasonal variation of barrier layer in the southeastern tropical Indian Ocean, *J. Geophys. Res*., **110**, C11003, doi:10.1029/2004JC002816.

Rayner, N. A., D. E. Parker, E. B. Horton, C. K. Folland, L. V. Alexander, D. P. Rowell, E. C. Kent, and A. Kaplan, 2003, Global analyses of sea surface temperature, sea ice, and night marine air temperature since the late nineteenth century, *J. Geophys. Res., 108*(D14), 4407, doi:10.1029/2002JD002670.

Reynolds, R.W., and T.M. Smith, 1994, Improved Global Sea Surface Temperature Analyses Using Optimum Interpolation. *J. Climate, 7,* 929–948.

Reynolds, R. W., N. A. Rayner, T. M. Smith, D. C. Stokes and W. Wang, 2002: An improved in situ and satellite SST analysis for climate. *J. Climate, 15*, 1609-1625.

Sato, K., T. Suga, and K. Hanawa, 2006, Barrier layer in the North Pacific subtropical gyre, *Geophys. Res Lett*, **31**, L05301, doi:10.1029/2003GL018590.

Schneider, N., A.J. Miller, M.A. Alexander, and C. Deser, 1999: Subduction of decadal North Pacific temperature anomalies: Observations and dynamics, *J. Phys. Oceanogr.*, **29**, 1056-1070.

Seager,R., D. S. Battisti, J. Yin, N. Gordon, N. Naik, A. C. Clement, M. A. Cane, 2002: Is the Gulf Stream responsible for Europe's mild winters?, *Quarterly Journal of the Royal Meteorological Society, 128,* 2563-2586.

Smith, T. M., and R. W. Reynolds, 2003: Extended reconstruction of global sea surface temperatures based on COADS data (1854 –1997), *J. Clim., 16,* 1495– 1510.

Soloviev, A., and R. Lukas, 1997: Observations of large diurnal warming events in the near-surface layer of the western equatorial Pacific warm pool, Deep Sea Res., 44, 1055– 1076.

Sprintall, J., and M. Tomczak, 1992: Evidence of the Barrier Layer in the Surface Layer of the Tropics, *J. Geophys. Res.*, **97**(C5), 7305–7316.

Sprintall, J., and M. Tomczak, 1993: On the formation of central water and thermocline ventilation in the Southern Hemisphere, *Deep Sea Res., Part I*, **40**, 827–848.

Stommel, H., and K. N. Fedorov, 1967: Small-scale structure in temperature and salinity near Timor and Mindanao, *Tellus*, **19**, 306-325.

Stuart-Menteth, A. C., I. S. Robinson, and P. G. Challenor, 2003: A global study of diurnal warming using satellite-derived sea surface temperature, *J. Geophys. Res.*, *108*(C5), 3155, doi:10.1029/2002JC001534.

Tandon, A., and L. Zhao, 2004: Mixed layer transformation for the North Atlantic for 1990–2000, *J. Geophys. Res.*, 109, C05018, doi:10.1029/2003JC002059.

Taylor, A.H., and J.A. Stephens, 1998: The North Atlantic Oscillation and the latitude of the Gulf Stream, *Tellus – A*, **50**, 134-142.

Timlin, M.S., M.A. Alexander, and C. Deser, 2002: On the Reemergence of North Atlantic SST Anomalies, *J. Clim*., **15**, 2702-2712.

Thadathil P, Thoppil P, Rao RR, et al., 2008: Seasonal variability of the observed barrier layer in the Arabian Sea, *J. Phys. Oceanogr*., **38**, 624-638.

Tomczak, M., and J. S. Godfrey, 1994, Regional Oceanography: An Introduction, Pergamon, New York. (Avalaible at www.cmima.csic.es/mirror/mattom/regoc/pdfversion.html)

Wang, W., and M.J. McPhaden, 2001: The Surface-Layer Heat Balance in the Equatorial Pacific Ocean, Part II: Interannual Variability, *J. Phys. Oceanogr.*, **30**, 2989-3008.

White, W.B., 1995: Design of a global observing system for gyre-scale upper ocean temperature variability, *Prog. Oceanogr.,* **36,** 169-217.

Weller, R. A., and A. J. Plueddemann, 1996, Observations of the vertical structure of the oceanic boundary layer, *J. Geophys. Res*., **101**, 8789–8806.

Xie and Arkin, 1997: Global Precipitation: A 17-Year Monthly Analysis Based on Gauge Observations, Satellite Estimates and Numerical Model Outputs, *BAMS,* **78**, 2539-2558.

Yeager, S.G., and W.G. Large, 2007: Observational Evidence of Winter Spice Injection. *J. Phys. Oceanogr*., **37**, 2895–2919.

Xie, S.-P., T. Kunitani, A. Kubokawa, M. Nonaka, and S. Hosoda, 2000: Interdecadal Thermocline Variability in the North Pacific for 1958–97: A GCM Simulation, *J. Phys. Oceanogr*., **30**, 2798-2813.